CHARLES UNIVERSITY IN PRAGUE

2nd FACULTY OF MEDICINE

and

INSTITUTE OF EXPERIMENTAL MEDICINE AS CR, v.v.i.

Lesia Dmytrenko, MSc.

Changes of the Extracellular Space Diffusion Parameters during Acute Pathological States in the Rodent Brain and the Role of AQP4 Channels in Cell Swelling

PhD thesis

Prague 2014

ACKNOWLEDGEMENT

I would like to express my gratitude to my supervisor, Assoc. Prof. MUDr. Lýdia Vargová, Ph.D., for all her advice and patient guidance from the very beginning of my research work. I would also like to thank Prof. MUDr. Eva Syková, DrSc. for her support during my PhD research, and finally to all the members of our research group, who assisted in studies, presented in this thesis, especially to Karel Šlais, Michal Cicanič, Ivan Voříšek and Miroslava Anděrová.

LIST OF PUBLICATIONS

All the experiments were performed in the Laboratory of Neurobiology, Department of Neuroscience, Institute of Experimental Medicine, v.v.i., Academy of Sciences of the Czech Republic and in the Department of Neuroscience, Charles University, 2nd Faculty of Medicine under the supervision of Assoc. Prof. MUDr Lýdia Vargová, Ph.D.

Publications related to the thesis and contributions of individual co-authors:

1. **Dmytrenko L.**, Cicanič M., Anděrová M., Voříšek I., Syková E., Vargová L. The impact of alpha-syntrophin deletion on the changes in tissue structure and extracellular diffusion associated with cell swelling under physiological and pathological conditions. *PLoS ONE, 2013* 8(7):e68044, IF=3.7.

CONTRIBUTIONS:
Immunohistochemistry: Anděrová M., Vargová L.
Measurements of extracellular space diffusion parameters *in vivo*: **Dmytrenko L.**
Measurements of extracellular space diffusion parameters *in vitro*: Cicanič M., **Dmytrenko L.**, Vargová L.
Measurements of extracellular K^+ concentration *in vivo*: **Dmytrenko L.**
Diffusion-weighted magnetic resonance imaging: Voříšek I.

2. Šlais K., Voříšek I., Zoremba N., Homola A., **Dmytrenko L.**, Syková E. Brain metabolism and diffusion in the rat cerebral cortex during pilocarpine-induced status epilepticus. *Experimental Neurology*, 2008 Jan; 209(1):145-54, IF=4.156.

CONTRIBUTIONS:
Measurements of extracellular space diffusion parameters *in vivo*: Šlais K., **Dmytrenko L.**
Local field potential recording: Šlais K., **Dmytrenko L.**
Measurements of extracellular K^+ concentration *in vivo*: Šlais K., **Dmytrenko L.**
Diffusion-weighted magnetic resonance imaging: Voříšek I.
Microdialysis: Zoremba N., Homola A.

Unpublished results used in this work:

Anděrová M., Benešová J., Mikešová M., Džamba D., Honsa P., Kriška J., Butenko O., Rusňáková V., Valihrach L., Kubista M., **Dmytrenko L.**, Cicanič M., Vargová L. Altered astrocytic swelling in the cortex of alpha-syntrophin-negative GFAP/EGFP mice. *Submitted to Glia.*

CONTRIBUTIONS:

Measurements of extracellular space diffusion parameters *in vivo*: **Dmytrenko L.**

Measurements of extracellular space diffusion parameters *in vitro*: Cicanič M., **Dmytrenko L.**, Vargová L.

Other author's impacted publications:

Bekku Y., Vargová L., Goto Y., Voríšek I., **Dmytrenko L.**, Narasaki M., Ohtsuka A., Fassler R., Ninomiya Y., Syková E., Oohashi T. Bral1: its role in diffusion barrier formation and conduction velocity in the CNS. *Journal of Neuroscience*, 2010 Feb 24; 30(8):3113-23, IF=7.178.

TABLE OF CONTENTS

LIST OF ABBREVIATIONS

α-syn	α-syntrophin
(a)CSF	(artificial) cerebrospinal fluid
ADC	apparent diffusion coefficient
ADC_W	apparent diffusion coefficient of water
ADK	adenosine kinase
Aldh1L1	10-formyltetrahydrofolate dehydrogenase
AMPA	2-amino-3-(3-hydroxy-5-methyl-isoxazol-4-yl)propanoic acid
Ado	adenosine
ATP	adenosine-5'-triphosphate
AQP	aquaporin
BBB	blood–brain barrier
BK_{Ca}	calcium-activated big (conductance) potassium channels
Bral1	brain link protein 1
CA	cardiac arrest
$[Ca^{2+}]_e$	extracellular calcium concentration
$[Ca^{2+}]_i$	intracellular calcium concentration
CIC	chloride channel
$[Cl^-]_i$	intracellular chloride concentration
CNS	central nervous system
CSPGs	chondroitin sulfate proteoglycans
Ctrl1	cartilage link protein-1
Cx	connexin
DG	dystroglycan
DNA	deoxyribonucleic acid
DP 71	dystrophin 71
DW-MRI	diffusion weighted magnetic resonance imaging
EAA	excitatory amino acids
EAAT	excitatory amino-acid transporter
ECM	extracellular matrix
ECS	extracellular space
EEG	electroencephalography
(E)GFP	(enhanced) green fluorescent protein

EMF	electromotive force
EN	endonucleotidase
ER	endoplasmic reticulum
FEP	fluorinated ethylene propylene
FFEM	freeze-fracture electron micrographs
FOV	field of view
FP	field potential
GABA	γ-aminobutyric acid
GAT	GABA transporter
GFAP	glial fibrillary acidic protein
GLAST	glutamate aspartate transporter
GLT-1	glutamate transporter-1
glu^-	glutamate
GLUT1	glucose transporter 1 (solute carrier family 2, facilitated glucose transporter member 1)
GS	glutamine synthetase
H-50	hypotonic solution 250 mOsmol/l
H-100	hypotonic solution 200 mOsmol/l
Hapln	hyaluronan and proteoglycan link protein
ICAM-1	intercellular adhesion molecule 1
IL-1β	interleukin-1 beta
IP_3	inositol trisphosphate
ISMs	ion-selective microelectrodes
$[K^+]_e$	extracellular K^+ concentration
Kir	inwardly rectifying potassium channels
Kv	voltage-gated potassium channels
LPs	link proteins
LTD	long-term depression
LTP	long-term potentiation
mGluR	metabotropic glutamate receptor
mPTP	mitochondrial permeability transition pore
mTOR	mammalian target of rapamycin
MAP	mitogen-activated protein
MIWC	mercurial-insensitive water channel

MRI	magnetic resonance imaging
MRS	magnetic resonance spectroscopy
$[Na^+]_e$	extracellular sodium concentration
NBC	electrogenic sodium bicarbonate cotransporter
NF-κB	nuclear factor kappa-light-chain-enhancer of activated B cells
NMDA	*N*-Methyl-D-aspartic acid (*N*-Methyl-D-aspartate)
NO	nitric oxide
NS	neurosteroids
OAPs	orthogonal arrays of particles
P2Y(R)	purinergic G protein-coupled (receptors)
PDZ	*p*ost synaptic density protein (PSD95), *D*rosophila disc large tumor suppressor (Dlg1), and zonula occludens-1 protein (zo-1)
PGE_2	prostaglandin E_2
pH_e	extracellular pH
pH_i	intracellular pH
PLA_2	phospholipase A_2
PSD-95	postsynaptic density protein 95
PTZ	pentylenetetrazol
PVC	polyvinyl chloride
ROI	region of interest
ROS	reactive oxygen species
$RSloK_{Ca}$	rat large-conductance Ca^{2+}-activated K^+ channel
rt-PCR	reverse transcription polymerase chain reaction
RTI	real-time iontophoretic method
RVD	regulatory volume decrease
RVI	regulatory cell volume increase
S100β	β-subunit of Ca^{2+}-binding protein
SE	status epilepticus
SICs	slow inward currents
siRNA	small interfering (short interfering or silencing) RNA
S.E.M.	standard error of the mean
SMAD2	mothers against decapentaplegic homolog 2
SNARE	SNAP (Soluble NSF (*N*-ethylmaleimide-sensitive factor) Attachment Protein) Receptor

SNV	Ser-Asn-Val
SSV	Ser-Ser-Val
STAT3	signal transducer and activator of transcription 3
TE	echo-time
TEA	tetraetylamonium
TMA	tetramethylammonium
TN	tenascin
TNF-α	tumor necrosis factor alpha
TGFα	transforming growth factor alpha
TGFβ(R)	transforming growth factor beta (receptor)
TRP	transient receptor potential
TRPV4	transient receptor potential vanilloid-related, type 4
TRPM7	transient receptor potential cation channel, subfamily M, member 7
TLE	temporal lobe epilepsy
TR	repetition time (time between measurements)
TS	tuberous sclerosis
TSC1	tuberous sclerosis protein 1
TSC1/2	tuberous sclerosis complex
VRAC	volume-regulated anion channel
VSOACs	volume-sensitive organic anion channels
Wnt3	wingless/integrated protein 3
20-HETE	20-hydroxyeicosatetraenoic acid

1. INTRODUCTION

1.1. Extracellular space of CNS

According to the current state of knowledge, the extracellular space (ECS) of the central nervous system (CNS) is the nerve cell microenvironment that composes of between 15 and 30% of the total CNS tissue volume in healthy adult brain with a typical 20%; during global ischemia it decreases to 5%. The ECS containes a fluid that is referred to as the interstitial fluid, which is in contact with cerebrospinal fluid (CSF) at the ventricles. The chemical composition of the brain interstitial fluid is close to the composition of that found in the CSF. In mammals the composition is as followed: 141 mM Na^+, 124 mM Cl^-, 3 mM K^+, 121 mM HCO_3^-, 1.2 mM Ca^{2+} and about 2.5 mM Mg^{2+} (Sykova E. and Chvatal A. 2000). The interstitial fluid also maintains long-chain macromolecules of the extracellular matrix (ECM).

Synaptic transmission requires the diffusion of neuroactive substances over short distances (across the synaptic cleft and in the close vicinity of the synapse), which allows communication between pre- and postsynaptic terminals and the astrocytic processes enwrapping the synapse. Astrocytes may suppress or facilitate neuronal activity by neurotransmitter uptake or release (Haydon P. G. 2001). The role of glial cells in synaptic transmission is illustrated in the model of a “tripartite synapse”. This model refers to a new concept, where the information flow between the pre-and postsynaptic neurons is modulated by astrocytic release or uptake of neurotransmitters into/from the synaptic cleft. Thus, all three elements (presynaptic terminal, postsynaptic terminal and astrocytic endfeet adjacent to the synapse) are considered to be equally important in synaptic signal transmission (Araque A. et al. 1999). Recently, a fourth important element - the extracellular space was added to this model, turning it into a “quadripartite synapse” (Fig. 1 left panel) (Sykova E. 2004).

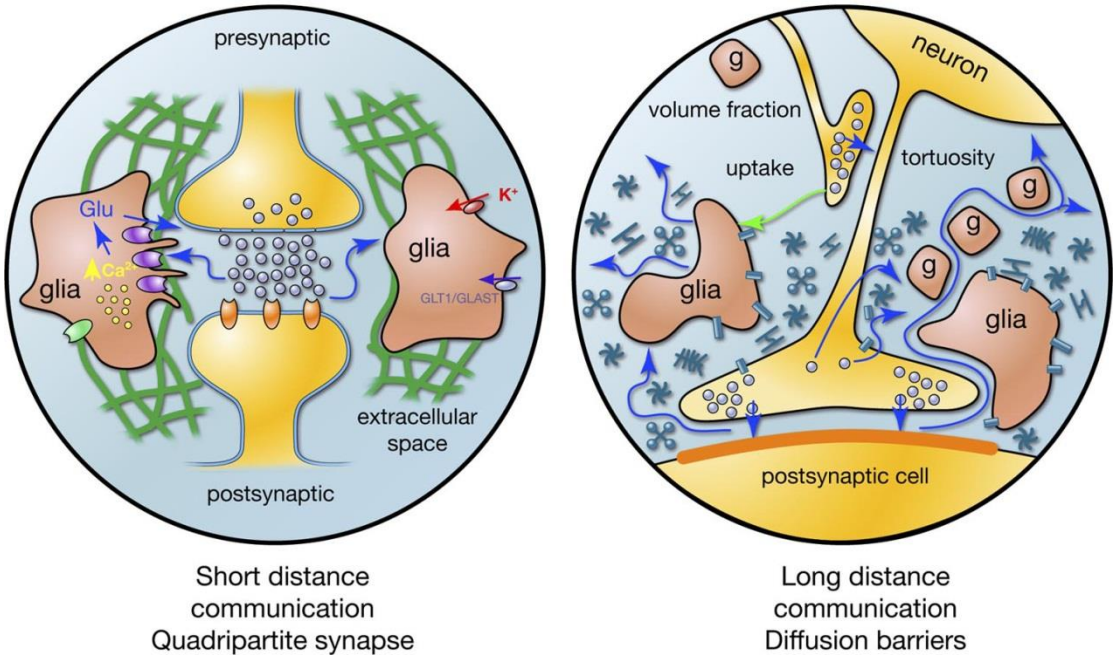

Fig. 1. Left panel: scheme of short-distance communication between cells and a quadripartite synapse, in which signal transmission is affected by four important elements: presynaptic and postsynaptic terminals, glial processes closely ensheathing the synapse and the extracellular space with its content, particularly the extracellular matrix. **Right panel:** The CNS architecture is composed of neurons, axons, glial cells (g), cellular processes, molecules of the ECM, and intercellular channels between the cells. Long-distance communication between nerve cells via diffusion is critically dependent on three ECS diffusion parameters: volume fraction α, tortuosity λ and non-specific uptake k' (Sykova E. and Nicholson C. 2008).

Beyond the close vicinity of the synapse, diffusion of transmitters and/or other neuroactive substances is an underlying mechanism of extrasynaptic or "volume" transmission, which is not only an alternative form of intercellular communication, but can modulate the synaptic transmission itself (Agnati L. F. et al. 1995; Zoli M. et al. 1999). Volume transmission acts over a time-scale of seconds or minutes, in both short and long distance modes and is also necessary for the phenomena known as "synaptic cross-talk" (Kullmann D. M. et al. 1996; Asztely F. et al. 1997). This heterosynaptic communication, whereby synapses of independent pathways may influence each other and modulate one another's activity, plays a role, for example, during long-term potentiation (LTP) and depression (LTD), during lactation or dehydration, where it can potentiate hormonal release (Oliet S. H. et al. 2001; Piet R. et al. 2004), or in the indirect modulation of the dopaminergic

system by excitatory input (Kiss J. P. et al. 2004). The synaptic cross-talk requires the escape of neurotransmitters from the synaptic cleft, referred to as "synaptic spillover". This process would otherwise be prevented in so-called "private" or "closed" synapses by the ensheathing of these synapses by glial processes and the ECM, which contributes to the high selectivity and signal-to-noise ratio of synaptic transmission (Fig. 1 left panel). Diffusion in the ECS is critically dependent on the nerve cell microenvironment; moreover, its properties vary in different brain regions and even around each cell. The private synapses that are tightly ensheathed by glial processes and molecules of the ECM, form perineural nets; other synapses are left more naked (so-called "public" or "open" synapses). Via diffusion, neurotransmitters such as glutamate (glu^-) or γ-aminobutyric acid (GABA) can thus reach extrasynaptic receptors in a neighboring synapse. Besides synaptic spillover, neuroactive substances and ions may be released into the ECS by various mechanisms, including extrasynaptic vesicular release from neurons or axonal varicosities (neuropeptides or catecholamines), the reversal action of glial transporters for neurotransmitters (glu^-, GABA, dopamine), ionic shifts from the intracellular to the extracellular compartment and also by the release of gaseous transmitters such as nitric oxide (NO) (Zoli M. et al. 1999). The diffusion of neurotransmitters and the accumulation of ions in the ECS are important for neuron-glia communication, since neurons can interact by both synaptic and extrasynaptic (volume) transmission, and because communication between neurons and glial cells is limited only to the extrasynaptic type.

1.1.1. Diffusion in the ECS

Diffusion is the spread of particles through random motion from regions of their higher concentration to regions of lower concentration. In a free medium, such as water or diluted agar, diffusion of substances is described by Fick's laws. Diffusion in the ECS, in contrast to a free medium, is obstructed by a number of factors, such as neuronal and glial processes, molecules of ECM, adhesion molecules, charged molecules, and cellular uptake, which hinder movement of the particles and, therefore, increases diffusion distance. Taking all these factors into account, the original Fick's diffusion equations were modified to describe diffusion in the ECS (Nicholson C. and Phillips J. M. 1981; Nicholson C. and Sykova E. 1998). Diffusion of substances in the ECS is dependent on the properties of the molecule (e.g., its size, shape, or charge), as well as on the properties of the ECS.

Diffusion properties of the ECS are characterized by three diffusion parameters (Fig. 1 right panel):

1. Extracellular volume fraction, α (α = ECS volume/total tissue volume), represents the volume available for diffusing particles. The ECS occupies about 20-25% of the adult healthy brain, and thus α = 0.2-0.25.

2. Tortuosity factor, λ, which is defined as $\lambda = (D/ADC)^{0.5}$, where D is the free diffusion coefficient and ADC is the apparent diffusion coefficient in the brain. The tortuosity value reflects the amount of obstacles in the ECS that hinder diffusion of molecules. The diffusion in the brain is about 2.5 times slower than in a free medium, so λ is approximated as 1.5 in the healthy brain tissue.

However, diffusion in the brain tissue is affected by the structure and organization of the diffusion barriers, so it is not uniform in all directions, i.e. anisotropic. Anisotropic diffusion facilitates movement of substances in the brain in one direction, e.g., along axons and is responsible for a partial specificity of the extrasynaptic transmission. It was found that diffusion anisotropy in white matter increases during development; the diffusion is isotropic in unmyelinated tissue, and becomes more anisotropic as myelination progresses. Studies using the tetramethylammonium (TMA) method have found anisotropy in the molecular layer of the cerebellum (Rice M. E. et al. 1993), and in the hypothalamic supraoptic nucleus (Piet R. et al. 2004). Other studies have revealed anisotropy in the myelinated white matter of the corpus callosum and spinal cord white matter (Vorisek I. and Sykova E. 1997; Chvatal A. et al. 1997; Prokopova S. et al. 1997). Anisotropy was also found in the hippocampus (Mazel T. et al. 1998), but later studies did not confirm this finding (Saghyan A. et al. 2012; Anderova M. et al. 2011).

3. Substances that diffuse in the ECS are also transported across membranes to cells or vessels by non-specific concentration-dependent uptake (k'). However, diffusion of some molecules (e.g., dopamine, glu^-) is also affected by the specific active transport systems. Substances that have negligible k' value, e.g., TMA^+, can be used as an extracellular marker.

According to recent studies (Hrabetova S. et al. 2003; Hrabe J. et al. 2004; Hrabetova S. et al. 2009; Sykova E. and Nicholson C. 2008) there are few factors that affect the tortuosity of an individual molecule in the ECS, in comparison to the diffusion in free medium:

1) Tissue structure, which creates obstacles and thus causes additional delay for the molecule diffusing in the ECS;

2) Dead-space microdomains that can be in the form of a “pocket”, glial wrapping, or even a local enlargement of the ECS. In such microdomains diffusing molecules are being trapped and lose time while exploring dead-ends;
3) Molecules of the ECM, such as hyaluronan;
4) Specific binding sites for the diffusing molecule on cell membranes or on molecules of the ECM;
5) Fixed negative charges that are usually on the molecules of the ECM that affect diffusion of charged molecules;
6) Size of the diffusing molecule.

1.1.2. Extracellular matrix

The ECM includes glycosaminoglycans (hyaluronic acid), oligomeric glycoproteins tenascins and chondroitinsulphate proteoglycans (CSPGs) (Fig. 2). Molecules of ECM are produced both by neurons and glial cells.

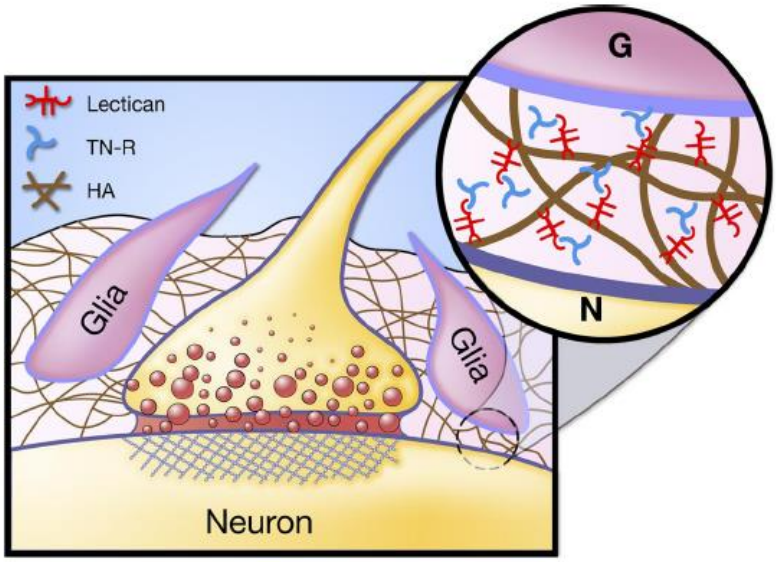

Fig. 2. Extracellular matrix. ECS is embedded in an extracellular matrix that includes lecticans, tenascin-R (TN-R), as well as tenascin-C in the developing brain, and hyaluronan (HA), G – glia; N – neuron (Sykova E. and Nicholson C. 2008).

Proteoglycans are major components of the ECM. They are a group of glycoproteins that carry covalently bound sulfated glycosaminoglycan chains. The diversity of proteoglycans is dependent on differential expression of genes encoding core proteins, transient splice variants of these genes, as well as variations in the length and types of glycosaminoglycan chains. In the CNS, the majority of the proteoglycans carry either chondroitin sulfate or heparin sulfate side chains (Bandtlow C. E. and Zimmermann D. R. 2000).

Lecticans are a family of chondroitin sulfate proteoglycans. There were four lecticans identified by molecular cloning: aggrecan, versican, neurocan and brevican. Aggrecan is a large cartilage proteoglycan, which was originally thought to be expressed exclusively in cartilage. Versican was identified in fibroblasts, and then later neurocan and versican were shown to be expressed in the nervous system (Yamaguchi Y. 2000; Oohashi T. and Bekku Y. 2007).

Three large ECM glycoproteins, tenascins (TN-C, TN-R and TN-Y), have been identified in the brain tissue (Joester A. and Faissner A. 2001). TN-C is expressed mainly during early development and tissue remodeling in neural and non-neural tissues. Later in adulthood, TN-C expression is present in areas that are known to display a high degree of functional plasticity, such as the hippocampus or hypothalamus (Theodosis D. T. et al. 1997). TN-R is expressed mainly by myelinating oligodendrocytes, and its neuronal expression persists until adulthood. Moreover, TN-R is a critical component of perineuronal nets surrounding neurons and is found in different brain areas, including the cerebral cortex and hippocampus (Bruckner G. et al. 2000; Sykova E. et al. 2005).

Hyaluronan is a glycosaminoglycan that is found ubiquitously in tissues where it can associate with hyaluronan-binding proteins (often called hyaladherins) in the ECM (Fig. 3). The link module superfamily forms a major group of hyaladherins that possess a common structural domain, ~100 amino acid residues in length. This superfamily includes lecticans and the link proteins (LPs). LP was primarily characterized as cartilage link protein 1 (Ctrl1). There have been a considerable amount of detailed studies on the hyaluronan-binding properties of various molecules, e.g. aggrecan and Ctrl1. However, until recently there had been no reports on other members of the LP family. In 2000 Hirakawa et al (Hirakawa S. et al. 2000) reported a new member of the LP family, brain link protein 1 Bral1. The LP family is now also known as the hyaluronan and proteoglycan link protein (Hapln) family (Oohashi T. and Bekku Y. 2007).

According to the current state of knowledge, the Hapln family has four distinct members: Crtl1 (Hapln1), Bral1 (Hapln2), Bral2 (Hapln4), and Lp3 (Hapln3). There are two types of

densely organized matrices in the brain: Bral1-associated ECM at the nodes of Ranvier and Bral2-binding ECM in perineuronal nets (Oohashi T. et al. 2002; Bekku Y. et al. 2003; Oohashi T. and Bekku Y. 2007). The C-terminal of lecticans can mediate binding to other ECM proteins such as tenascins. It was proposed that the hyaluronan-associated ECM could serve as an "extracellular ion pool" at the perinodal ECS, as both hyaluronan and chondroitin sulfate provide a strong negatively charged environment corresponding to the nodal diameter that binds positively charged ions (Oohashi T. et al. 2002; Bekku Y. et al. 2009; Bekku Y. et al. 2010).

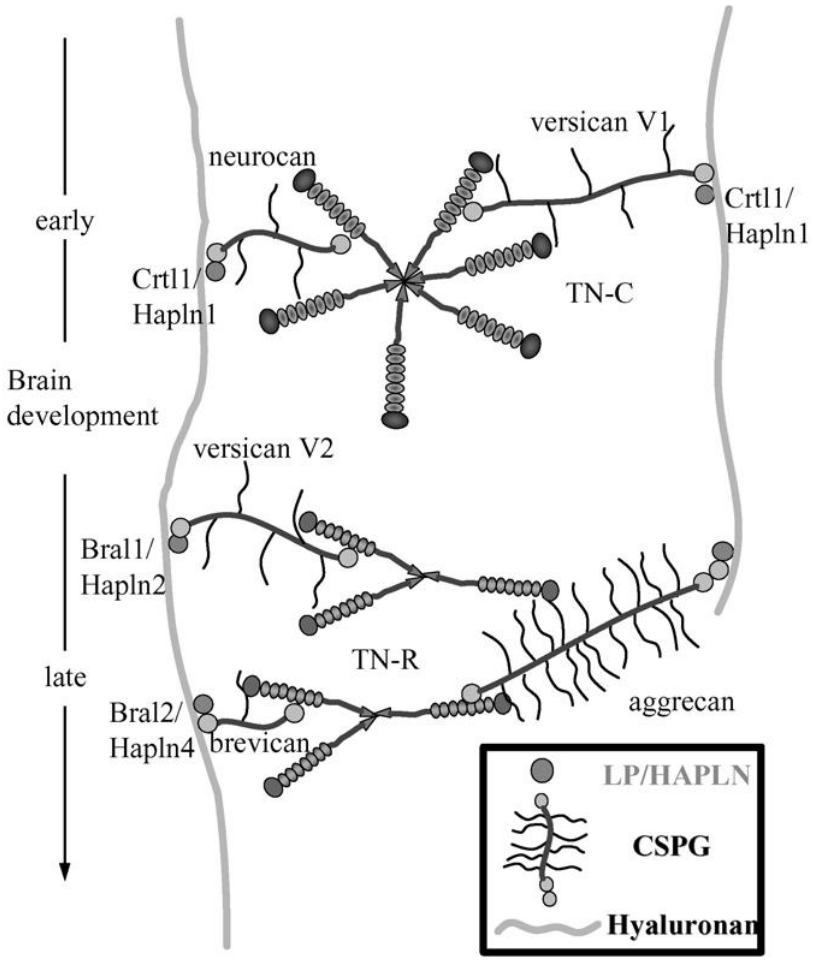

Fig. 3. A summary of the hyaluronan-binding proteoglycan complex during brain development. The arrow indicates the time course of brain development. There are developmental changes in the expression of lecticans and Lp/Haplns in the brain. Used abbreviations: Crtl1 – cartilage link protein 1; Hapln (1, 2, 4) – hyaluronan and proteoglycan link protein (1, 2, 4); Bral(1, 2) – brain link protein (1, 2); TN(-R, C) – tenascin(-R, C); LP – link protein; CSPG – chondroitin sulfate proteoglycan (Oohashi T. and Bekku Y. 2007).

The content of various ECM molecules and adhesion molecules can dynamically change during development, aging, wound healing and many pathological processes. ECM molecules play a role in tissue cytoarchitecture by maintaining the optimal size of intercellular pores, thus affecting the ECS volume fraction. A significant decrease in ECS volume was found in genetically modified animals, lacking certain molecules of ECM such as tenascin-R (Sykova E. et al. 2005) or Bral1 (Bekku Y. et al. 2010). On the other hand, an increase in α has been found in pathological states with overproduction of ECM: during astrogliosis (Roitbak T. and Sykova E. 1999), in the tissue of primary brain tumors (Zamecnik J. et al. 2004), or in focal cortical dysplasias (Zamecnik J. et al. 2012). Moreover, it was found that a decrease in the amount of CSPG and fibronectin in the hippocampus of old rats coincided with a decrease in the ECS volume (Sykova E. et al. 2002). The ECM is also one of the key factors that create diffusion barriers and affect tortuosity. In summary, overproduction of ECM leads to the increase in λ and to hindered diffusion (tumors, dysplastic or astrogliotic tissue), while diffusion is facilitated in conditions with attenuated ECM content (Bral1 deficiency).

1.2. Astrocytes

1.2.1. Definition and basic characteristics of astrocytes

Glial cells, also known as neuroglia or simply glia, represent nonexcitable neural cells that are unable to generate an action potential in their plasma membrane. In the late 1800s, glial cells were recognized as distinct cellular elements in the CNS. In 1895 Mihaly von Lenhossek proposed that the term “neuroglia” be used to cover all supporting CNS cells, and suggested the name “astrocyte” to specify a distinct type of glial cells (Montgomery D. L. 1994) (Fig. 4). Astrocytes constitute about 20-25% or even 50% of the total volume in some brain areas. For a long time astrocytes were believed to play only supportive and structural roles, reacting in a stereotypical manner to injury and disease. However, recent breakthroughs in cell culture and increasingly specific methods for identifing these cells have lead to greater knowledge about astrocytic development, function, and its role in disease.

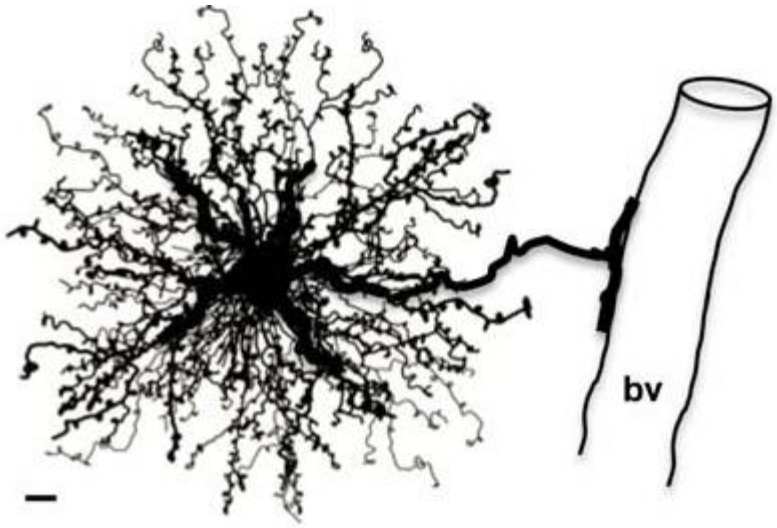

Fig. 4. Astrocyte morphology and interactions with blood vessels. Protoplasmic astrocyte giving rise to a dense network of finely branching processes throughout its local gray matter neuropil, as well as to a large stem branch that extends foot processes along a blood vessel (bv) (Sofroniew M. V. and Vinters H. V. 2010).

Based on their morphological appearance and distribution in the CNS, mature astrocytes come in three forms, the spherically bushy variant, the less bushy process-bearing form, and the elongated, non-excitable version. The first two forms are the protoplasmic astrocytes of grey matter and the fibrous astrocytes of white matter. The elongated cells are the Bergmann glia of the cerebellum and the Muller cells of the retina (Kimelberg H. K. and Nedergaard M. 2010). Based on morphological and immunohistochemical findings, a second classification of astrocytes has been proposed, in which astrocytes are divided into two types: type 1 and type 2, that are analogues to protoplasmic and fibrous astrocytes, respectively (Miller R. H. and Raff M. C. 1984; Montgomery D. L. 1994). Neuroanatomical studies indicate that both astrocyte types develop extensive contacts with blood vessels. It was also revealed that the processes of protoplasmic astrocytes envelop synapses, the processes of fibrous astrocytes contact nodes of Ranvier, and both types of astrocytes form gap junctions between distal processes of neighboring astrocytes (Sofroniew M. V. and Vinters H. V. 2010).

The main ultrastructural feature of astrocytes is the presence of intermediate filaments (glial fibrils) that are more prominent in fibrous than in protoplasmic astrocytes. The major component of glial fibrils, glial fibrillary acidic protein (GFAP), is specific for astrocytes in the CNS. This discovery was made approximately 40 years ago by Larry Eng during the lipid

studies of the multiple sclerosis brains (Eng L. F. et al. 2000). GFAP is the main 8-9 nm intermediate filament protein, which is one of a family of intermediate filament proteins, including vimentin, nestin, as well as others, and is found almost exclusively in mature astrocytes. GFAP is also expressed in the peripheral nervous system, in Schwann cells and enteric glia of the autonomous nervous system, and is now used as a prototypical marker for immunohistochemical identification of astrocytes (Jessen K. R. and Mirsky R. 1985; Jessen K. R. et al. 1990; Pekny M. and Pekna M. 2004).

The high abundance of the GFAP in astrocytes suggests that it plays an important role in the CNS. Although GFAP has been extensively studied, its precise functions still remain unclear. GFAP plays an important role in modulating astrocyte motility and provides structural stability to astrocytic processes, thus creating the shape of the cell. Following injury, as a result of trauma, disease, or genetic disorders, astrocytes become reactive and respond in a typical manner, referred to as astrogliosis. This process is characterized by rapid synthesis of GFAP and is demonstrated by an increase in protein content or by immunostaining with GFAP antibody. Thus, expression of GFAP is the most common marker to define the astrocyte population (Eng L. F. et al. 2000). It was also proposed that GFAP determines the complex astrocyte morphology including multiple processes that contact blood vessels, unsheathe neuronal synapses, abut nodes of Ranvier, and interweave with one another at the pial surface forming the glial limitans (Johansson C. B. et al. 1999; Doetsch F. et al. 1999).

Taking these functional predictions into account, it was suggested that mice knockout for GFAP would not be able to survive prenatal development. Surprisingly, after four groups independently produced GFAP-null mice, it occurred that the mice were vital, demonstrating seemingly normal behavior and life span (Gomi H. et al. 1995; Pekny M. et al. 1995; McCall M. A. et al. 1996; Liedtke W. et al. 1996). As a result, attempts to investigate functions of GFAP have largely relied on studies of changes in astrocyte properties or their effects on other cells in the GFAP-null mice. Following studies reported several differences between GFAP-null mice and control animals. GFAP-null mice display altered interactions in both LTD in the cerebellum (Shibuki K. et al. 1996) and LTP in the hippocampus (McCall M. A. et al. 1996). These mice also appear more severely affected by autoimmune encephalomyelitis and show deficits in myelination at an advanced age. Studies done by Liedtke et al. (Liedtke W. et al. 1996) suggested a role for GFAP in the architecture of white matter and blood-brain barrier. Nawashiro et al. (Nawashiro H. et al. 1998) showed that GFAP-deficient mice are hypersensitive to cervical spinal cord injury. Morphological analysis using confocal

microscopy and quantification of xy intensity profiles in a confocal plane demonstrated a lower density of processes in GFAP -/- astrocytes compared to GFAP +/+ astrocytes (Anderova M. et al. 2001). Moreover, this group showed that the changes in ECS diffusion parameters, induced by cell swelling in 50 mM K^+ or in hypotonic solution, are smaller and slower in GFAP -/- compared to that of GFAP +/+ mice (Anderova M. et al. 2001).

Due to the intracellular localization of GFAP, immunostaining can only be performed on permeabilized, i.e. dead cells. However, transgenic animals with expression of enchanced green fluorescent protein (EGFP) under the control of the human GFAP promoter (Besnard F. et al. 1991; Masood K. et al. 1993) were generated to allow imaging of astrocytes in living brain slices. In recent years, the green fluorescent protein (GFP) of the jellyfish *Aequorea victoria* has become a very useful and valuable tool in neuroscience for living cells. EGFP is the red-shifted variant of GFP that exhibits a substantially brighter fluorescence compared to the original protein (Patterson G. H. et al. 1997). In such regions of the CNS as the cortex, cerebellum, striatum, corpus callosum, hippocampus, retina, and spinal cord, EGFP-positive cells with morphological properties of astrocytes could be readily visualized by direct fluorescence microscopy in living brain slices. Moreover, EGFP marks the typical radial glia of the cerebellum, the protoplasmic astrocytes of the gray matter displaying vascular endfeet, and typical fibrous astrocytes of the white matter. EGFP is found to be co-expressed with GFAP, the astrocyte-specific intermediate filaments (Nolte C. et al. 2001).

The GFAP/GFP transgene has already been successfully used to label astrocytes in transgenic mice by Zhuo et al. (Zhuo L. et al. 1997). Thereafter, Nolte and colleagues (Nolte C. et al. 2001) have confirmed these observations, but have also employed the EGFP protein as a reporter molecule that provides a much brighter fluorescence compared to a previous S65T-GFT transgenic mouse line. EGFP can be detected at levels as low as ~100 nM, which is 10 times lower than the detection limit for GFP. Furthermore EGFP labeling enables the detection of smaller cellular details, compared to GFAP labeling (Nolte C. et al. 2001). There is a coexpression of GFAP and EGFP in many astroglial types, such as in the radial glia or in reactive astrocytes, however, some subpopulations of astrocytes show differential distribution of these two proteins. For example, there is high GFAP and low EGFP immunoreactivity in retinal and hypothalamic astrocytes (Nolte C. et al. 2001).

There are also some other molecular markers that have been used for immunohistochemical detection of astrocytes and reactive astrocytes, including glutamine synthetase and β-subunit of Ca^{2+}-binding protein (S100β); although, these substances are not exclusive to astrocytes (Goncalves C. A. et al. 2008). Some studies have been carried out to

identify more astrocyte molecular markers. The protein 10-formyltetrahydrofolate dehydrogenase (Aldh1L1) was defined as such marker. Its promoter targets the expression of reporter molecules such as GFP to astrocytes and it is possible sensitive chemical markers for astrocytes in healthy tissue (Barres B. A. 2008). In addition, glutamate transporter GLT-1 and glutamate aspartate transporter GLAST (Chaudhry F. A. et al. 1995) as well as glutamine synthetase (GS) (Wu Y. et al. 2005) were identified as astrocytic markers.

Astrocytes possess two membrane specializations, gap junctions and orthogonal assemblies, which are closely related to certain functions. Gap junctions are composed of hollow transmembrane proteins, known as connexons, which are themselves each constructed out of six connexin molecules. Connexons join with a homologous protein on adjacent cells to create hydrophobic channels that allow the interchange between coupled cells of small molecules with molecular weights less than 1000 such as ions, oligosaccharides, amino acids, nucleotides, or trophic factors (Dermietzel R. et al. 1991). The main connexins expressed in astrocytes are connexin 43 (Cx43) (Dermietzel R. et al. 1991) and connexin 30 (Cx30) (Kunzelmann P. et al. 1999; Nagy J. I. et al. 1999). Their relative levels vary according to the developmental stage and brain region (Giaume C. et al. 2010). There is also a variation in gap junction expression throughout the brain (Batter D. K. et al. 1992). Around blood vessels, connexin immunoreactivity is larger than this in the parenchyma. Outside blood vessels, Cx43 staining is abundant, whereas Cx30 immunoreactivity is much weaker (Rouach N. et al. 2008). Gap junctional coupling of astrocytes form multicellular network that play role in healthy brain and in CNS disorders (Nedergaard M. et al. 2003). Gap junctional networking facilitates extracellular glu^- and potassium removal during synaptic activity through modulation of astroglial clearance rate and extracellular space volume. This regulation limits neuronal excitability, release probability, and insertion of postsynaptic α-amino-3-hydroxy-5-methyl-4-isoxazolepropionic acid (AMPA) receptors, silencing synapses, thus, underlining importance of connexins in synaptic plasticity (Pannasch U. et al. 2011).

Orthogonal assemblies are paracrystalline arrays composed of 7-nm particles that can be viewed only in freeze-fracture preparations. These arrays are most numerous on the astrocytic endfeet facing and surrounding blood vessels and on the astrocytic processes facing the pia mater. They may function in cell adhesion and in the transport of substances between astrocytes and blood or CSF (Montgomery D. L. 1994).

1.2.2. Functions of astrocytes

Over the past 25 years it has become evident that astrocytes are responsible for a wide variety of very complex and essential functions in the healthy nervous system. Their functions can be divided into several important groups.

1. **Developmental function:**

- **Regulation of neuro- and gliogenesis.** In primates neurogenesis in the adult brain is restricted to the hippocampus and subventricular zone, and in both locations, astroglia are the stem elements that produce neurons. These "stem" astrocytes differ from "classical" mature astrocytes by specific expression of the protein nestin that is a marker for newly derived cells. There are additional markers of neural stem astrocytes, such as vimentin, a type III intermediate filament protein, is also often used as a marker of mesenchymally-derived cells (Eriksson J. E. et al. 2009); brain lipid-binding protein, the expression of which is spatially and temporally correlated with neuronal differentiation in many parts of the mouse CNS (Feng L. et al. 1994); RC1 (Edwards M. A. et al. 1990) and RC2 (Park D. et al. 2009), markers of radial glial cells. Some of the astrocytes form cilia. "Stem" astrocytes that reside in the hippocampus and subventricular zone give rise to both neurons and glia. In contrast to neurogenesis, gliogenesis occurs everywhere in the adult brain (Verkhratsky A. and Butt A. 2007). Astrocytes regulate neurogenesis by the secretion of factors such as wingless/integrated protein 3 (Wnt3), interleukin-1β, interleukin-6, and insulin-like growth factor binding protein 6 (Parpura V. et al. 2012).
- **Neuronal guidance.** Molecular boundaries formed by astrocytes take part in guiding the migration of developing axons and certain neuroblasts (Sofroniew M. V. and Vinters H. V. 2010). Neurons migrate along the processes of glial cells during development of the CNS. These guiding glial cells are called radial glia. The processes of radial glia contain vimentin and GFAP, and these glial cells are believed to be immature astrocytes. Migration depends on neuron-glial interactions, adhesion and recognition that are under the influence of cell membrane bound molecules and extracellular matrix molecules. With further maturation of the CNS, vimentin positivity in radial glia disappears and, after neuronal migration is completed, radial glia differentiates into mature astrocytes (Montgomery D. L. 1994; Verkhratsky A. and Butt A. 2007).

- **Regulation of synaptogenesis.** Astrocytes play an essential role in the formation and function of developing synapses by releasing molecular signals (Barres B. A. 2008). Christopherson and collegues (Christopherson K. S. et al. 2005) found that astrocytes release a large matrix-associated protein called thrombospondin, which is sufficient to induce synapses that have normal presynaptic and postsynaptic ultrastructure as well as normal clustering of presynaptic and postsynaptic proteins, such as synapsin and postsynaptic density protein 95 (PSD-95), respectively. Several distinct soluble factors have been identified that are released by glial cells and affect synapse maturation. One of these is tumor necrosis factor α (TNFα), which regulates the insertion of glu^{-} receptors into post-synaptic membranes; another one is activity-dependent neurotrophic factor (ADNF), which after being secreted by astrocytes, increases the density of *N*-Methyl-D-aspartic acid (NMDA) receptors in the membrane of neighbouring postsynaptic neurons (Barres B. A. 2008; Verkhratsky A. and Butt A. 2007). Astrocytes also appear to influence developmental synaptic pruning (Sofroniew M. V. and Vinters H. V. 2010).

2. **Structural function:**

- **Astroglia form the scaffold of the nervous system**, thus defining the functional architecture of the brain and spinal cord.
- **Astrocytes form a continuous syncytium** that integrates other neural cells. Such structural organization of the astrocytes is possible through gap junctions. Taking into account communication between brain cells, the term "astroglial network" was proposed to show neuroglial-gliovascular interaction (Giaume C. et al. 2010; Araque A. and Navarrete M. 2010).

3. **Vascular function:**

- **Formation and regulation of the blood-brain barrier:** astrocytes make extensive contacts and have multiple bidirectional interactions with blood vessels. The main cellular elements of the blood–brain barrier (BBB) are cerebral capillary endothelial cells that form tight junctions and are surrounded by a basal lamina, perivascular pericytes, and astrocyte endfeet (Sofroniew M. V. and Vinters H. V. 2010; Kimelberg H. K. and Nedergaard M. 2010).
- **Regulation of cerebral microcirculation:** astrocytes produce and release various molecular mediators, such as prostaglandins, nitric oxide, and arachidonic acid, that are able to increase or decrease blood flow (Gordon G. R. et al. 2007). The production

of arachidonic acid in astrocytes by Ca^{2+} sensitive phospholipase A_2 (PLA_2) has been shown to be common to both constriction and dilation mechanisms. Constriction results from the conversion of arachidonic acid to 20-hydroxyeicosatetraenoic acid (20-HETE) and dilation from the production of prostaglandin E_2 (PGE_2) or epoxyeicosatrienoic acid and the level of nitric oxide appears to dictate which of these two pathways is recruited. Additionally, the activation of Ca^{2+} activated K^+ channels in astrocytic endfeet and the efflux of K^+ has also been suggested to modify vascular tone by hyperpolarization and relaxation of smooth muscle cells.

Moreover, astrocytes release several regulatory factors: transforming growth factor α (TGFα), and glial-derived neurotrophic factor that induce the formation of tight junctions between endothelial cells and stimulate the polarization of their luminal and basal cell membranes. In turn, the endothelial cells signal to astrocytes, in particular through leukaemia-inhibitory factor, which promotes maturation of astrocytes (Verkhratsky A. and Butt A. 2007).

4. **Metabolic function:**

- **Providing energy substrates for neurons:** astrocytes are the main storage sites of glycogen granules in the CNS and the greatest accumulation of astrocytic glycogen occurs in areas of high synaptic density (Sofroniew M. V. and Vinters H. V. 2010). Glucose transporter GLUT1 is expressed on the astrocytic endfeets that provides astrocytes with an easy access to glucose supply. After the uptake, glucose is phosphorylated to glucose-6-phosphate, which can enter the glycolytic pathway, phosphate pathway (Parpura V. et al. 2012), or alternatively act as a substrate for glycogen synthesis (Walls A. B. et al. 2009; Schousboe A. et al. 2010). Astrocytic glycogen utilization can sustain neuronal activity during hypoglycemia and during periods of high neuronal activity (Sofroniew M. V. and Vinters H. V. 2010).
- **Collecting neuronal waste.**

5. **Control of the CNS microenvironment:**

- **Maintenance of ion and volume homeostasis:** astrocytes play a role in the homeostasis of K^+, Cl^-, H^+ (pH), neurotransmitters such as glu^- and in cell volume maintaining. The next chapter is dedicated to this astrocytic function.
- **Removal of neurotransmitters from the extracellular space:** astrocyte processes at synapses express high levels of transporters for different neurotransmitters (such as glu^-, GABA, and glycine) that assist in clearing them from the synaptic cleft.

Following their uptake into the astrocyte, the transmitters are converted by enzymes into precursors and then recycled back to the synapses for reconversion into active transmitters (e.g. glutamate-glutamine cycle) (Seifert G. et al. 2006).

- **Brain water homeostasis:** astrocytes are capable of cell volume regulation by the release of osmoticaly active molecules, such as taurine. Taurine is an abundant, free, sulfur-containing, β-amino acid that exerts an osmoregulatory effect and is predominantly concentrated in glial cells in the supraoptic nucleus. This glial osmoregulatory control may be a complement to that exerted by central and peripheral osmoreceptors regulating neurosecretion in response to changes in plasma osmolarity (Simard M. and Nedergaard M. 2004). Rates of taurine accumulation and taurine synthesis are enhanced by cell shrinkage, whilst taurine efflux from cells and brain tissue is accelerated by cell swelling (Kreisman N. R. and Olson J. E. 2003).

6. Signaling:

- **Synaptic transmission is modulated by controlling the concentrations of neurotransmitters:** they are either released into or takenup from the synaptic cleft via glial transporters. These findings gave rise to the "tripartite synapse" hypothesis, which functionally involves astrocytes into synaptic transmission (Halassa M. M. et al. 2007; 2009).
- **Release of gliotransmitters and contribution to extrasynaptic transmission:** astrocytes have been shown to be capable of releasing a wide range of gliotransmitters, such as glu^-, purines (adenosine-5'-triphosphate [ATP] and adenosine), GABA, D-serine, TNFα, prostaglandins, atrial natriuretic peptide, brain-derived neurotrophic factor, etc. (Perea G. and Araque A. 2010). The molecular mechanisms responsible for the release of gliotransmitters are still under debate; although convincing results indicate that gliotransmitter release is based on Ca^{2+} and SNARE (an acronym derived from "SNAP [Soluble N-ethylmaleimide-sensitive factor Attachment Protein] Receptor") protein-dependent mechanisms through vesicle and lysosome exocytosis (Perea G. and Araque A. 2010). Despite this evidence supporting Ca^{2+}-dependent release of gliotransmitters, a study performed on transgenic mice has questioned Ca^{2+} dependence (Fiacco T. A. et al. 2007). Several astrocytic glu^- release mechanisms have been identified, such as: 1) through sodium-dependent glu^- transporters operating in reverse mode (Rossi D. J. et al. 2000); 2) Ca^{2+}-dependent release via exocytosis of glutamate containing vesicles (Bezzi P. et al.

2004; Parpura V. et al. 2004); 3) through purinergic receptors (Parpura V. et al. 2004); 4) hemichannels (Parpura V. et al. 2004); or 5) via activation of volume-sensitive organic anion channels (VSOACs) in the context of hypoosmolar stress and cellular volume regulatory response (Kimelberg H. K. et al. 1990). Transmitters released from astrocytes modulate synaptic transmission in neighboring neuronal circuits (Verkhratsky A. and Butt A. 2007; Perea G. et al. 2009) and thus contribute to extrasynaptic transmission.

- **Long-range signaling within the glial syncytium:** astrocytes via gap junctions act as an electrical syncytium that serves for spatial buffering and long-range Ca^{2+} waves propagation (Verkhratsky A. et al. 1998; Cornell-Bell A. H. et al. 1990).
- **Integration of neuronal-glial networks:** Astrocytes can integrate neuronal activity through activation of their channels, receptors, and transporters, and modulate in turn synaptic transmission and plasticity, via the release of gliotransmitters or uptake of neuroactive substances. Since astrocytes are interconnected via gap junctions, which allow the intercellular trafficking and redistribution of neuroactive substances, they can integrate and modulate large neuronal ensembles (Pannasch U. et al. 2011; Pannasch U. et al. 2012). Astrocyte-neuronal signaling operates both locally and distantly; Ca^{2+} waves can affect excitability of the neurons that are involved in the astrocyte network via secretion of neurotransmitters, through the reduction of free Ca^{2+} in the synaptic clefts (Verkhratsky A. et al. 1998).

1.2.3. Role of astrocytes in the ionic homeostasis

The extracellular concentration of K^+ ($[K^+]_e$) is ~2-3 mM. Due to the restricted volume of the ECS and low $[K^+]_e$, even relatively small numbers of K^+ released by neurons may significantly affect K^+ extracellular concentration and bring the neurons' membrane potential closer to the action potential threshold. This depolarization results in increased neuronal activity, however further increase in the $[K^+]_e$ leads to the inactivation of Na^+ channels and neuronal activity inhibition.

Glial cells, particularly astrocytes, are the key elements in the maintenance of $[K^+]_e$ at a level necessary to keep continued neuronal activity. The main mechanisms by which astrocytes remove excessive K^+ from the ECS are represented by *local* K^+ *uptake* and K^+

spatial buffering. In the case of K^+ uptake, excess K^+ ions are temporarily sequestered into glial cells by transporters or K^+ channels. To preserve electroneutrality, K^+ influx into glial cells is accompanied by either influx of anions, such as Cl^-, or by efflux of cations such as Na^+. Eventually, K^+ ions accumulated in glia are released back into the extracellular space and the overall distribution of K^+ across the cellular compartments is restored (Kofuji P. and Newman E. A. 2004).

The *local K^+ uptake* occurs in the individual cells and is mediated by K^+ channels and transporters (Fig. 5):

1. By the Ca^{2+}-activated K^+ channels, which open when the $[K^+]_e$ is increased, leading to the depolarization of the membrane of glial cells, that in turn results in the influx of Ca^{2+} to the cells and activation of Ca^{2+}-dependent K^+ channels (MacVicar B. A. 1984).
2. By the KCl uptake. This mechanism is also known as Donnan-mediated KCl uptake and is thought to be a minor contributor to overall K^+ homeostasis, due to the low Cl^- permeability in astrocytes under physiological conditions (Leis J. A. et al. 2005).
3. By Na-K-2Cl cotransporters that mediate the coupled, electrically neutral movement of Na^+, K^+ and Cl^- across the cell membrane and is considered a major contributor of KCl accumulation (Russell J. M. 2000). This cotransporter is stimulated by elevated $[K^+]_e$ (Hertz L. et al. 2000). The Na-K-2Cl cotransporter-1 has been shown to play an important role in the mediation of astrocyte swelling (Chen H. and Sun D. 2005; Jayakumar A. R. and Norenberg M. D. 2010).
4. By activation of the Na^+/K^+ pump that leads to the exchange of the extracellular K^+ ions for the intracellular Na^+ ions. This pump is present in both neurons and glia (Walz W. and Hinks E. C. 1986; Syková E., Chvátal, A., Vargová, L., Voříšek, I. 1996) and determines the rate of $[K^+]_e$ recovery during high-frequency stimulations (Leis J. A. et al. 2005).

However, the capacity for *local K^+ uptake* is limited due to the increase in intracellular K^+ concentration and the fact that water follows the ions, resulting in cell swelling. Another mechanism for excess $[K^+]_e$ removal was proposed by Wolfgang Walz and Richard Orkand and is now known as *spatial K^+ buffering* (Orkand R. K. et al. 1966; Coles J. A. and Orkand R. K. 1983). This mechanism is based on the fact that astrocytes form a syncytium via the network of gap junctions, which is essential for the rapid redistribution of K^+ from areas of high neuronal activity through astrocyte cytoplasm and the system of gap junctions; these

excess K^+ ions can be released in distant regions with decreased K^+ concentration (Leis J. A. et al. 2005). Excess intracellular K^+ is shunted to the vascular system via outwardly rectifying K^+ currents, inwardly rectifying potassium channel Kir4.1, voltage-gated potassium channel Kv1.5, and rat large-conductance Ca^{2+}-activated K^+ channel ($RSloK_{Ca}$), and swell-activated K^+ currents during cellular regulatory volume decrease (RVD) (Simard M. and Nedergaard M. 2004). The main K^+ channels that are responsible for spatial buffering are inwardly rectifying channels of Kir4.1 type (Horio Y. 2001; Dibaj P. et al. 2007). In Muller cells, expression of Kir2.1 accompanies that of Kir4.1 (Kofuji P. et al. 2002).

However, the exact role of glial K^+ uptake or spatial buffering in various parts of the CNS remains unclear, as research has shown that the relative contributions may vary across species and between CNS regions. For example, $[K^+]_e$ buffering in the rat optic nerve seems to be more dependent on the active uptake mechanism than on K^+ spatial buffering as post-stimulus recovery of $[K^+]_e$ is highly sensitive to sodium pump inhibition, but not to glial K^+ channel blockers. By contrast, in the CA3 region of rat hippocampus, both the sodium pumps and glial K^+ channels seem critical for setting the baseline $[K^+]_e$ and the post-stimulus recovery of $[K^+]_e$. In this preparation, sodium pumps are necessary for the clearance of excess K^+ during afferent stimulation, whereas glial K^+ channels are necessary to prevent large $[K^+]_e$ undershoots following post-tetanus (Kofuji P. and Newman E. A. 2004).

As glial cells are not electrically excitable, they have a relatively small distribution of voltage-gated Na^+ channels, which allow Na^+ influx via the H^+/Na^+ antiport, and the Na-K-Cl cotransporter. Na^+K^+-ATPase pump extrudes Na^+ in exchange for K^+ from the ECS that generates an inwardly directed gradient for Na^+ ions, which in turn energizes other secondary ion transporters, like Na^+-Ca^{2+} exchange (Simard M. and Nedergaard M. 2004).

Several chloride channels have been described in astrocytes. Hypoosmotic swelling of cultured astrocytes has been shown to evoke an outwardly rectifying anion current that is regulated by tyrosine and mitogen-activated protein (MAP) kinase (Ordaz B. et al. 2004). It was also demonstrated in rat cortical astrocytes that an inwardly rectifying Cl^- current is augmented by extracellular acidosis and reduced by alkalosis (Makara J. K. et al. 2001). The swell-activated Cl^- channels extrude Cl^- during the process of RVD (Simard M. and Nedergaard M. 2004). Moreover, it has also been demonstrated that Cl^- may be transported into the astrocytes by a Na^+-K^+-$2Cl^-$ cotransporter and extruded via the Cl^-/HCO_3^- anion exchange system coupled to pH regulation (Simard M. and Nedergaard M. 2004).

Glial cells are able to respond to external stimuli with the generation of intracellular Ca^{2+} signals. Local Ca^{2+} release from the endoplasmic reticulum (ER) creates microdomains

of an increased Ca^{2+} concentration that triggers neighboring Ca^{2+} release channels. This results in a propagating wave of excitation, that serves as a substrate for long-range signaling in the glial syncytium (Verkhratsky A. 2006).

Astrocytes express all types of known neurotransmitter receptors. Synaptic activity triggers activation of glial receptors resulting in the release of Ca^{2+} from intracellular stores as well as extracytosolic sources, which leads to an increase in intracellular calcium concentrations ($[Ca^{2+}]_i$). These Ca^{2+} signals in astrocytes control the release of gliotransmitters (e.g. glu^-, D-serine, ATP), which can in turn modulate neuronal excitability, synaptic activity and plasticity, affecting neurons by either exciting them or modulating the ongoing synaptic transmission (Verkhratsky A. 2006). A local $[Ca^{2+}]_i$ increase in a single perivascular digit spreads throughout the entire process of the astrocyte, including the endfoot, and then propagates to adjacent endfeet. Connexin channels contribute to the intercellular propagation of Ca^{2+} waves *in vivo* and during pathological states, it is suggested that they participate in the regulation of blood flow by increasing the number of endfeet involved in the response (Giaume C. et al. 2010).

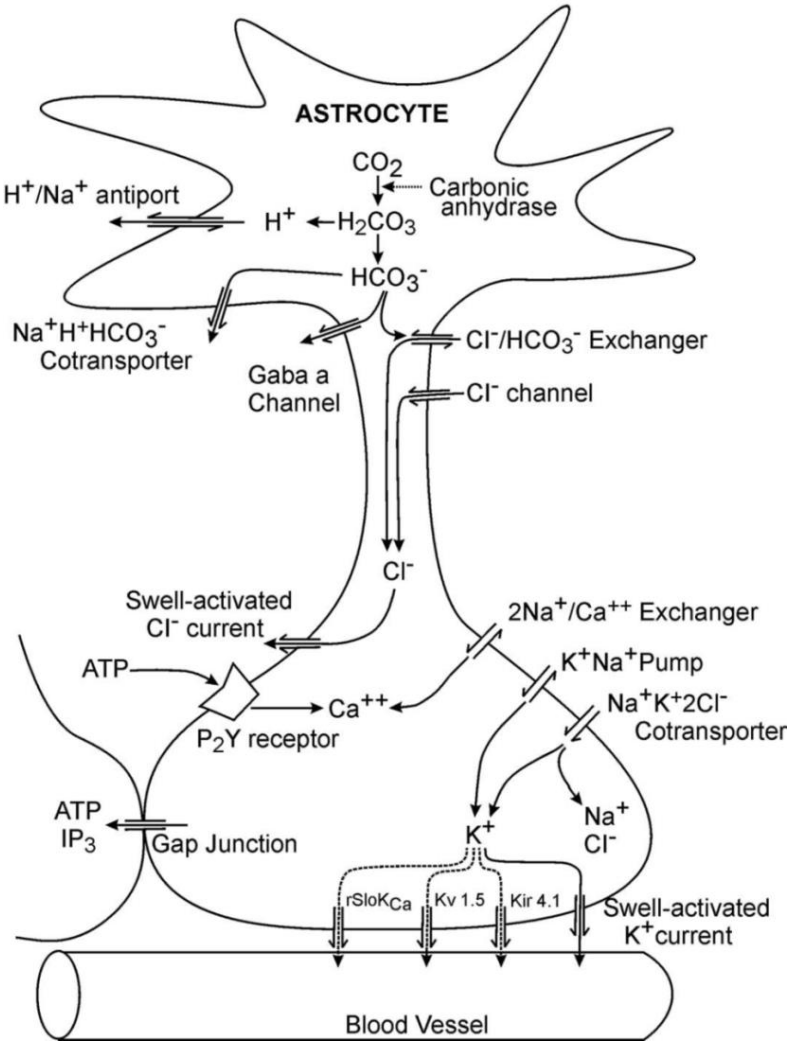

Fig. 5. Ionic homeostasis in glia. Used abbreviations: GABA - γ-Aminobutyric acid; ATP – adenosine triphosphate; IP_3 – inositol trisphosphate; P_2Y receptor – purinergic G protein-coupled receptor; $RSloK_{Ca}$ – rat large-conductance Ca^{2+}-activated K^+ channel; Kv 1.5 – potassium voltage-gated channel, member 5; Kir4.1 – inwardly rectifying potassium channel, member 4.1 (Simard M. and Nedergaard M. 2004). For detailed explanation see text.

The extracellular pH (pH_e) varies between 7.1 and 7.3, whereas intracellular pH in both neurons and glia lies in a range of 6.8 to 7.5. This means that the concentration of free protons, H^+, is quite low, being somewhere around 50 nM in the extracellular milieu and 30-160 nM in the cytosol of neural cells. Maintenance of extracellular pH is physiologically important, as even small fluctuations of pH_e may significantly affect synaptic transmission and neuronal excitability (Verkhratsky A. and Butt A. 2007). Most of the H^+ produced during energy metabolism is rapidly buffered by proteins and other ampholytes, thus the concentration of free H^+ ions in the cytoplasm constitutes only a minute fraction of the total acid loan. The clearance of H^+ from the cytoplasm into the extracellular space is mediated in astrocytes by several transporters such as the Na^+-HCO_3^- cotransporters, Na^+/H^+ exchanger and either Na^+-dependent or Na^+-independent Cl^-/HCO_3^- antiporters. This movement of H^+ results in acidification of the extracellular space and alkalization of the cell interior (Simard M. and Nedergaard M. 2004). Moreover, the glial cell membrane is easily permeable for CO_2, which reacts with water to form carbonic acid, which in turn is quickly dissociated to water and protons. This reaction is catalyzed by the enzyme carbonic anhydraze that is present in glia. Some of this membrane transport mechanisms result in alkaline shifts in pH_e (acid loaders), while others result in acid shifts in pH_e (acid extruders). It has been shown that acid loaders are dominant in neurons, while acid extruders are dominant in glia (Chesler M. 1990; Sykova E. et al. 1992).

A model of a nonspecific feedback mechanism suppressing neuronal activity that explains the connection between ionic and volume changes has been proposed (Fig. 6). The model can be simplified in to the following points:

1. Neuronal activity results in accumulation of $[K^+]_e$.
2. Extracellular K^+ depolarizes glial cells and depolarization in turn activates alkaline shift in intracellular pH (pH_i).
3. Glial cells absorb HCO_3^- that leads to an acid shift in pH_e.
4. Acidification of the ECS suppresses neuronal excitability by causing changes in receptor proteins.

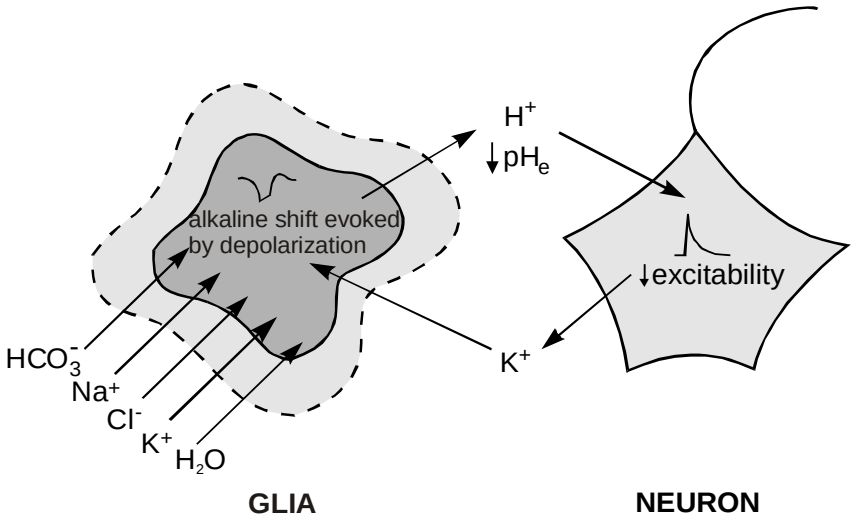

Fig. 6. Schematic picture of the mechanism of nonspecific feedback suppressing neuronal excitability (Sykova E. 1997).

All transmembrane ionic shifts (K^+, Na^+, Ca^{2+} and H^+) and membrane transport mechanisms, such as glu^- uptake, are followed by water movement, thus causing swelling of neural cells, particularly glia. Cell swelling further facilitates nonspecific feedback mechanism suppressing neuronal excitability.

1.3. Aquaporin family of water channels

Water constitutes more than 90% of the molecules in the human body and its movement across cell membranes is a crucial property of life. It can pass freely through the lipid layer; however this form of transport is relatively slow. Another form of water transport across the cell membrane was initially discovered in 1988 by Peter Agre. He identified the first member of the aquaporin (AQP) family of water channels, AQP1, and was awarded the Nobel Prize in chemistry in 2003.

The aquaporins are a family of small, hydrophobic proteins, consisiting of about 300 amino acids that assemble in cell membranes as tetramers. Each monomer has six membrane-spanning α-helical domains surrounding a water pore and intracellularly located NH_2- and COOH-termini (Preston G. M. and Agre P. 1991; Preston G. M. et al. 1994). The molecular weights of the monomers range from 26 kDa (AQP7) to 34 kDa (AQP4). Transport through AQPs is possible in both directions (Agre P. et al. 2002; Verkman A. S. 2005). Water

movement is driven by the osmotic pressure or by the solute concentration difference between the intracellular and extracellular space. Single channel permeability of AQPs and their abundance in the cell membrane determine the intensity of the water flux; both these parameters can be regulated (Zelenina M. 2010).

To date, over 13 different members of this family have been identified in mammals. AQPs facilitate regulated transmembrane water transport and are expressed in various tissues including the kidney, lung, gastrointestinal tract and CNS.

The aquaporin family contains two subfamilies: aquaporins and aquaglyceroporins. AQP0, AQP1, AQP2, AQP4, AQP5 and AQP8 are primarily water selective, whereas aquaglyceroporins (AQP3, AQP7, AQP9 and AQP10) are also permeable to glycerol and other small solutes (in case of AQP9) (Agre P. et al. 2002). Most AQPs are not permeable to ions. AQP6 and AQP8, which possess ion permeability, as well as AQP11 and AQP12 that lack characteristic structural features of AQPs, have all been assigned to an unorthodox AQP subgroup (Table 1) (Rojek A. et al. 2008; Verkman A. S. 2005).

Table 1. Function and expression pattern of aquaporins

AQP	Permeability	Tissue expression
AQP0	?	Eye lens fiber cells
AQP1	Water	Kidney tubules, endothelia, erythrocytes, choroid plexus, ciliary epithelium, intestinal lacteals, corneal endothelial
AQP2	Water	Kidney collecting duct
AQP3	Water, glycerol	Kidney collecting duct, epidermis, airway epithelium, conjunctiva, large airways, urinary bladder
AQP4	Water	Astroglia in brain and spinal cord, kidney collecting duct, glandular epithelia, airways, skeletal muscle, stomach, retina
AQP5	Water	Glandular epithelia, corneal epithelium, alveolar epithelium, gastrointestinal tract
AQP6	Chloride?	Kidney collecting duct intercalated cells
AQP7	Water, glycerol	Adipose tissue, testis, kidney proximal tubule
AQP8	Water	Liver, pancreas, intestine, salivary gland, testis, heart
AQP9	Water, small solutes	Liver, white blood cells, testis, brain
AQP10	Water, glycerol	Small intestine
AQP11	?	Kidney, liver
AQP12	?	Pancreatic acinar cells

Adapted from Verkman, Journal of Cell Science 118: 3225-3232, 2005.

It was shown that AQP4 has the highest water permeability coefficient, followed by AQP1, AQP2 and AQP5. AQP3 and AQP0 have the lowest water permeability coefficient (Yang B. and Verkman A. S. 1997). AQPs are inhibited by nonspecific, mercurial sulfhydral-reactive compounds, such as $HgCl_2$, that interact with free sulfhydryls. AQP4 is the only identified mercury-insensitive aquaporin as it lacks a mercury-sensitive site (Amiry-Moghaddam M. and Ottersen O. P. 2003). AQP6 is also unusual because it is activated by

$HgCl_2$ (Hazama A. et al. 2002). Reducing agents like β-mercaptoethanol can reverse inhibition by mercury. AQP0, AQP3 and AQP8 are metal sensitive, whilst AQP0 and AQP3 are sensitive to extracellular pH, and AQP6 to intracellular pH (Zelenina M. 2010).

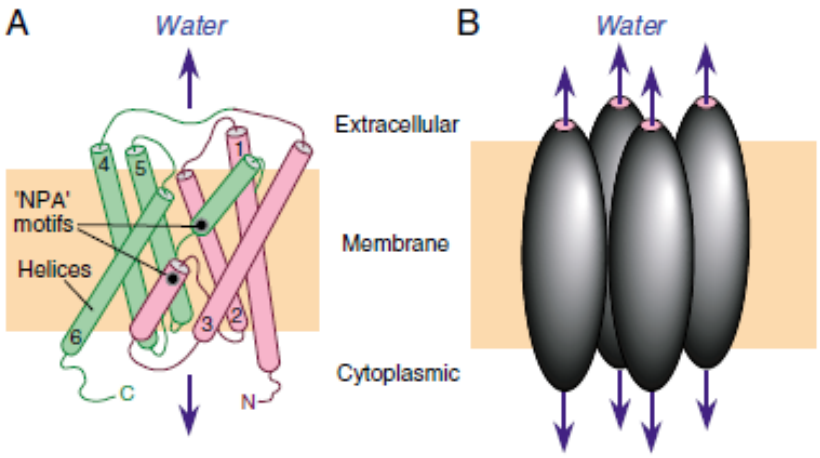

Fig. 7. Structure of AQP1 monomers and their tetrameric assembly in membranes. (A) Crystal structure of AQP1 monomer showing titled transmembrane α-helical domains (numbered 1-6) surrounding a water pore. Conserved Asn-Pro-Ala (NPA) motifs are indicated. **(B)** Tetrameric assembly of AQP1 in a membrane in which individual monomers contain water pores (Verkman A. S. 2005).

There are two main mechanisms of regulation of AQPs and channels in general:

1. **Short-term** (or **dynamic**) **regulation** that can be mediated by conformational changes or channel gating as a result of
    - Activation-deactivation of intracellular signaling pathways that induces phosphorylation-dephosphorylation events;
    - Changes in intracellular or extracellular pH that lead to changes in the protonation state of certain protein amino acids;
    - Binding or chemical reaction with metal ions;
    - Protein-protein interactions;
    - Internalization/incorporation into the cell membrane;
    - Binding of an inhibitor.

As a result of short-term regulation, permeability of AQP channels or AQP abundance in the membrane may change within seconds or minutes.

2. **Long-term regulation** that is mediated by AQP mRNA changes, protein synthesis and degradation rate that alter, within hours or days, AQP abundance, which changes the permeability of the membrane (Zelenina M. 2010).

1.3.1. Aquaporins in the brain

Water homeostasis in the brain is of central importance since it is coupled with the neuronal activity. Roughly 78% of the brain is water, but still little is known about brain water transport. The main portion of the brain water is intracellular, but it is also distributed in the extracellular space, cerebral ventricles and subarachnoid space. Water enters the brain across the choroids plexus or through the blood-brain barrier. Under physiological conditions, the extracellular fluid flows into the cerebral ventricles or subarachnoid space and after circulation through CSF compartments, exits to the venous system through the arachnoid granulations (Abbott N. J. 2004).

In earlier works it has been demonstrated that there is a high osmotic-diffusion ratio of the choroids plexus, and it was hypothesized that there exists some pore-like pathway for water molecules (Wright E. M. et al. 1977). The first studies showing the brain to contain water channels were carried out by Jung and colleagues (Jung J. S. et al. 1994) and Hasegawa with coauthors (Hasegawa H. et al. 1994). It is now known that there are three brain aquaporins: AQP1, AQP4 and AQP9. Data by reverse transcription-polymerase chain reaction showed expression of AQP3, AQP5, and AQP8 in neuronal primary cultures and astrocyte cultures. AQP8 was found on oligodendrocytes, and AQP5 on astrocytes (Yamamoto N. et al. 2001).

AQP4 is the most abundant brain aquaporin channel and is expressed in the basolateral membrane of the ependymal cells that line cerebral ventricles and in the plasma membranes of astrocytes (Nielsen S. et al. 1997; Rash J. E. et al. 1998). There are three key location areas of AQP4 distribution in astrocytes: 1) in perivascular astrocyte endfeet, where it is involved in the blood-brain barrier function; 2) in perisynaptic astrocyte processes, where it helps with neurotransmitter clearance; 3) in the processes that are in contact with the nodes of Ranvier and nonmyelinated axons, where it is involved in clearance of K^+ (Zelenina M. 2010). Besides that, AQP4 expression has been reported in neural stem cells from the human and murine subventricular zone (Cavazzin C. et al. 2006). Moreover, high AQP4 expression is found in spinal cord gray matter in direct contact with neuronal cell bodies and synapses (Oshio K. et al. 2004; Vitellaro-Zuccarello L. et al. 2005). Studies using electron microscopy have also

confirmed that AQP4 is expressed in the microvascular endothelial cells (Amiry-Moghaddam M. et al. 2004). The lungs, skeletal muscles, stomach, inner ear and kidneys also contain AQP4 (Amiry-Moghaddam M. and Ottersen O. P. 2003). Additionally, a low, but significant AQP4 mRNA hybridization was reported in the neocortex, in the CA1-CA3 areas of the hippocampus, nucleus of stria terminalis, and medial habenular nucleus (Venero J. L. et al. 1999).

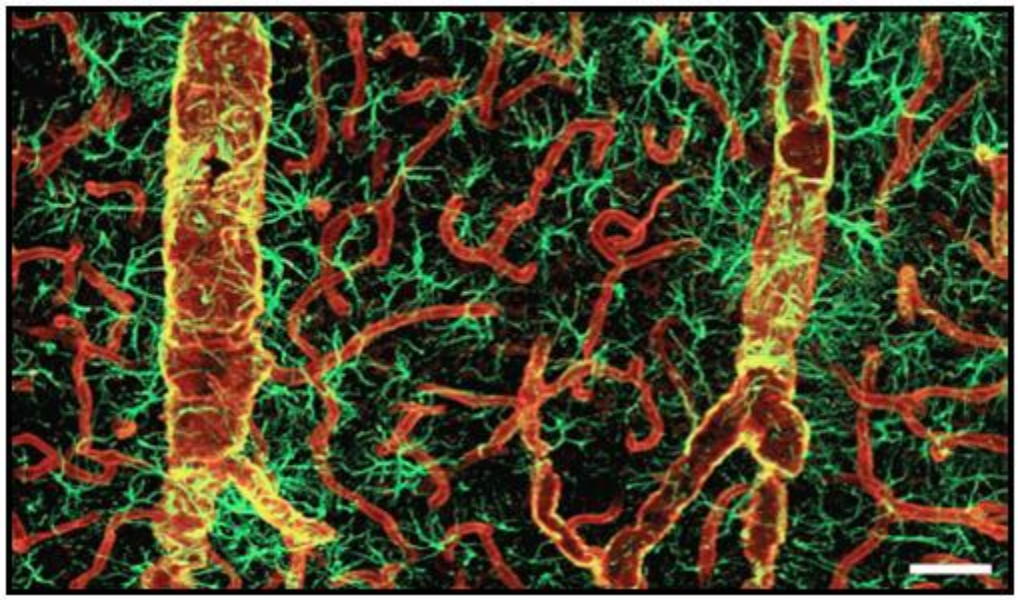

Fig. 8. Double immunolabeling of AQP4 (red) and GFAP (green). Aquaporin-4 immunolabeling reveals that the entire network of vessels, including capillaries, is covered by astrocytic processes, albeit GFAP negative. Smaller vessels and capillaries are mostly GFAP negative but display intense labeling against the astrocyte-specific channel AQP4. The AQP4 labeling reveals continuous coverage by astrocytic end feet. Scale bar: 60 μm (Simard M. et al. 2003).

1.3.2. Structure and functions of the AQP4 water channel

AQP4 channel was initially named mercurial-insensitive water channel (MIWC), and was cloned from the mouse lung. Another isoform of AQP4 with a longer N-terminus was later identified in the rat brain (Hasegawa H. et al. 1994; Jung J. S. et al. 1994; Manley G. T. et al. 2004). There are three known isoforms of AQP4 that differ by the length of their NH_2-termini (Hasegawa H. et al. 1994; Jung J. S. et al. 1994; Moe S. E. et al. 2008). M23 is the shortest (301 amino acids) brain AQP4 isoform (Neely J. D. et al. 1999). AQP4 M1 has an additional 22 amino acids and, finally, AQP4 Mz isoform has another 41 amino acids compared to

AQP4 M1 in its NH_2-terminus. This isoform has been found in rat, not human or mouse, at very low levels (Moe S. E. et al. 2008). AQP4 M23 isoform dominates in the brain (Neely J. D. et al. 1999), however, during ischemia, an expression of AQP4 M1 isoform is significantly increased (Hirt L. et al. 2009). Glial processes show highly polarized expression of AQP4, with a severalfold higher density of gold particles along the membrane domains facing capillaries and pia than along membranes facing the neuropil (Nielsen S. et al. 1997).

It has also been identified that AQP4 is a structural component of membrane "orthogonal arrays". Using freeze-fracture electron micrographs (FFEM) it has been shown that astrocyte foot processes membranes contain numerous arrays of intramembrane particles that are regular square arrays with a characteristic cobblestone pattern and are referred to as square arrays or orthogonal arrays of particles (OAPs) (Yang B. et al. 1996; Rash J. E. et al. 1998). Based on the finding that AQP4 is expressed in the same cells in which OAPs were identified, it was proposed that AQP4 is an OAP protein (Frigeri A. et al. 1995). The evidence of this theory came from FFEM studies of brain, kidney and skeletal muscle tissue from AQP4-deficient mice (Fig. 9). There were OAPs identified in every sample from AQP4 +/+ mice, while there was no sample from AQP4 -/- mice (Frigeri A. et al. 1995; Verbavatz J. M. et al. 1997; Manley G. T. et al. 2004). Later the same research group demonstrated that M23 and M1 isoforms have opposing effects on intramembrane organization of AQP4 and that the interaction of the M1 and M23 isoforms of AQP4 regulates OAP size (Furman C. S. et al. 2003). The biological role of OAP formation by AQP4 remains unknown, though it has been proposed that OAPs might facilitate AQP4 water transport, polarization to astrocyte foot processes, and cell-cell adhesion (Verkman A. S. et al. 2011).

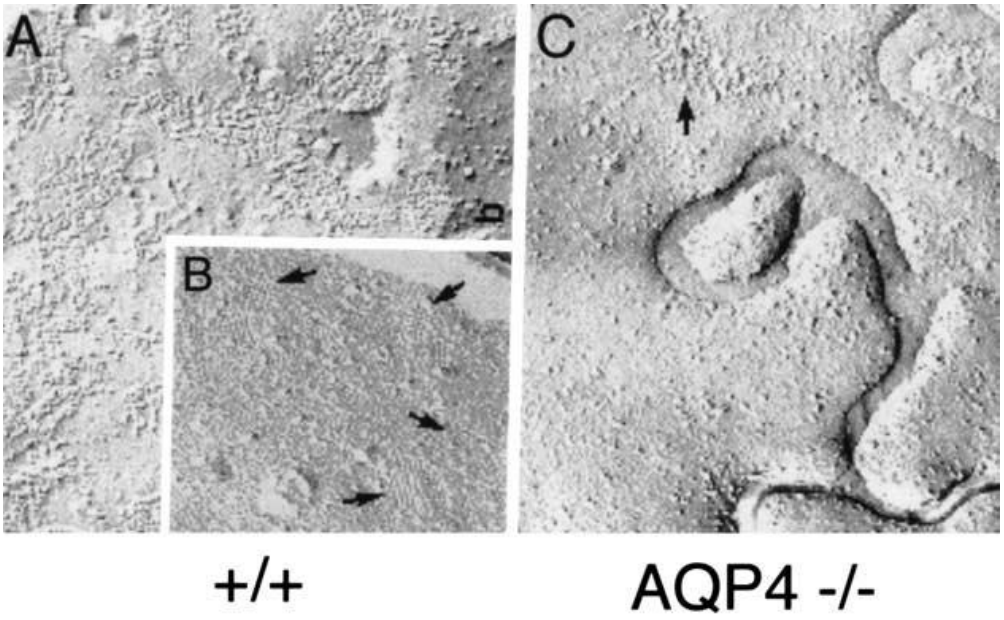

Fig. 9. Freeze-fracture electron micrographs of brains from wild-type (+/+) and AQP4-null (-/-) mice. (A) OAPs on Pf (protoplasmic)-face electron micrograph of brain from wild-type (+/+) mice. (B) Immunogold labeling of OAPs with anti-AQP4 (arrows). (C) Pf (protoplasmic)-face electron micrograph of brain from AQP4-null (-/-) mice demonstrating a lack of OAPs (Manley G. T. et al. 2004).

AQP4 expression in the brain is regulated during development. AQP4 appears between one and two weeks of postnatal development and then at four weeks reaches its adult level in the rat brain (Wen H. et al. 1999). In the cerebral cortex of the sheep, AQP4 mRNA and protein were detectable as early as at 60% of gestation, which then increased dramatically by 80% of gestation, and did not differ from adult levels by 90% of gestation (Ron N. P. et al. 2005). Expression of AQP4 in astrocytes is dependent on the cell cycle; it appears as though this protein is only expressed in the G0/G1 phase (Yoneda K. et al. 2001).

1.3.3. AQP4 protein-protein interactions

Neely and colleagues (Neely J. D. et al. 2001) have shown that the AQP4 water channel is tethered in perivascular astrocyte endfeet by the binding of the AQP4 C terminus to the *p*ostsynaptic density 95, *d*isc-large, *z*ona occludens 1 (or PDZ) domain of syntrophin, a component of the dystrophin-associated protein complex. Dystrophin is a part of a large membrane assembly connecting the cytoskeleton to the extracellular matrix. It was identified as the gene mutated in Duchenne/Becker muscular dystrophies (Neely J. D. et al. 2001).

Dystrophin bridges actin protein with the transmembrane protein β-dystroglycan, which is in turn associated with a laminin/agrin-binding protein, α-dystroglycan. Dystrophin binds to dystrobrevin on the cytoplasmic site of the complex, forming a scaffold for binding up to four syntrophin (syn) molecules (Peters M. F. et al. 1997; Newey S. E. et al. 2000). The syntrophin family includes five proteins (α, β_1, β_2, γ_1, γ_2) containing two pleckstrin homology domains (a principal substrate of protein kinase C), a PDZ domain and a C-terminal syntrophin-unique region (Kachinsky A. M. et al. 1999). The PDZ domain serves as an adaptor for recruiting membrane channels, receptors, kinases, and other signaling proteins. Variations in the dystrophin complex, which are tissue-specific, are in part caused by different syntrophins. The α-syntrophin isoform is expressed primarily in skeletal and cardiac muscle and at lower levels in the brain (Peters M. F. et al. 1997; Peters M. F. et al. 1997). Interaction between AQP4 and syntrophin was suggested to occur as a result of the interaction between a PDZ binding domain in the COOH-terminus of AQP4 molecule and a PDZ domain in syntrophin (Adams M. E. et al. 2001).

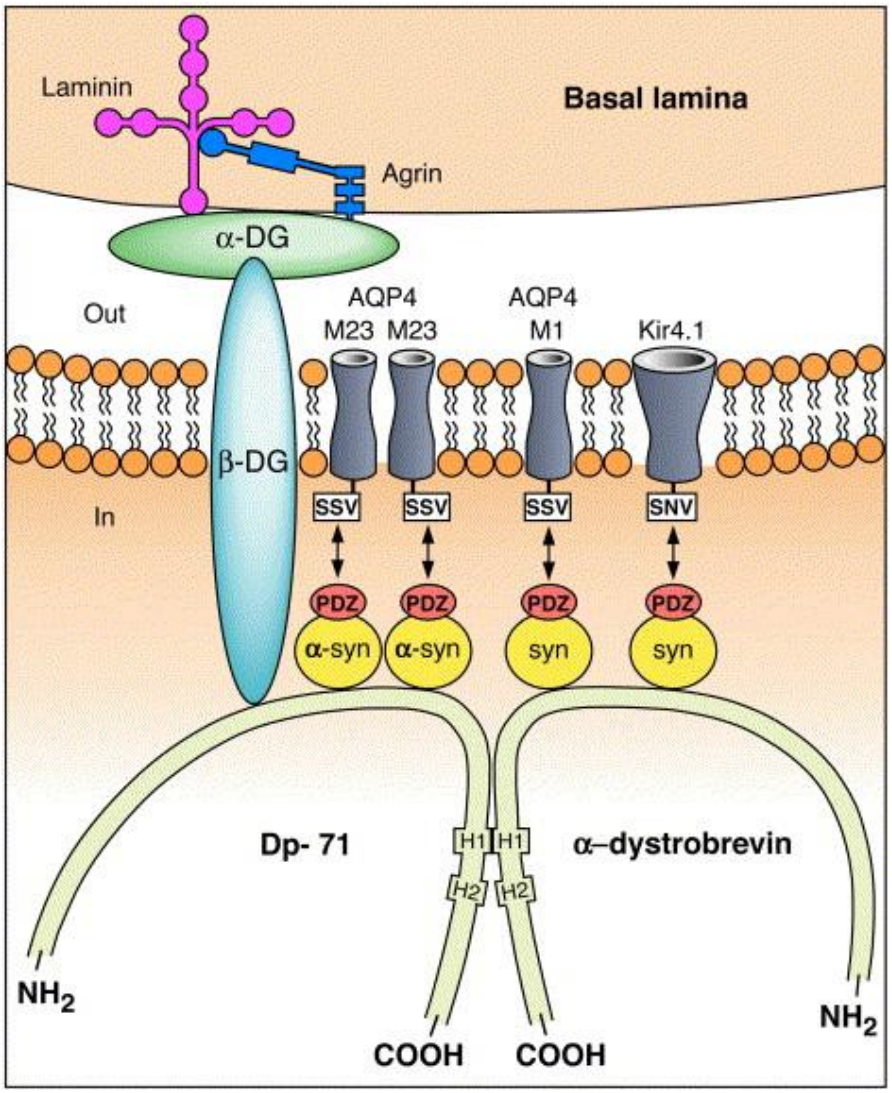

Fig. 10. Schematic picture of assumed molecular complex of AQP4 in perivascular and subpial membranes. The coupling between AQP4 and syntrophin may be indirect (indicated by double arrows). The PDZ binding domains of syntrophin are indicated. H1 indicates the coiled-coil motif interaction between Dp71 (the major dystrophin isoform in brain) and α-dystrobrevin. Used abbreviations: SSV (Ser-Ser-Val) for AQP4; SNV (Ser-Asn-Val) for Kir4.1, SXV-containing membrane molecules; α-DG and β-DG, α and β dystroglycan; Dp-71, dystrophin isoform 71; PDZ, postsynaptic density 95/zona occludens 1 (Amiry-Moghaddam M. et al. 2004).

Mice lacking α-syntrophin exhibit a marked reduction of AQP4 in perivascular and subpial membranes, but not in other locations in the brain, since total brain AQP4 protein content is not reduced (Neely J. D. et al. 2001).

Some studies reported association of AQP4 with Na^+, K^+-ATPase both in the cerebellum and kidneys (Illarionova N. B. et al. 2010). This association suggests an involvement in the clearance of extracellular K^+ and in neurotransmitter uptake by astrocytes. AQP4 has also been shown to interact with metabotropic glu^- receptor (mGluR) 5 that can play a role in the regulation of AQP4 by glu^-. It has been proposed that AQP4, Na^+, K^+-ATPase and mGluR 5 may form a protein complex in the plasma membrane of astrocytes, since the same region of AQP4 NH_2-terminus has been shown to be involved in association of AQP4 with both these proteins (Illarionova N. B. et al. 2010).

It has also been indicated that there is a cooperative action between AQP4 and Cx43, which occurs in the regulation of water and $[K^+]_e$ homeostasis. Cx43 is highly expressed in the process end-feet of astrocytes that are also enriched with AQP4 (Simard M. et al. 2003; Benfenati V. and Ferroni S. 2010). In mouse primary cultured astrocytes, AQP4 suppression by small interfering RNA (siRNA), induced the downregulation of Cx43 and alteration in astrocyte cell-to-cell coupling, thus, providing evidence of the AQP4 and Cx43 interaction (Benfenati V. and Ferroni S. 2010). The increase in $[K^+]_e$ observed as result of the high neuronal activity during ischemia augmented both the level of gap-junctional coupling and AQP4 expression (Ribeiro Mde C. et al. 2006). On the contrary, downregulation of AQP4, Cx43 and Kir4.1 was reported in a mouse model of hyperammonemia (Lichter-Konecki U. et al. 2008). AQP4-containing OAPs were detected near to Cx43-containing gap junctions (Rash J. E. and Yasumura T. 1999). AQP4 has also been proposed to interact with F-actin and to influence actin microfilament organization in astrocytes (Nicchia G. P. et al. 2005).

1.3.4. Interactions between Kir4.1 and AQP4 in astrocytes

Among the various Kir channels cloned so far at least five of these (Kir2.1, 2.2, 2.3, 4.1, 5.1) have been found in astrocytes. But various studies have demonstrated that Kir4.1 underlies the majority of the astrocytic Kir conductance. The weakly-rectifying nature of Kir4.1 drives bidirectional movement of K^+ in and out of the cell depending on the transmembrane K^+ gradient. In the brain, Kir4.1 is enriched at the endfeet of astrocytic

processes enwrapping synapses and facing blood vessels and pia matter or perivascular processes in Muller glial cells (Benfenati V. and Ferroni S. 2010).

The process of spatial redistribution of K^+ in the astroglial syncytium by Kir channels assumes that these channels are compartmentalized in astrocytes. Such a clustered pattern of expression suggests the presence of cellular microdomains, formed of plasma membrane proteins arranged in multi-molecular functional complexes. Kir4.1 was found to colocalize with syntrophin proteins and to form a macromolecular assembly with dystrophin 71 (Dp71), β–dystroglycan, α-dystroglycan and α-syntrophin, both in retinal Müller glial cells and astrocytes (Ishii M. et al. 1997; Guadagno E. and Moukhles H. 2004; Hibino H. et al. 2004; Noel G. et al. 2005; Connors N. C. and Kofuji P. 2006). α-syn was shown to be crucial for dystrophin-associated protein complex connection interaction with Kir4.1 in the brain and retina, depicting a critical role of scaffolding proteins in $[K^+]_e$ homeostasis (Connors N. C. et al. 2004; Connors N. C. and Kofuji P. 2006).

Confocal and immunogold electron microscopy showed that AQP4 is tightly co-localized with Kir4.1 in Muller cells and in astrocyte endfeet of the neocortex *in situ* (Nagelhus E. A. et al. 1999). Moreover, double immunoelectron microscopy indicated that AQP4 is colocalized with Kir4.1 on the cell membranes nearby to the vitreous body and blood vessels in the retina (Nagelhus E. A. et al. 1999). Based on these findings, Nagelhus and colleagues (Nagelhus E. A. et al. 1999; Nagelhus E. A. et al. 2004) proposed that AQP4 works as a molecular partner of inwardly rectifying K^+ channels in spatial buffering of K^+ by facilitating the water movement through the plasma membrane. It was suggested that this involvement of AQP4 in K^+ spatial buffering may also be responsible for the extracellular volume changes at the sites of neuronal activation (Agre P. et al. 2002).

Moreover, Nagelhus and colleagues (Nagelhus E. A. et al. 2004) proposed that there is a functional relationship between AQP4, Kir4.1, electrogenic Na^+-dependent bicarbonate transporter (NBC) and activity-dependent volume changes. They proposed that the buildup of K^+ causes a depolarization of the neighboring astrocyte membrane that helps an uptake of sodium and bicarbonate through NBC. This causes the increase of intracellular osmolarity and drives water into the glial cells through AQP4 that, in turn, leads to the astrocyte swelling and, thus, to the local shrinkage of the extracellular space (Sykova E. and Chvatal A. 2000).

1.3.5. Role of AQP4 in brain water balance

AQP1 and AQP4 water channels are mostly expressed at tissue-fluid interfaces, revealing a potential role in facilitating water flux between these compartments, and, thus, taking part in maintaining brain water balance. Studies done on the transgenic mice lacking AQP1 and AQP4 have helped to determine the role of these channels in the physiology of brain water homeostasis under normal and pathological conditions. Using a mouse model of obstructive hydrocephalus it was shown that AQP4-deficient mice have a faster course of ventricle enlargement and intracranial pressure elevation, compared to wild-type mice (Bloch O. et al. 2006).

Other studies describe the role of brain aquaporins in cerebral edema, an abnormal increase in brain water content due to a loss of water homeostasis. Two distinct forms of cerebral edema were classified by Igor Klatzo (Klatzo I. 1994) based on their pathogenesis:

1. In vasogenic (extracellular) edema, the blood-brain barrier is disrupted, permitting the entry of plasma fluid from the brain capillary to the extracellular space of the brain parenchyma. Vasogenic edema can be seen in experimental models of CNS inflammation, tumors (Davies D. C. 2002) and cold injury (Chan P. H. et al. 1991).
2. Cytotoxic (intracellular) brain edema is characterized by acute cellular swelling in the presence of an intact blood-brain barrier. This type of edema can occur during water intoxication and such anoxia-generating conditions as stroke, trauma and hypoxia (Kimelberg H. K. 1995).

It was shown that mice lacking AQP4 have reduced cerebral edema in response to water intoxication and stroke, with improved neurological deficit scores and better improvement in survival compared with the AQP4 +/+ mice (Manley G. T. et al. 2000).

It has been proposed that AQP4 channel modulates the function of nearby electrically excitable cells through the regulation of activity dependent volume changes of the extracellular space (Pellerin L. and Magistretti P. J. 2004). The expression of AQPs in the central nervous system is sensitive to different experimental manipulations, for example after brain injury or cell swelling. It was indicated that expression of AQP4 protein in astrocytes of rodents is upregulated in response to hyponatremia (Vajda Z. et al. 2000), after middle cerebral occlusion (Taniguchi M. et al. 2000) and in cerebral edema caused by brain injury (Ke C. et al. 2001). In primary astrocyte culture from AQP4-deficient mice, it was shown that they have a seven-fold reduced water permeability as compared with controls (Solenov E. et

al. 2004). In contrast, another group has demonstrated that wild-type mice have a nearly complete loss of perivascular AQP4 pool after ischemia reperfusion with no change in the number of perivascular population of α-syntrophin. It seems that the link between AQP4 and α-syn proteins is impaired after ischemia. Thus, it was proposed that other molecules play a role in the regulation of the link between these two molecules (Neely J. D. et al. 2001).

The possible role of AQP4 channels in water movement was proposed by Amiry-Moghaddam and co-authors (Amiry-Moghaddam M. et al. 2004). Normally (Fig.11A), siphoning of K^+ is associated with water uptake in astrocytes and subsequent water release through the perivascular and subpial membranes that are strongly enriched in AQP4 (activity dependent fluxes). Constitutive water fluxes are based on a net secretion of water from the capillary bed and a net production of water from the energy metabolism. The enrichment of AQP4 in endfeet and non-endfeet membranes at the cortical surface serves to facilitate the transport of water into the subarachnoidal space, which acts as a sink. The activity dependent efflux of water through perivascular endfeet is likely to join the constitutive flux of water (asterisk on Fig. 11), as osmotic gradients may not favor a net transendothelial water flux from brain to blood. After α-syntrophin knockout (Fig. 11B) the distinct swelling of perivascular and subpial endfeet may reflect a reduced capacity for water efflux through the endfeet membranes.

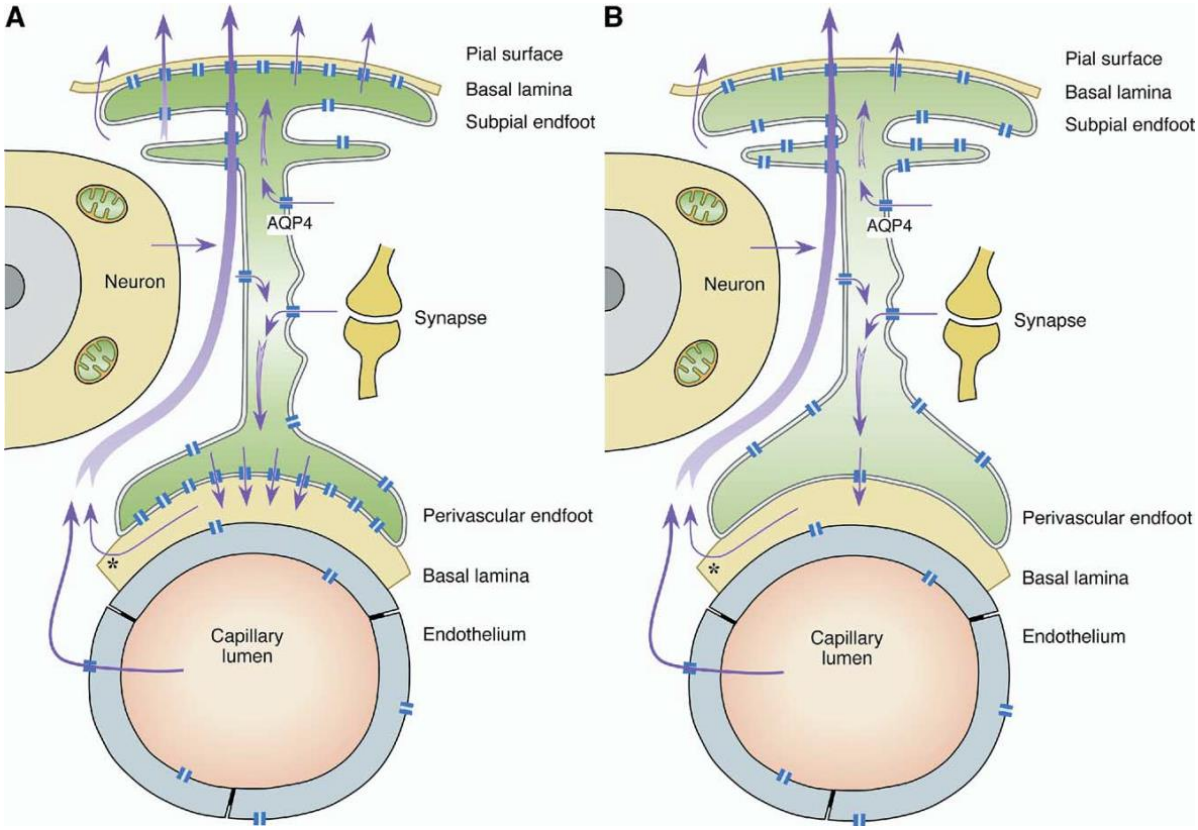

Fig. 11. Diagram showing the possible involvement of AQP4 in activity dependent and constitutive water flow in the neocortex of wild type (A) and α-syn -/- animals (B). Arrows show the putative direction of water flux (Amiry-Moghaddam M. et al. 2004). For detailes see text.

1.4. Cell volume regulation in astrocytes

Cell volume and cell water content are determined by the cellular content of osmotic active compounds and by the extracellular tonicity. The osmotic water permeability of animal cells is several orders of magnitude greater than the permeability to Na^+, K^+, and Cl^-. Cells maintain impermeable, polyvalent anionic macromolecules, and are continuously threatened by colloid osmotic cell swelling as diffusible ions and water are entering the cell (Hoffmann E. K. et al. 2009).

Astrocytes have the ability to sense changes in extracellular osmolarity and to regulate their cell volume in response to such changes. Moreover, astrocytes are in the strategic position to control homeostasis of ions and water through the movement of anorganic and organic molecules and the balance of osmotic gradients, as they are contacting neurons and cells that line the fluid-filled compartments. The astroglial endfeet uptake and secrete ions, organic molecules, and water at the neuron-astrocyte interface (Simard M. and Nedergaard M. 2004). The osmolality of the CNS extracellular fluid and the cell volume homeostasis are challenged all the time by the generation of local, transient osmotic microgradients of ions and molecules that are associated with physiological neuronal activity (Simard M. and Nedergaard M. 2004). Recent data obtained from rodents have shown that the accurate regulation of astroglia-mediated homeostasis tightly depends on the water channels and ion channels interactions and their anchoring with proteins forming macromolecular complexes that are able to mediate specific cellular processes (Benfenati V. and Ferroni S. 2010).

Maintenance of physiological neuronal activity is crucially dependant on the astroglial architecture that is functional to the homeostatic role of astrocytes (Fig 12). Neurotransmitters and ions are released in the perineuronal milieu, as a result of action potential firing. Astrocytes uptake the extracellularly accumulated potassium ions and glu^- in order to maintain their levels within the physiological range to allow further action potential generation. Glutamate uptake is carried through the astroglial Na^+/glu^- co-transporter (GLT-1) (in conjunction with GLAST co-transporter). The Kir4.1 is the main inwardly rectifying channel, which mediates the K^+ influx at perineuronal endfeet. The excess in intracellular K^+ is spatially redistributed via gap junctions through the syncytium toward areas where extracellular K^+ is low or directly into the interstitial space opposed to fluid-filled cavities (Müller glial cells). The transient osmotic gradient created upon K^+ uptake, is rapidly counteracted by water flux that is mediated by AQP4. Intracellular chloride concentration

($[Cl^-]_i$), which is controlled by transporters, is critical to set the condition for the passive KCl uptake when operative. The role of Cl^- channels of the ClC family that have been described in astroglia *in vitro* and *in situ* is still not fully elucidated. Volume-regulated anion channels (VRACs) have been identified *in vitro* and might contribute to cell volume homeostasis. The expression of the Ca^{2+} permeable channel named transient receptor potential vanilloid-related type 4 (TRPV4) has been reported both *in vivo* and *in vitro*, but its functional role is uncertain (Benfenati V. and Ferroni S. 2010).

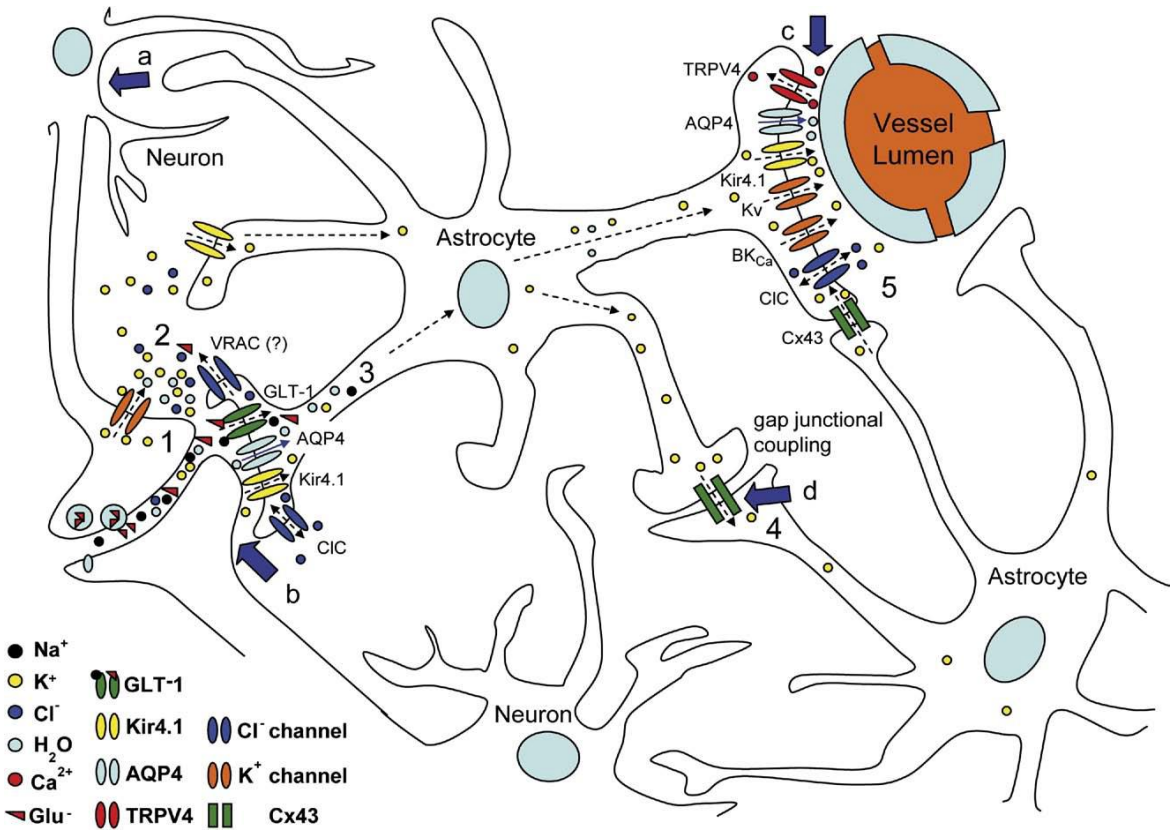

Fig. 12. Hypothetical astroglial channel-mediated mechanisms involved in extracellular homeostasis. (a) process endfeet that cover soma; **(b)** process endfeet, which enwrap synapses; **(c)** processes that take contact with the surface of the brain or about the blood vessels forming a perivascular sheet; **(d)** gap-junctions that allow synchronization of the responses in distal cells of the astroglial syncytium. **(1)** action potential firing; **(2)** release of ions and neurotransmitters; **(3)** uptake of K^+ and glu^- by astrocytes; **(4)** K^+ spatial buffering to sites with lower K^+ concentration; **(5)** K^+ spatial buffering directly into the interstitial space opposed to fluid-filled cavities (Müller glial cells). Used abbreviations: glu^- - glutamate; VRAC - Volume-Regulated Anion Channel; GLT-1 – glutamate transporter; AQP4 – aquaporin 4; Kir4.1 - inwardly rectifying potassium channels, type 4.1; CIC - chloride channel family; TRPV4 – transient receptor potential vanilloid-related, type 4; BK_{Ca} – calcium-activated big (conductance) potassium channels; Cx43 – connexin 43 (Benfenati V. and Ferroni S. 2010). For details see text.

Most cell types are able to counteract volume perturbations following a shift in extra- or intracellular osmolarity. Osmotically swollen cells release KCl, nonessential organic osmolytes, and cell water, thereby reducing the cell volume towards the original value, the process of regulatory volume decrease (Hoffmann E. K. et al. 2009). Ion channels responsible for cell volume regulation include the K^+ channels Kv1.3, Kv1.5, and KCNE1/KCNQ1 and the chloride channels CIC-2 and CIC-3 (Lang F. 2007).

A number of integral membrane proteins, such as integrins, growth factor receptors (GFRs), cytokine receptors, and calcium-sensing receptors, have been recognized as upstream sensors of cell volume perturbations. Moreover, members of several transient receptor potential (TRP) channel subfamilies have been demonstrated to be activated by osmotic stimuli and in some cases contribute to the following volume regulatory response (Hoffmann E. K. et al. 2009).

The ensuing process of RVD is based on the extrusion of intracellular solutes paralleled by obliged water efflux. VRAC, by permeating inorganic (Cl^-) and organic osmolytes such as taurine, and excitatory amino acids (EAA), has a critical role in RVD *in vitro* but its relevance *in vivo* is unclear (Benfenati V. and Ferroni S. 2010). TRP channels mediate an increase in $[Ca^{2+}]_i$ that further stimulates RVD by activating efflux of K^+ and Cl^- via Ca^{2+} activated K^+ and Cl^- channels. It was also demonstrated that the absence of TRPV4 or TRPM7, transient receptor potential cation channel, subfamily M, member 7, attenuates RVD (Hoffmann E. K. et al. 2009). A contribution of K^+ efflux is also likely but the specific volume-sensitive K^+ channels involved remain to be identified. The osmolyte extrusion creates the gradient for water efflux and promotes RVD to recover the initial volume. Various pumps and transporters also contribute to the transmembrane movement of ions (Fig. 13) (Benfenati V. and Ferroni S. 2010).

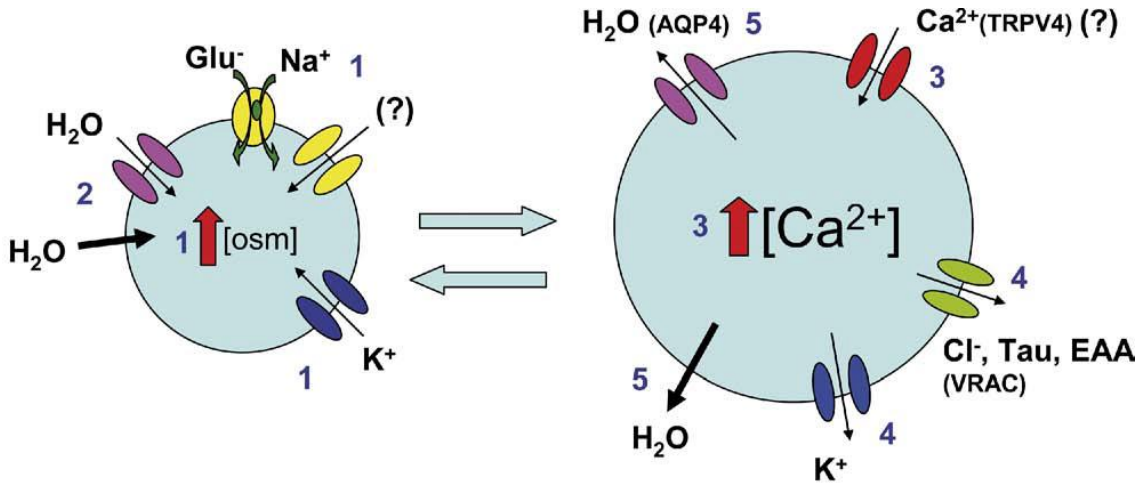

Fig. 13. Astroglial swelling and possible routes promoting cell volume recovery. Used abbreviations: Glu^- - glutamate; AQP4 – aquaporin 4; TRPV4 - transient receptor potential vanilloid-related, type 4; Tau – taurine; EAA – excitatory amino acids; VRAC - volume-regulated anion channel (Benfenati V. and Ferroni S. 2010).

Conversely, cellular loss of osmolytes or cell exposure to hypertonic medium leads to the exit of water according to the osmotic gradient. The result is cell shrinkage that leads to the activation of the Na^+-K^+-$2Cl^-$ cotransporters and/or the combined activation of the Na^+/H^+ exchanger in parallel to the Cl^-/HCO_3^- exchanger. The H^+ and the HCO_3^- extruded by the Na^+/H^+ exchanger and the Cl^-/HCO_3^- exchanger, respectively, are replenished in the cell from CO_2 via H_2CO_3. The net effect of those two carriers is NaCl entry. Na^+ accumulated by either Na^+-K^+-$2Cl^-$ cotransport or Na^+/H^+ exchange is extruded by the Na^+/K^+ ATPase in exchange for K^+. Therefore, the transporters eventually lead to the uptake of KCl. This ion uptake underlies mechanism of regulatory cell volume increase (RVI) (Lang F. 2007).

Under a lot of different pathophysiological conditions cell volume is challenged. For example, cell swelling occurs during:

1) hypoxia/ischemia;
2) status epilepticus;

3) hyponatremia, which occurs in situations where hormonal and renal function is impaired;
4) hypothermia, which inhibits the Na^+-K^+-ATPase;
5) increases in the extracelluar K^+ concentration;
6) intracellular acidosis/diabetic ketoacidosis.

Cell shrinkage occurs during:

1) hypernatremia, following excessive Na^+ intake or water loss;
2) reduced $[K^+]_e$;
3) hyperglycemia and alkalosis.

1.5. Ischemia

In medicine, ischemia is the restriction of blood supply that results in tissue damage. In practice, ischemia is accompanied with hypoxia that is the deprivation of adequate oxygen supply, or, in most serious cases with anoxia, which refers to the complete deprivation of oxygen supply. Ischemia in brain tissue, for example due to head injury or stroke, causes a process known as the ischemic cascade, in which harmful chemical substances, such as proteolytic enzymes, reactive oxygen species, etc, damage nervous tissue. Without the restoration of the blood supply, this process can lead to brain tissue death or cerebral infarction/ischemic stroke.

Two types of ischemia are distinguished: focal ischemia and global ischemia. Focal ischemia results from the interruption of the oxygen supply and glucose following a blockade of an artery. Global brain ischemia occurs when blood flow to the brain is halted or drastically reduced; commonly it is caused by cardiac arrest. Symptoms may be transient if sufficient circulation is restored within a short period of time. However, if a significant amount of time passes before restoration, brain damage may be permanent. Cerebral flow falls to zero within seconds, loss of consciousness occurs after approximately 10 s, electroencephalographic (EEG) activity ceases after 30-40 s, cellular damage is initiated after a few minutes, and death occurs within 10 min (Nedergaard M. and Dirnagl U. 2005). Further following early glial changes occur, preceding neuronal cell death: astrocytic cell swelling; rough endoplasmic reticulum proliferation; reactive astrogliosis; the thickening and retraction of astrocytic processes; and the interruption of oligodendrocytic processes (Hertz L. 2008).

Within seconds to minutes after the loss of blood flow to a region of the brain, the ischemic cascade is rapidly initiated. Ischemic cascade comprises a series of subsequent biochemical events that eventually result in cell membrane disintegration and neuronal death at the core of infarction. Ischemic stroke begins with severe focal hypoperfusion, that leads to excitotoxicity and oxidative damage which in turn cause microvascular injury, blood-brain barrier dysfunction and initiate post-ischemia inflammation. All these events intensify the initial injury and can lead to permanent brain damage (Fig. 14). The degree and duration of ischemia determines the extent of cerebral damage (Lakhan S. E. et al. 2009).

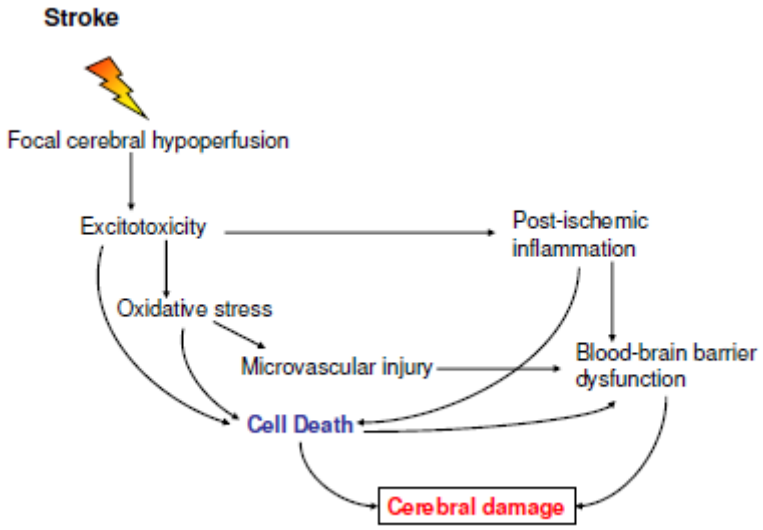

Fig. 14. Ischemic cascade leading to cerebral damage (Lakhan S. E. et al. 2009). For details see text.

As a result of residual perfusion from the collateral blood vessels, regions where blood flow drops to approximately 30 ml/100 g/min ischemic cascade progresses at a slower rate. Neuronal cells may tolerate this level of reduced (20-40% of control values) blood flow for several hours from the stroke onset with full recovery of function following restoration of blood flow (Lakhan S. E. et al. 2009).

1.5.1. Ischemic cascade

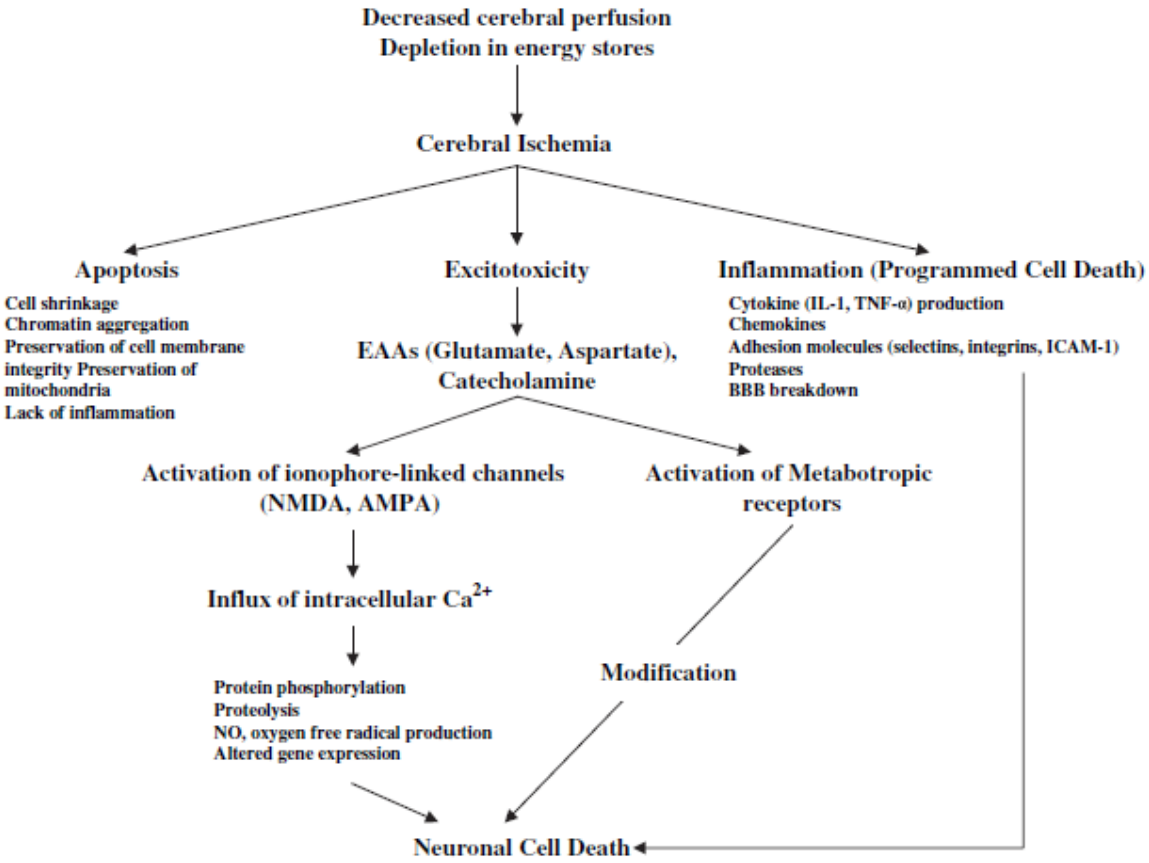

Fig. 15. Schematic diagram representing events leading to ischemic brain injury (Harukuni I. and Bhardwaj A. 2006).

The ischemic cascade includes the following biochemical and molecular events:

1. Lack of oxygen causes the neuron's normal production of making ATP for energy to fail. The brain's ATP supply is dependent on continuous perfusion and approaches zero within roughly 4 min of complete ischemia (White B. C. et al. 2000).

2. ATP-dependent ion transport pumps stop working leading to energy depletion that leads to depolarization. Breakdown of ion gradients blocks all subsequent exchanger systems or even reverts them, leading to uncontrolled deregulation of intracellular ion homeostasis (Kahlert S. and Reiser G. 2004).

3. During depolarization ions, including Ca^{2+}, flow into the cell. Since ion pumps can no longer transport Ca^{2+} out of the cell, resulting in an increase in $[Ca^{2+}]_i$. that affects

intracellular communication. A Ca^{2+} overload is generally linked to apoptotic or necrotic cell death. A possible pathway through which a high Ca^{2+} load is toxic for brain cells is the opening of the mitochondrial permeability transition pore (mPTP) and the release of cytochrome C. Such Ca^{2+} concentrations are possibly reached by increased mitochondrial Ca^{2+} loads leading to the generation of reactive oxygen species (ROS), which by themselves are releasing further Ca^{2+} from stores and therefore further raise the mitochondrial Ca^{2+} load (Kahlert S. and Reiser G. 2004).

4. The Na^+/K^+-ATPase activity is coupled to the intracellular Na^+ concentration. The block of Na^+/K^+-ATPase leads to a breakdown of the Na^+/K^+ gradient, which fuels the astrocytic glu^- uptake system. The Na^+ gradient is also involved in the maintenance of the Ca^{2+} gradient via Na^+/Ca^{2+}-exchanger (Kahlert S. and Reiser G. 2004). High $[Ca^{2+}]_i$ triggers the release of EAA neurotransmitters (glu^-, aspartate).

5. Glu^- activates three major families of ionophore-linked receptors (NMDA, AMPA, and kainate) and metabotropic receptors that activate second messenger systems. NMDA receptors are Ca^{2+}-permeable, thus their opening allows more Ca^{2+} into cell (Harukuni I. and Bhardwaj A. 2006).

6. Excess release of Ca^{2+} and its intracellular influx triggers the generation of harmful chemicals like free radicals, reactive oxygen species and Ca^{2+}-dependent enzymes such as calpain, endonucleases (leading to fragmentation of genomic deoxyribonucleic acid [DNA] and energy failure due to mitochondrial dysfunction), ATPases, and phospholipases (leading to cell membrane breakdown, arachidonic acid, and free radical formation) in a process known as excitotoxicity. Moreover, Ca^{2+} can also cause the release of more glu^- (Harukuni I. and Bhardwaj A. 2006).

7. After the cell membrane is broken down by phospholipases, it becomes more permeable, allowing more ions and harmful chemicals to flow into the cell.

8. Mitochondria break down, releasing toxins and apoptotic factors into the cell.

9. The caspase-dependent apoptosis cascade is initiated.

10. After the cell dies through necrosis, it releases glu^- and toxic chemicals into the environment around it. Toxins poison nearby neurons, and glu^- can overexcite them.

The ischemic cascade usually goes on for hours but can last for days, even after the restoration of blood circulation. Although reperfusion of ischemic brain tissue is critical for restoring normal function, it can paradoxically result in secondary damage, called ischemia/reperfusion injury. The definitive pathophysiology regarding reperfusion injury still remains obscure. However, oxidative stress mediators such as ROS, released by inflammatory cells around the reperfusion injured areas, are suggested to play an important role (Wong C. H. and Crack P. J. 2008). The increase in oxygen free radicals triggers the expression of a number of pro-inflammatory genes by inducing the synthesis of transcription factors, including nuclear factor kappa-light-chain-enhancer of activated B cells (NF-κB), hypoxia inducible factor 1, interferon regulator factor 1, and signal transducer and activator of transcription 3 (STAT3). As a result, cytokines are unregulated in the cerebral tissue and consequently, the expression of adhesion molecules on the endothelial cell surface is induced, including intercellular adhesion molecule 1 (ICAM-1), P-selectin and E-selectin which mediate adhesion of leukocytes to endothelia in the periphery of the infarct (Lakhan S. E. et al. 2009).

1.5.2. Effect of ischemia on brain diffusivity

Neuronal activity results in an increase in extracellular K^+ concentration, a decrease in extracellular calcium concentration ($[Ca^{2+}]_e$), and a rapid extracellular alkaline shift followed by a slower but longer-lasting acid shift. After adequate sustained stimulation of the afferent input or after repetitive electrical stimulation, the ionic transients reach a certain steady, the so-called "ceiling level". When stimulation is continued beyond this, a gradual decrease of both transients, $[K^+]_e$ and pH_e, occur after the ceiling levels are reached because of homeostatic mechanisms in neurons and glia. Transmembrane ionic fluxes are accompanied by the movement of water and cellular, particularly glial, swelling. Changes in ECS diffusion parameters are the consequence of activity-related transmembrane ionic shifts and cellular swelling (Sykova E. 1997).

The normal resting level for K^+ in the ECS is 2.7-3.5 mM, but it can reach up to 50-80 mM during ischemia. As energy deprivation will compromise neuronal function before glial function is affected, this will lead to the early failure of neuronal contributions to K^+

regulation. Thus, glial cell K^+ uptake plays a very important role under ischemic conditions (Leis J. A. et al. 2005).

In 1994, Enkvist and McCarthy proposed that through the concomitant increase in gap junctional conductance that results from K^+-induced membrane depolarization, K^+ could facilitate its own spatial buffering by increasing inter-astrocytic communication. Membrane depolarization has been observed to open gap junction hemichannels (Hofer A. and Dermietzel R. 1998), whereas experiments with mouse spinal cord astrocytes have suggested the involvement of a calmodulin kinase pathway (De Pina-Benabou M. H. et al. 2001).

As it has been shown in the rat cortex and corpus callosum, changes in ECS diffusion parameters have several phases during ischemia (Vorisek I. and Sykova E. 1997; Xie Y. et al. 1995; Walz W. et al. 1993):

I phase: no statistically significant change in ECS volume and geometry is seen. Energy depletion is low and the anaerobic metabolism is maintained by Na^+/K^+ pump. During this phase, there is Ca^{2+}-dependent K^+ rise in the ECS of 1-2 mM, which also corresponded to an initial small acid shift. Extracellular sodium concentration ($[Na^+]_e$) and $[Ca^{2+}]_e$ still maintained their normal levels.

II phase: energy is further depleted, leading to a block of the Na^+/K^+ pump, release of K^+ from neurons, entry of Na^+ into neurons, increase in cytosolic Ca^{2+}, glu^- and aspartate release. $[K^+]_e$ is elevated by 6-12 mM and pH_e shows slow acid shift of 0.1-0.2 pH units. The tortuosity increases and the ECS volume decreases by 10-15%.

III phase: complete loss of ionic homeostasis: $[K^+]_e$ is elevated by 50-70 mM, $[Na^+]_e$ and $[Ca^{2+}]_e$ rapidly decrease. pH_e decreases by ~0.5-0.6 pH units. Glial cells are depolarized, which results in the opening of Cl^- and HCO_3^- channels that, in turn, leads to passive K^+, Cl^-, and HCO_3^- fluxes into glial cells. ECS volume decreases rapidly and dramatically, while tortuosity increases.

IV phase: swelling is not accompanied by further $[K^+]_e$, $[Na^+]_e$, or $[Ca^{2+}]_e$ changes. However, there is an additional acid shift in pH_e by 0.3-0.5 mM units.

The transmembrane ionic shifts during ischemia/anoxia are accompanied by the corresponding redistribution of water, in order to maintain the same osmolality inside and outside cells. Resulting cell swelling is compensated by ECS shrinkage, so that the total brain tissue volume remains constant (Sykova E. 1983). Astrocyte swelling is believed to be mostly responsible for the extracellular space volume decrease that is observed under ischemic conditions (Nakane M. et al. 2001; Sykova E. 2005). Additionally, a group of authors, using 1H magnetic resonance spectroscopy/magnetic resonance imaging (MRS/MRI) and 31P

MRS, demonstrated a decrease of the *ADC* of tissue water (ADC_W) after the induction of global ischemia of which the time course correlated with the time course of the decrease in the ECS volume fraction and the increase in ECS tortuosity (van der Toorn A. et al. 1996). After reperfusion, ECS volume fraction and ADC_W rapidly returns to its physiological size (Dijkhuizen R. M. et al. 1998; Zoremba N. et al. 2008). This phenomenon was also demonstrated in the CA1 region of hippocampus, where ADC_W values obtained 6 hours after transient global ischemia induction were comparable to control values. In the early phases of reperfusion (1 to 3 days), neuronal cell death and developing gliosis were accompanied by the increase of ADC_W and tortuosity. Surprisingly, ECS volume fraction significantly decreased only during the first day after ischemia. In the late phases of reperfusion (starting from 1 month after ischemia) when the CA1 region consisted mainly of glial cells with altered morphology, all ADC_W, ECS volume fraction, and tortuosity were increased (Anderova M. et al. 2011).

Initial diffusion weighted magnetic resonance imaging (DW-MRI) studies on animal models of cerebral ischemia showed a rapid decrease ADC_W, of up to 40%, after the onset of ischemia (Benveniste H. et al. 1992; Knight R. A. et al. 1991; Moonen C. T. et al. 1991). During persistent ischemia, values of ADC_W remained decreased for about 18-24 hours and then began to return to normal (Helpern J. A. et al. 1993; Knight R. A. et al. 1991). Increased ADC_W above its normal levels after prolonged ischemia is associated with tissue necrosis (Helpern J. A. et al. 1993).

1.6. Status epilepticus

Epilepsy is a common chronic neurological disorder characterized by the periodic and unpredictable occurrence of seizures. Epilepsy affects 1% to 3% of the population, and about 10% of the population will have one or more seizures during their life span. Seizures are time-limited paroxysmal events that result from abnormal, involuntary, rhythmic neuronal discharges in the brain. Epilepsy syndromes are defined by many factors, such as the type of seizures, family history of seizures, age at the onset of seizures, findings at physical examination, EEG, and neurologic imaging studies. Epilepsy syndromes fall into two main categories: generalized and partial (localization-related) syndromes. In generalized epilepsies, seizures begin simultaneously in both cerebral hemispheres. In contrast, in partial epilepsies,

seizures originate in one or more localized foci, although they can spread to involve the entire brain. Partial epilepsies are usually believed to be as result of one or more CNS insults (Chang B. S. and Lowenstein D. H. 2003).

Seizures are either unprovoked (spontaneous) or provoked. Spontaneous seizures occur in persistent brain disease that is epilepsy. Provoked seizures are trigged by certain factors in the healthy brain, for example, by acute metabolic processes, acute neurologic insult, drugs, and excessive physiological conditions (Shneker B. F. and Fountain N. B. 2003). There is often a delay from the time of the specific insult (febrile seizures, status epilepticus, hypoxic-ischaemic injury or head injury) to the occurrence of seizures (sometimes more than 20 years). The risk of developing epilepsy remains for more than 10 years after a serious head injury. Immediate seizures within the first week after an insult have a better prognosis than later seizures (Walker M. C. et al. 2002).

Status epilepticus (SE) is one of the most serious neurologic problems worldwide in which the brain is in a state of persistent seizure. It is defined due to the international classification as a seizure that lasts for more than 30 minutes or as recurrent seizures without regaining consciousness between seizures for more than 30 minutes. SE occurs when seizures fail to stop, and is a life-threatening medical emergency. In contrast to SE, epilepsy is any disorder in which the main symptom is the spontaneous recurrence of unprovoked seizures.

Each generalized or partial complex SE has short and long lasting negative affects on brain functions. They trigger the mechanisms of secondary brain damage that may lead to cell death. Irreversible changes appear only a few minutes after any type of SE. At least two mechanisms, common with those during ischemia, are involved in neuronal death during SE:

1) Excitotoxic cascade activation:
    - Elevated calcium levels due to modifications in excitatory amino acids;
    - Activation of nitric oxide synthase;
    - Oxidative stress and production of oxygen free radicals.
2) Induction of apoptosis.

The use of *in vitro* models on brain slices made a significant breakthrough in the pathophysiology research of SE. Hippocampal brain slices are often used, which are washed out using solutions with modified ion composition, for example, with high Ca^{2+} concentration (Jefferys J. G. and Haas H. L. 1982; Taylor C. P. and Dudek F. E. 1982), with no Mg^{2+} (Anderson W. W. et al. 1986) or with elevated K^{+} concentrations (Traynelis S. F. and Dingledine R. 1989). Other models that are used to study the epileptic neuronal activity

include the use of K^+ channel blockers, such as 4-aminopyridine on bulbus olfactory brain slices (Galvan M. et al. 1982), or the use of GABA antagonists on hippocampus slices accompanied with elevated K^+ concentration (Hablitz J. J. 1987; Swann J. W. and Brady R. J. 1984).

1.6.1. Dysfunction of astrocytes in epilepsy

Since astrocytes modulate neuronal communication and are involved in the control of brain network activities, it may be suggested that astrocytes have the potential to be involved in the development of a number of brain disorders, including Alzheimer's disease, Parkinson disease and epilepsy. Astrocytes exhibit significant morphological and functional changes in the development of various brain disorders. This condition is known as reactive gliosis and is characterized by hypertrophy and hyperproliferetion of astrocytes, altered morphology with hypertrophic soma and processes, spatial overlapping and different functional changes of astrocytes, and increased expression of GFAP (Vijayan V. K. et al. 1990; Kalman M. and Ajtai B. M. 2000; Nolte C. et al. 2001; Eclancher F. et al. 1990), vimentin and S100β (Perillan P. R. et al. 1999; Perillan P. R. et al. 2000). Reactive gliosis is common in the human epileptic brain and is observed in temporal lobe epilepsy (TLE), post-traumatic and infection-induced epilepsy. In pilocarpine- and the kainate-induced animal models of epilepsy, gliosis is observed early, during the period that precedes recurrent seizure onset (Losi G. et al. 2012). TLE is the most common form of epilepsy with a focal onset in temporal structures such as the hippocampus, entorhial cortex, and amygdala. The most prevalent pathology found in patients with TLE is hippocampal sclerosis; more generally known as mesial temporal sclerosis. This state is characterized by neural cell loss in specific hippocampal areas, gliosis, microvascular proliferation, and synaptic reorganization (Blumcke I. et al. 1999).

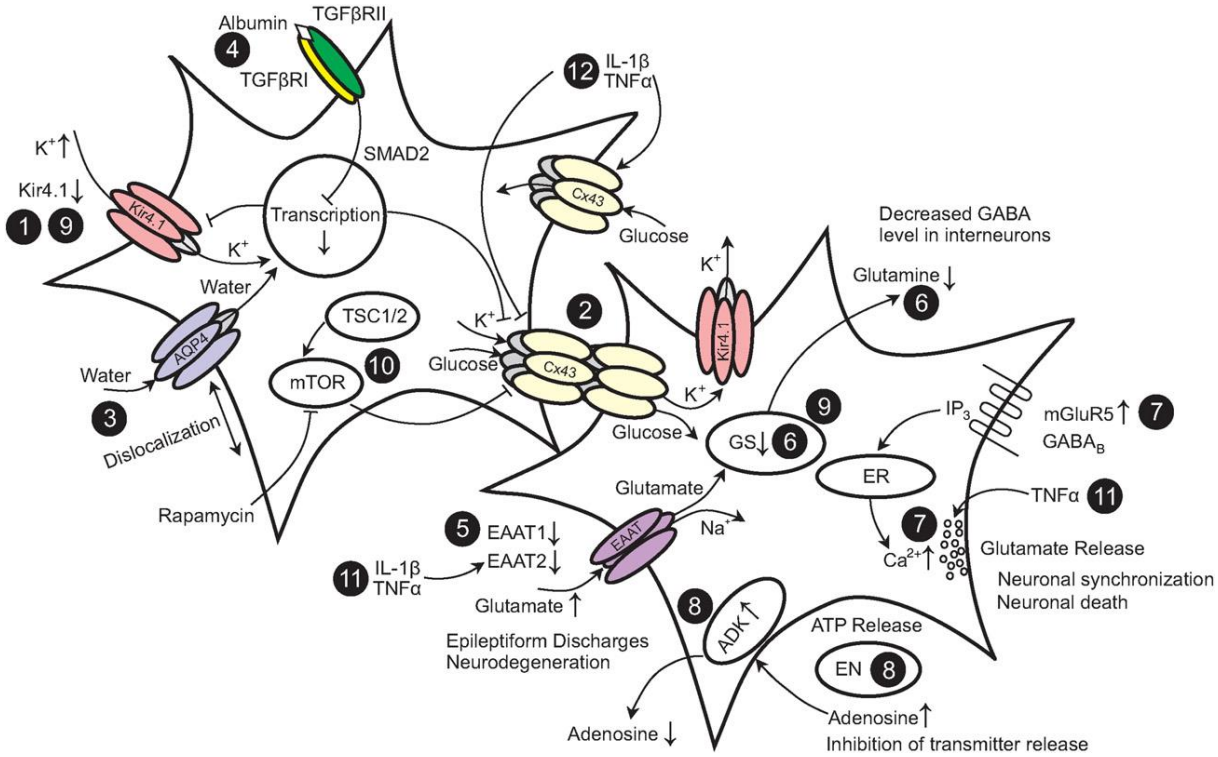

Fig. 16. Epilepsy-associated alterations of functional properties in astrocytes: (1) increase in extracellular potassium concentration; (2) genetic ablation of gap junctions; (3) aquaporin 4 (AQP4) dislocation; (4) disruption of blood-brain barrier (BBB); (5) elevated extracellular glu$^-$; (6) decreased level of glutamine synthetase (GS); (7) elevated astrocytic Ca^{2+} mediated by metabotropic receptors; (8) upregulation of the astrocytic enzyme adenosine kinase (ADK) and decreased ambient adenosine concentration; (9) decreased levels of inwardly rectifying potassium channel Kir4.1 and glutamine synthetase protein (epilepsy patients with tuberous sclerosis [TS]); (10) deletion of tuberous sclerosis protein 1 (TSC1) in astrocytes leads to downregulation of connexin 43 (Cx43) and impaired K^+ buffering; (11) interleukin-1 beta (IL-1β) and tumor necrosis factor alpha (TNFα) inhibit glu$^-$ uptake and increase glial glu$^-$ release. Used abbreviations: EN – endonucleotidases; TGFβRI (II) – transforming growth factor beta receptor I (II); mTOR – mammalian target of rapamycin; TSC1/2 – tuberous sclerosis complex; EAAT – excitatory amino-acid transporters; GABA – γ-Aminobutyric acid; ER – endoplasmic reticulum; ATP – adenosine triphosphate; mGluR5 – metabotropic glu$^-$ receptor 5; SMAD2 – mothers against decapentaplegic homolog 2 (Seifert G. et al. 2010). For details see text.

The following epilepsy-associated alterations of functional properties in astrocytes can be distinguished (Fig. 16; numbers on the picture correspond to the numbers in the text):

1) Increase in $[K^+]_e$: since even small increases in $[K^+]_e$ significantly increases neuronal network activity, it was hypothesized that increased $[K^+]_e$ is a causal factor for epileptiform activity. Moreover, seizure activity itself leads to a significant $[K^+]_e$ increase of up to 10-12 mM. Additionally, downregulation of Kir channels was observed in astrocytes in human and experimental epilepsy (Losi G. et al. 2012).
2) Genetic ablation of gap junctions entails impaired K^+ buffering and hyperactivity: normally, gap junctions mediate spatial redistribution of K^+. Cx43 and Cx30 are the main connexins that form gap junctions in astrocytes, and, thus, their deletion in mice led to a decreased threshold for evoking seizure activity and to the generation of spontaneous epileptiform activity (Pannasch U. et al. 2011).
3) Dislocation of AQP water channels contributes to impaired K^+ buffering.
4) Blood–brain barrier disruption, albumin intake, and activation of transforming growth factor beta (TGFβ) receptors lead to the downregulation of Cx43, Cx30 and Kir4.1 transcripts and impaired K^+ buffering.
5) Elevated extracellular glu^-. It is well-known that astrocytes are primarily responsible for glu^- uptake. Reduction of EAAT1 and EAAT2 was observed in human epileptic hippocampus, indicating that elevated extracellular glu^- decreases the threshold for seizure induction.
6) Decreased level of glutamine synthetase (GS): GS converts glu^- into glutamine. In a human epileptic hippocampus, loss of GS resulted in elevated extracellular glu^- levels. Moreover, downregulation of GS was observed in experimental epilepsy in the chronic phase.
7) Elevated Ca^{2+} in astrocytes that is mediated by metabotropic receptors: enhanced mGluR5 levels are observed in experimental and human epileptic tissue.
8) In experimental epilepsy, seizure induction results in the upregulation of the astrocytic enzyme adenosine kinase (ADK) and decreased ambient adenosine concentration, while genetic reduction of ADK prevents seizures. Ambient adenosine levels are controlled by ATP release, endonucleotidases and the activity of ADK.
9) Astrocytes from epilepsy patients presenting with tuberous sclerosis display decreased levels of Kir4.1 and GS protein.
10) Deletion of tuberous sclerosis protein 1 in astrocytes results in the downregulation of Cx43 and impaired K^+ buffering.

11) The inflammatory cytokines interleukin-1 beta (IL-1β) and TNFα inhibit glu^- uptake and increase glial glu^- release, which produces hyperactivity.
12) IL-1β and TNFα inhibit Cx43-mediated gap junction communication, but increase activity of Cx43 hemichannels. This might represent an alternative pathway for glucose entry under pathological condition (Seifert G. et al. 2010).

According to a classical paradigm epileptiform activities may arise from a brain network that becomes hyperexcitable as a result of an imbalance in glutamatergic and inhibitory GABAergic transmission. GABAergic transmission may favor epileptic activity by synchronizing large neuronal populations and even depolarize, at least under certain conditions, the neuronal membrane thereby enhancing neuronal excitability (Losi G. et al. 2012).

Astrocytes are an extrasynaptic source of glu^- that then triggers synchronized activities in groups of neurons from different brain regions. Paired patch-clamp recording experiments from two pyramidal neurons showed that the release of glu^- from astrocytes in response to Ca^{2+} elevations evoked by different agents or direct mechanical stimulations, induced in both neurons NMDA receptor-mediated slow inward currents (SICs) that could occur with a high level of synchrony. Experiments performed both *in vivo* and on brain slices showed that during epileptiform activity, the frequency of Ca^{2+} oscillations in astrocytes is significantly increased, while it is reduced by anticonvulsant drugs (Losi G. et al. 2012).

High extracellular glu^- levels have been reported in human epileptic tissue (Cavus I. et al. 2005). It has been hypothesised that an increased glutamatergic transmission may be an early event that contributes to the generation of epilepsy. However, controversial results have been reported in studies investigating the EAAT levels from the tissue of TLE patients (Eid T. et al. 2008). The potential of the astrocytic EAAT family to participate in seizure generation was also demonstrated in a transgenic mouse line, in which a deletion of EATT2 in astrocytes resulted in epileptiform activities (Tanaka K. et al. 1997). Additionally, reduced glu^- and K^+ clearance capacity was reported in an animal model of focal epilepsy induced by a BBB disruption that mimics post-traumatic epilepsy (David Y. et al. 2009). Moreover, glu^- released from rodent astrocytes during SE contributes to neuronal death (Ding S. et al. 2007) that supports the hypothesis that increased excitability in the neuron-astrocyte network favors neuronal synchronization.

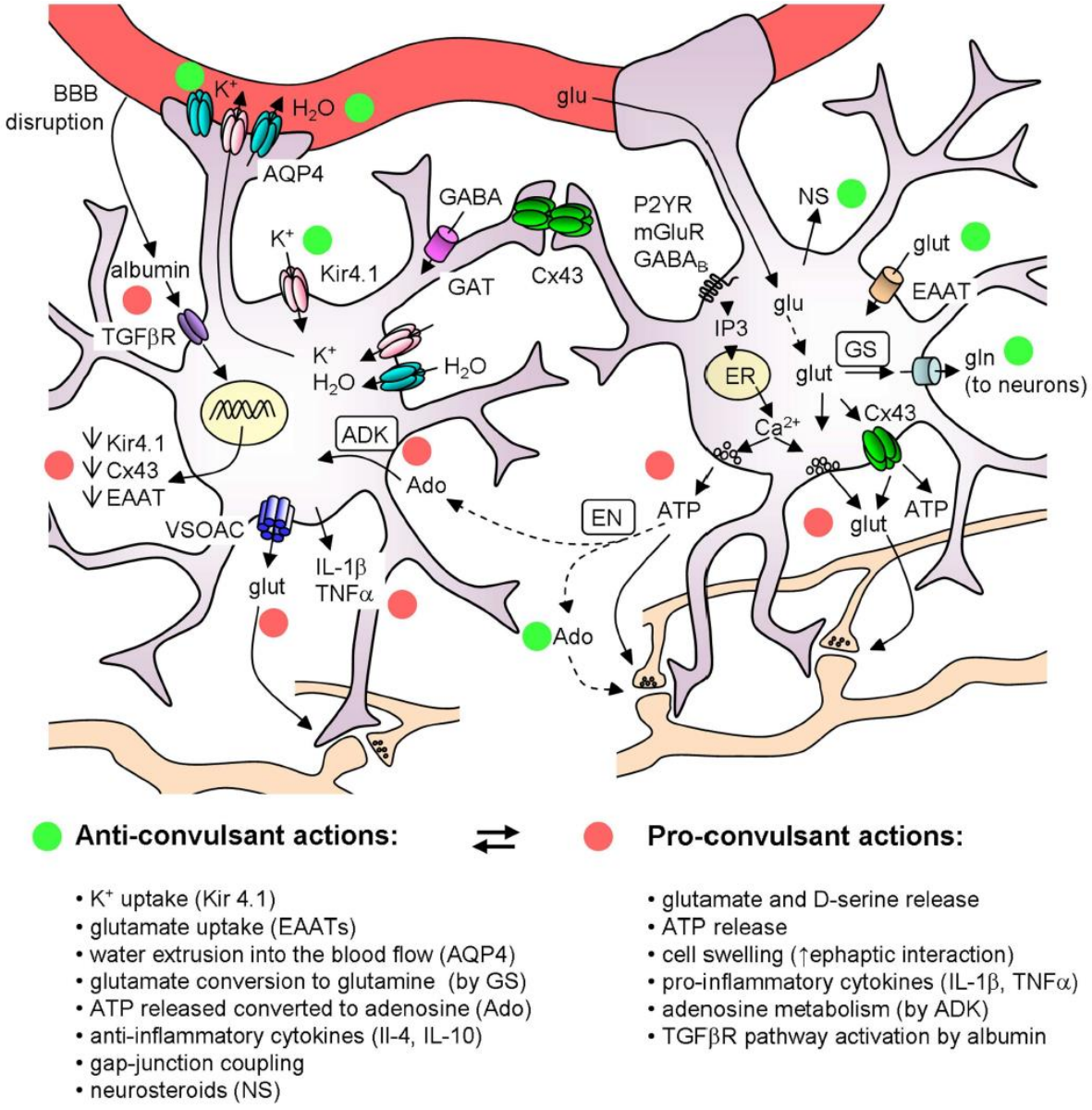

Fig. 17. Schematic of the main astrocyte actions that can affect epileptiform activities. The colored circles mark the anticonvulsant (green) and the proconvulsant (red) actions of astrocytes. Note that (i) ATP can have *per se* a proconvulsant action, but after its conversion to Ado it is anticonvulsant; (ii) astrocytic cytokines can have either pro- or anti-inflammatory actions. Used abbreviations: ADK – adenosine kinase; Ado – adenosine; AQP4 – aquaporin 4; BBB – blood brain barrier; Cx43 – connexin 43; EAAT – excitatory amino acid transporters; EN – ectonucleotidase; ER – endoplasmatic reticulum; GAT – GABA transporters; glu – glucose; glut – glutamate; gln – glutamine; GS – glutamine syntethase; NS – neurosteroids; VSOACs – volume-sensitive organic anion channels; TP – adenosine triphosphate; GABA - γ-Aminobutyric acid; TGFβR – transforming growth factor beta receptor; mGluR – metabotropic glutamate receptor; IL-1β – interleukin-1 beta; P2YR - purinergic receptor; TNFα – tumor necrosis factor alpha; Il-4 – interleukin 4; IL-10 – interleukin-10; IL-1β – interleukin-1 beta (Losi G. et al. 2012).

1.6.2. Astrocytic swelling during epilepsy

Astrocyte swelling leads to a reduction of the extracellular space that enhances network excitability and favors epileptiform discharges. Brain excitability is very sensitive to osmolarity and the size of the ECS. Decreased ECS volume contributes to the hyperexcitability and enhanced epileptiform activity, while increased volume of ECS resulting from hyperosmolar medium application attenuates epileptiform activity (Kilb W. et al. 2006). Such experimental data correlates with extensive clinical experience indicating that hypo-osmolar states, such as hyponatremia, lower seizure threshold while hyperosmolar states elevate seizure threshold (Binder D. K. and Steinhauser C. 2006). Astrocyte swelling can also result in an increased release of gliotransmitters, such as glu^-, via VSOACs that further enchances network excitability (Losi G. et al. 2012).

Water influx in astrocytes is mediated by AQP4 channels. It has been shown that AQP4-deficient mice have slower K^+ influx and prolonged seizures. Decreased expression of AQP4 channels has also been observed in the kainic acid model of epileptogenesis in wild-type mice. An altered distribution of AQP4 may thus reduce the transfer of water from astrocytes into blood vessels. This would lead to astrocyte swelling, reduced clearance of extracellular K^+ and glu^-, an increase in glu^- release, and through volume-sensitive anion channels that all together will facilitate cell swelling. Hypo-osmotic stress also triggers Ca^{2+} increase in astrocytes and this response depends on AQP4 and P2Y receptors (Losi G. et al. 2012).

Binder and colleagues have studied seizure susceptibility of AQP4-/- mice using the convulsant $GABA_A$ antagonist pentylenetetrazol (PTZ). At 40 mg/kg i.p. administration of PTZ, all wild-type mice exhibited seizure activity, whereas AQP4 -/- mice did not. At 50 mg/kg PTZ, both groups were exhibiting seizure activity; however, the latency to generalized (tonic-clonic) seizures was longer in AQP4 -/- mice. Since a disposition to seizure is very sensitive to the change in the ECS volume (Schwartzkroin P. A. et al. 1998), the expanded ECS in AQP4 -/- is consistent with the increased seizure threshold (Binder D. K. et al. 2004; Binder D. K. et al. 2012). AQP4 -/- mice were also found to have remarkably prolonged stimulation-evoked seizures compared to wild-type animals (Binder D. K. et al. 2004).

Alteration in the expression and subcellular localization of AQP4 has been described in sclerotic hippocampi obtained from patients with mesial temporal sclerosis. Using immunohistochemistry, reverse transcription polymerase chain reaction (rt-PCR), and gene

chip analysis, an overall increase in AQP4 expression in sclerotic hippocampi was demonstrated (Lee T. S. et al. 2004). However, using quantitative immunogold electron microscopy, the same group found that there was mislocalization of AQP4 in the human epileptic hippocampus, with a reduction in perivascular membrane expression. It was hypothesized that the loss of perivascular AQP4 perturbs water flux, impairs K^+ buffering, and results in an increased propensity for seizures (Eid T. et al. 2005; Binder D. K. and Steinhauser C. 2006).

Moreover, it was shown that AQP4 -/- mice have substantially slower K^+ reuptake in models of seizure and spreading depression *in vivo*, which is associated with a near-threefold increase in seizure duration (Binder D. K. et al. 2006; Binder D. K. and Steinhauser C. 2006). It was also demonstrated in hippocampal slices from human patients with TLE, where even submillimolar increases in $[K^+]_e$ strongly enhance epileptiform activity (Feng Z. and Durand D. M. 2006; Gabriel S. et al. 2004; Binder D. K. et al. 2012).

2. AIMS OF THE STUDY

The primary goal of the following studies was to monitor the changes in the ECS diffusion parameters in acute cell swelling and assess the role of AQP4 water in the development of cytotoxic edema. To reach this goal, the following experimental models of acute cell swelling were used: pilocarpine-induced status epilepticus, terminal ischemia/anoxia, as well as hypotonic and hyperkalemic stress.

The specific aims of the experiments included:

1) Determination of the changes in the ECS diffusion parameters and ADC_W *in vivo*:
   - During pilocarpine-induced status epilepticus;
   - During terminal ischemia/anoxia evoked by cardiac arrest.
2) In the model of status epilepticus:
   - Elucidation of changes in local field potentials and extracellular K^+ concentration;
   - Establishment of the real changes in extracellular concentration of brain metabolites (lactate, pyruvate, glucose and glutamate) in relation to altered ECS volume fraction.
3) Investigation of the role of α-syntrophin protein in the ECS diffusion parameters changes during acute cell swelling in experimental models *in vivo* as well as *in vitro* using genetically modified mice.

3. METHODS

3.1. Ion-selective microelectrodes

The ion-selective microelectrode (ISM) is a very important tool for dynamic measurement of the activity of given ions in tissue, usually on a real time basis.

Ion-selective microelectrodes are miniaturized transducers, or sensors that convert the activity of specific ions dissolved in a solution into an electrical potential, which can be measured by a voltmeter. The main component of the ISMs is an electrochemical membrane that separates two solutions of different ionic concentration and is, ideally, selectively permeable to a single ion. Ions move from the area of a high concentration to that of a low concentration of the ion of interest, carrying its charge with it. Aligning the potential difference on both sides of the membrane stops the flow of ions and creates a state of equilibrium. The size of the potential (E), established using the ISM, is described by the Nernst equation:

$$E = E_o + s \log a_i \qquad [1],$$

where E_o is the reference potential in millivolts, s is the Nernst response ("slope"), and a_i is the activity of the reference ion. Nernst response at 25°C is defined as:

$$s = 2{,}303\, RT / z_i F = 59{,}16/z_i \qquad [2],$$

where R is the gas constant (8.314 $JK^{-1}mol^{-1}$), T is the absolute temperature [K], F is the Faraday electrochemical equivalent (9.6487 x 10^4 $Cmol^{-1}$) and z_i is the charge of the ion. However, in practice we must also reckon with the ISM interference with other ions and, therefore, the ISM potential is better reflected by the Nikolsky equation:

$$E = E_o + s \log [a_i + \sum_{kij}{}^{pot} (a_j)^{zi/zj}] \qquad [3],$$

where a_j is the activity of the interfering ion, zj is the charge it carries, and $\sum_{kij}{}^{pot}$ is the coefficient of potentiometric selectivity. In practice, concentration is commonly used instead

of activity. In that case, ISM potential in the solution of two interfering ions is described by a simplified form of the Nikolsky equation:

$$E_1 - E_2 = s \log(C_1 + k)/(C_2 + k) \quad [4],$$

where E_1 and E_2 are the potentials of the electrodes at different concentrations (C_1 and C_2) of the measured ion and k is the interference. In practice, the problem of the interference is solved by adding the interfering ions to the calibration solutions.

Modern ISMs that are used in neurophysiology, are two-channel microelectrodes (double-barreled ISMs), where one channel is the reference and the second is served as the ion-selective electrode. When ISM is introduced into a tissue or calibrating solution where ionic activity is to be measured, a Nernst potential develops across the ion-exchanger membrane. However, in the neural tissue the microelecrode also picks up other biopotentials (action or synaptic potentials) that may corrupt the measurement of ion activity changes (Syková E. 1992). This effect is abolished if the reference electrode is very close to the tip of the ISM, or, better, in its immediate vicinity, as it is achieved in the double-barrelled microelectrodes. In our measurements we used two-channel electrodes, where one channel is filled with a NaCl solution, or other indifferent solution, and serves as the reference channel. The ion-selective channel of the electrode consists basically of a liquid ion-exchange membrane in the tip of a glass micropipette, the main component of which is an ionophore (carrier, ion-carrying agent, ion-bearer). The rest of the channel is back-filled with a solution of known ionic composition. Non-wanted electrical potentials that both channels register can be then subtracted from the potential that is measured by the ISM and, thus, register the activity of the given ion only.

The neutral carriers are able to transport selected ions from the sample solution, across the membrane to another aqueous solution. Liquid membranes in ISM consist of:

- The neutral carrier for the selected ion;
- The membrane solvent, for example nitrobenzene;
- The membrane matrix (polymer), for example polyvinyl chloride (PVC);
- Other membrane additives.

Liquid membranes are commercially available (Fluka Chemical Corp.) for a lot of different ions (e.g. Ca^{2+}, K^+, H^+, Na^+, Mg^{2+}, Li^+) as complete “cocktails”.

For measurement of the TMA^+ ion concentration original K^+ ion-exchanger Corning 477317 (Rochester, NY) is used.

3.1.1. Preparation of the double-barrelled ion-selective microelectrodes

In our laboratory we produced ISM from glass borosilicate tubings (Ruckl and sons, Otvovice) 2.5 mm in diameter, and 11 cm and 5.5 cm long, which melts at relatively low temperatures. Two glass tubes with different length were fixed together with a polythene ring. After heating the middle of the tubing above a small Bunsen burner tubes were twisted through 360˚ and pulled approximately 3 mm apart (Syková E. et al. 1981). On the vertical microelectrode puller (Narishige, Japan) two double-barreled microelectrodes were pulled. Tensile strength of the magnet and the intensity of glowing platinum spiral determine the shape and length of the electrode tip.

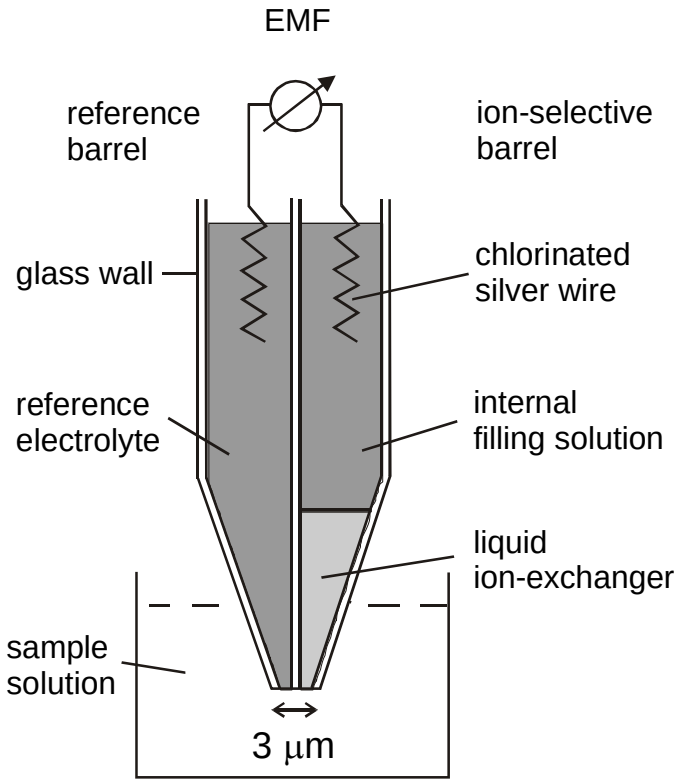

Fig. 18. **Schematic cross-section of a double-barreled ion-selective microelectrode.** The hole in the tip of the electrode for extracellular measurements is 2-4 μm. The reference channel is filled with a reference electrolyte, usually NaCl. The ion-selective channel has the liquid ion exchanger in its tip; the rest of the channel is back-filled with a solution containing the reference ion. Both channels are connected to the amplifier with silver chlorinated wires (Syková E. 1992). Used abbreviations: EMF – electromotive force.

3.1.2. Silanization of the electrodes

The glass surface is highly hydrophilic and, therefore, repels organic liquids, such as ion exchanger. By applying a thin layer of silane to the tip of inner surface of the ion-selective channel, the tip of the ISM becomes hydrophobic and better "holds" the ion exchanger. Generally, two methods of silanization are distinguished:

1) Immersion of the ISM tip into the solution containing a reactive silicone compound (such as chlorosilane, amino silane, siloxane), which is dissolved in an organic solvent (such as carbon tetrachloride or xylene).
2) Silanization by vapors, when the electrode is exposed to vapors of the silicone compound (e.g., dimethylaminotrimethylsilane) in a closed chamber at high temperature (Syková E. 1992). This method is usually used for the silanization of electrodes for intracellular measurements.

We used the first method for silanization of ISM in this work. Before silanization, the reference channel of ISM was filled with a small amount of distilled water that filled the tip by capillarity and protected it from silane entering. The ISM was then dipped into silane and a column of about 200-500 μm was drawn up only into the ion-selective barrel. We used tributylchlorosilane diluted in 1-chloronaphatalene (1:6; Fluka). The electrodes with silane were heated to 150-200˚C for 1 hour in an oven to evaporate water and silicon solution from the barrels. Silane joined with covalent bond to free hydroxyl groups in glass and created hydrophobic surface in the tip of ion-exchanger channel making them ready for filling.

3.1.3. Filling of the electrodes

In this work we used the method of front filling of the electrodes (Syková E. 1992). At first, the tip of the electrode was broken at 2-3 μm under the microscope. The reference channel was back-filled with a solution of 150 mM NaCl and then dipped into the ion-exchanger (Corning 477317) for 10-60 s. An ion-selective channel of the TMA^+-ISM was then back-filled with 100 mM of TMACl solution above the ion-exchanger. For K^+-ion-selective microelectrodes, which were used for the measurement of changes in extracellular K^+ concentration, the ion-selective channel was back-filled with 150 mM KCl. Air bubbles

that appeared between the ion-exchanger and solution were removed under the microscope by electrokauter and rat (cat) whiskers.

For diffusion measurements, the iontophoresis pipette was prepared, and its shank was bent before back-filling it with 150 mM TMACl, so that the shank aligned parallel to that of the ISM. Electrode arrays were made by gluing together an iontophoresis pipette and an ISM with a tip separation of 90-160 μm (Fig. 19).

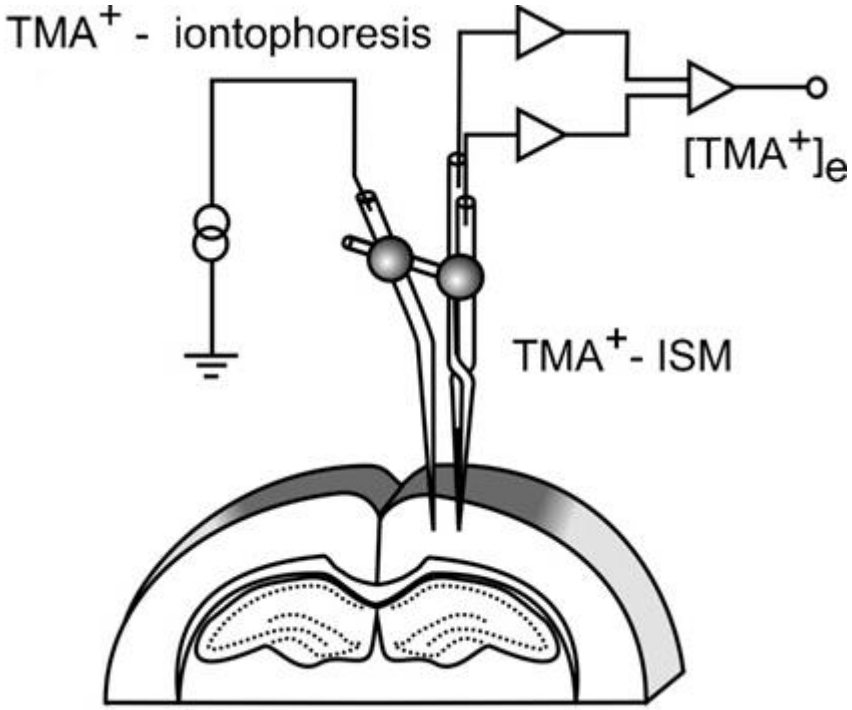

Fig. 19. Experimental setup of RTI method. A TMA^+-selective double-barreled ion-selective microelectrode was glued to a bent iontophoresis microelectrode with a known inter-tip distance, and this array was introduced into the tissue (Sykova E. et al. 1998).

3.1.4. Electrical connection of the ion-selective microelectrodes

Reference and ion-selective channels of ISM were connected by silver chlorinated wires (Ag-AgCl) with a low-noise differential amplifier, with input impedance of 10^{14} Ω and compensation of capacitance by negative feedback (Ujec E. 1988). Typical iontophoresis parameters involved a +20 nA bias current that was continuously applied to maintain a

constant transport number, with a +100 nA current step of 24 s duration to generate the diffusion curve. The TMA^+ diffusion curve was then captured on a digital oscilloscope and transferred to PC, where it was analyzed by non-linear curve fitting algorhythm (see chapter 3.2). The changes in potentials were recorded by the acquisition program Lab-Trax (WPI).

3.1.5. Calibration of the ion-selective microelectrodes

TMA^+-ISM was calibrated in solutions of 0.25, 0.5, 1, 2, 4, 8 and 16 mM of TMA^+ with respective background of NaCl to keep the ionic strength of the solution constant (Kriz N. et al. 1974). TMA^+ concentration versus time curves were first recorded in 0.3% agar gel made up in 147 mM NaCl, 3 mM KCl and 0.5 mM TMA^+.

K^+-ISMs were calibrated in a sequence of solutions containing 0.5, 1, 2, 3, 4, 6, 8, 12, 16, 24, 32, 48, 64, 96 and 128 mmol/L KCl, with a background of either 149.5, 149, 148, 147, 146, 144, 142, 138, 134, 126, 118, 102, 86, 54, or 22 mmol/L NaCl to keep the ionic strength of the solution constant (Kriz N. et al. 1974).

The data were fitted to the Nikolsky equation to determine the electrode slope and interference. Based on these electrode characteristics, the measured voltage was converted to extracellular concentrations. Potential change of the electrodes was recorded on a two-channel recorder TZ 4200 and on the PC by Lab-Trax.

3.2. Measurement of the ECS diffusion parameters

3.2.1. Diffusion parameters of the extracellular space

The structure of the nervous tissue can be presented as foam, where the gaseous phase represents the cells and ECS corresponds to the water phase. Within the ECS, the main mechanism of molecular transport is diffusion that is constrained by the labyrinthine nature of the ECS. Diffusive motion of molecules in a free water medium is describe by Fick's laws, which reflect the macroscopic Brownian motion of molecules. This movement is a result of short straight movements of diffusing molecules in random directions and their collisions with molecules of the solvent. If in the system a dissolved substance solvent concentration gradient

∇C exists, then the microscopic flow of diffusing molecules J in the direction of the concentration gradient is presented as a vector, for which the following equation applies:

$$J = -D \nabla C \quad [5]$$

This equation describes Fick's first law, where D is the diffusion coefficient of the diffusing substance in water, C is its concentration, and ∇C is the gradient operator. However, ECS is a complex medium and its geometrical structure with a size of intercellular pore makes the inevitable barriers for free diffusion. Moreover, diffusion can be limited by possible interactions with macromolecules in the cell membranes, which bear an electrical charge on their surface, or by the uptake of diffusing substances into the cells or capillaries. Diffusion in the brain may, therefore, be described after the introduction of the parameters of extracellular volume fraction α and tortuosity λ into the diffusion equations for diffusion in porous media. Extracellular volume fraction α is defined as:

$$\alpha = V_{ECS}/V_{Tissue} \quad [6],$$

where V_{ECS} is volume of the ECS and V_{Tissue} is a total tissue volume. In a "free" medium (aqueous solution or very dilute gel) $\alpha = 1$.

The presence of various obstacles prolongs the diffusion path of the molecule in the complex medium comparing to the free medium (water or a dilute agar). Therefore, the apparent diffusion coefficient ADC for a given substance in a complex medium is smaller than the diffusion coefficient D in the free medium. This extension of the diffusion path expresses tortuosity factor λ, which is defined as:

$$\lambda = (D/ADC)^{1/2} \quad [7]$$

Taking all this into account, the equation [5] for a homogeneous isotropic porous medium would be modified (Nicholson C. and Phillips J. M. 1981):

$$J = -\alpha ADC \nabla C \quad [8],$$

where C is the concentration of the substance in the ECS measured by the ion-selective microelectrode. J and C are the average values in the entire tissue sample.

Another modification, the introduction of the third diffusion parameter that represents the non-specific cellular uptake k', expresses the loss of diffusing molecules from the ECS into cells or capillaries, resulting in a modified form of the second Fick's law (Nicholson C. and Phillips J. M. 1981):

$$\partial C / \partial t = (D / \lambda^2)\ \nabla^2 C + (Q / \alpha) - k'C \qquad [9],$$

where t is time, and Q is the flow of substance diffusing from the source.

If the diffusing molecule is injected into the tissue by iontophoresis, with a duration of S, changes in the molecule concentration in time are presented by a diffusion curve with rising and falling phases. The following is applied for the rising phase of the curve:

$$C = \mathrm{G}(t) \qquad t<S$$

And for the falling phase of the curve:

$$C = \mathrm{G}(t) - \mathrm{G}(t - S) \qquad t>S,$$

where C is the concentration of the ion at the time t and distance r.

Using mathematical modifications of the first and second Fick's equations we get the diffusion curve function $G(u)$, where $u = t$ or $t - S$ for rising, or falling phase of the curve:

$$\mathrm{G}(u) = (Q\lambda^2 / 8\pi D\alpha r)\ \{\exp\ [r\lambda(k' / D)^{1/2}]\ \mathrm{erfc}\ [r\lambda / 2(Du)^{1/2} + (k'u)^{1/2}] + \exp\ [- r\lambda(k' / D)^{1/2}]\ \mathrm{erfc}\ [r\lambda / 2(Du)^{1/2} - (k'u)^{1/2}]\} \qquad [10]$$

The quantity of TMA^+ that is delivered to the tissue per second is $Q = In/zF$, where I is the step increase in current applied to the iontophoresis electrode, n is the transport number, z is the number of charges associated with the substance iontophoresed (+1 for TMA^+), and F is Faraday`s electrochemical equivalent. The function “erfc” is the complementary error function. During calibration in agar, by definition, $\alpha = 1 = \lambda$ and $k' = 0$, the values of n and D

are extracted by the curve fitting. Knowing n and D, parameters α, λ, and k' can be obtained when the experiment is repeated in the neural tissue.

3.2.2. The real-time iontophoretic method (RTI) using TMA^+-ion-selective microelectrodes

Method for measurement of diffusion parameters was originally developed by Nicholson and Phillips (Nicholson C. and Phillips J. M. 1981). The method of direct diffusion measurement is based on the introduction of ions into the tissue by pressure or iontophoresis and measurement of their concentration distribution in space and time using ion-selective microelectrodes. The ion that is applied should fulfill the following conditions:

- cell membranes should be relatively impermeable for this ion and the ion should stay in the ECS;
- it should be relatively small to freely diffuse in the extracellular space;
- there must be a detection tool for it, for example an ISM.

TMA^+ and tetraetylamonium (TEA^+) fulfill these requirements. Ion-exchanger for K^+ (Corning 477317) is highly sensitive to TMA^+ and TEA^+ ions. These ions in low (micromolar) concentrations are not toxic and do not cross cell membrane, and are therefore good candidates for monitoring dynamic changes in the ECS (Lehmenkuhler A. et al. 1993; Nicholson C. and Phillips J. M. 1981; Sykova E. and Chvatal A. 1993). In our measurements we used TMA^+-ISM. The TMA^+ ions were administered by a current passing into the ECS through an iontophoretic micropipette. TMA^+-ISM records changes in ion concentration at an appropriate distance (90-160 μm). This way, absolute values, as well as their changes, can be calculated from the recorded diffusion curves by fitting them to the modified diffusion equation [10].

3.3. Diffusion-weighted magnetic resonance imaging

3.3.1. Basic principles of the magnetic resonance imaging

MRI is a medical imaging technique that is used to visualize detailed internal structures. This method uses quantum-mechanical properties of nuclei with odd nucleus numbers, which have their own magnetic moment and can interact with an external magnetic field. The practical significance on magnetic resonance have nuclei that are abundant in the measured tissues, which must also provide sufficient response to the excitation electromagnetic signal, such as ^{1}H, ^{13}C, ^{19}F, ^{31}P. The hydrogen nucleus is the most important in terms of the use of MRI in biology and medicine. It has the greatest sensitivity of all other nuclei and is present in most biologically important compounds, including water that has two hydrogen nuclei or protons.

Magnetic moments of individual nuclei are randomly oriented in space and after inserting the sample into the external magnetic field, the average magnetic moment of many protons becomes aligned with the direction of this field. The state of nuclei that are oriented in the direction of the magnetic field have lower energy then the state with an opposite orientation of the magnetic moment, thus more nuclei will appear in this state (at 37˚C for protons in the magnetic field with intensity 1 T the ratio of energy levels is about 1 000 007 : 1 000 000). Even this small difference results in the formation of macroscopic magnetic moment of sample magnetization in the direction of external magnetic field.

This electromagnetic field has a frequency, resonance frequency, which is absorbed and flips the spin of the protons in the magnetic field. After the sample is removed from the electromagnetic field, the spins of the protons return to thermodynamic equilibrium and the bulk magnetization becomes re-aligned with the static magnetic field. During this relaxation, a radio frequency signal is generated, which can be measured with receiver coils.

Held in a magnetic field the magnetic moments of individual nuclei make periodic tilted motion called precession. The frequency (ω_0) of this movement depends on the type of nuclei and field strength (B_0). This relationship is called the Larmor equation:

$$\omega = \gamma \cdot B_0$$

ω is the Larmor frequency;

γ is the gyromagnetic ratio, which describes the ratio of mechanic and magnetic properties of the nucleus and depends on the type of nucleus;
B_0 is the strength of the magnetic field.

The constant γ is the gyromagnetic ratio that gives the precession frequency of the nuclei in a field intensity of 1 T. In the resting conditions, moments of the precession movement of individual nuclei cancel out, and thus, the precession causes no external magnetic moment. This occurs after the tissue is exposed to the electromagnetic waves of the same frequency as the precession. The magnetic moments of individual nuclei begin to rotate in phase, leading to formation of macroscopic magnetic moment in the direction that is perpendicular to that of external magnetic field. Yet this process is temporary and expires due to the spin-to-spin interaction with neighboring nuclei leading to the energy emission in the form of electromagnetic waves, which can be captured by the receiver placed near the sample. When the sample is exposed to electromagnetic waves, the nuclei switch to a higher energy state (with a magnetic moment oriented anti-parallel to the direction of the magnetic field). Depending on the amount of supplied energy on the sample, it may result in the disappearance of the longitudinal macroscopic magnetic moment (the transverse component may still be present) or to its reverse against the direction of the external magnetic field. The electromagnetic pulse that causes the above process is referred to as a 90-degree or 180-degree pulse. The longitudinal component of the magnetic moment returns to the equilibrium state due to spin-lattice interaction. The time taken for a sample to reach equilibrium state, dependends on both of these interactions as, when used in imaging techniques based on magnetic resonance imaging, their influence is different in various tissues. The process of returning to the equilibrium state from an excited state is called the spin-lattice relaxation process or longitudinal relaxation process, a time constant known as T_1. It is named in contrast to T_2, the spin-spin relaxation time.

For practical measurements on MR devices the so-called pulse sequence is used, a sequence of pulses of electromagnetic waves with a concomitant magnetic field gradient. The most common is the spin-echo sequence, which is schematically illustrated in Fig. 20. It begins with a 90-degree pulse to excite a measurable response. Due to magnetic field inhomogeneities, the signal decreases more rapidly than it would do with the relaxing time T_2, this time thus corresponds to the T_2* time constant. The local magnetic field around the nucleus is partially shielded by the electron cover influenced by the type of chemical bonds. It means that the individual nuclei have a slightly different resonant frequency, which results in

a faster spin focusing. In particular time τ after the first pulse followed by a 180-degree pulse, which not only turns the longitudinal magnetization vector, but also moves slower spins before faster that will cause in time τ rephasing of all nuclei spins. Spin phasing gives rise to another measurable signal (echo). This way spins could be phased several times using the 180-degree pulse. Every other echo is smaller and their size decreases with a time constant T_2. Time from the first pulse to echo generation is called echo-time (TE). The whole measurement is repeated many times, the time between measurements is denoted by TR. Typical TE values are 10 to 100 ms and for TR1 - 10 s.

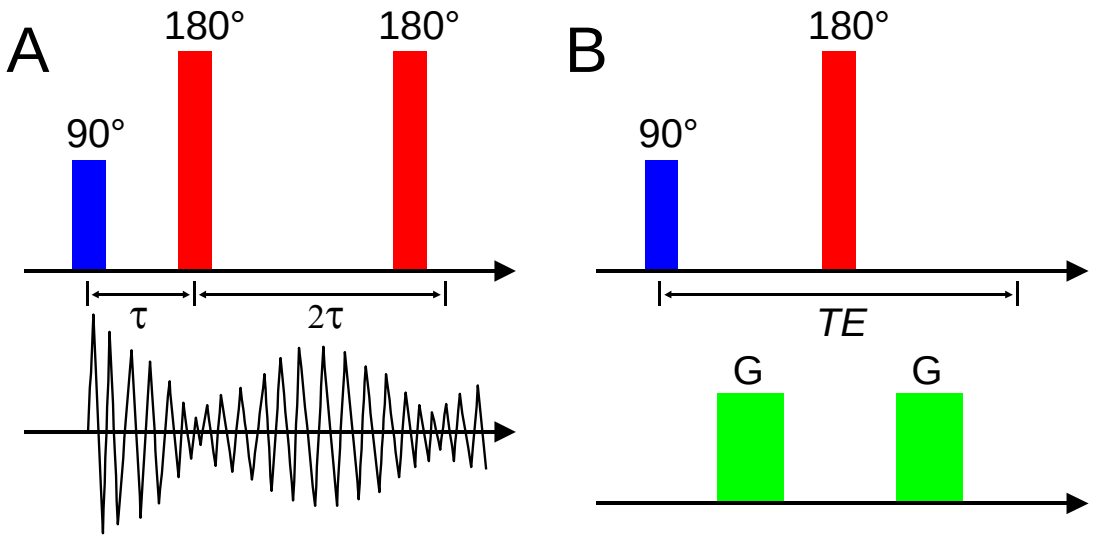

Fig. 20. Spin echo sequence (A) and diffusion-weighted sequence (B). Spin echo sequence could be sensitized to random movements of water molecules (diffusion) by adding two pulses of gradient magnetic field.

For imaging use it is necessary to distinguish the direction of the signal. This can be done with a weak magnetic field gradient. If the gradient is applied during the whole measurement, points with different values of magnetic field intensity can be distinguished on the basis of different resonant frequencies (frequency coding). The second method is known as phase encoding, where a gradient is applied only at the beginning of the measurement that leads to a shift of phase precession and other ways to distinguish different spatial regions.

To improve the quality of measured images, the measurements are usually repeated several times and then the received signals are averaged. The number of repetitions is marked

as NA. Signal / noise ratio improves with the square root of the number of repetitions. When NA = 4, we can expect twice the improvement in the quality of images.

3.3.2. Measurement of the water diffusion coefficient

In the MR experiments molecules or ions (more precisely the atomic nuclei which are their components) could be marked and then their diffusion can be traced. Practically, this method can be used for *in vivo* measurements of water diffusion coefficient in tissue. The measurement may also use a modified spin echo sequence (see Fig. 20). During the measurement, the gradient magnetic field is turned on twice for a short period of time (σ): once before the 180-degree pulse and once after. The first gradient causes the precession phase shift in the sample. During the following period (Δ) a portion of labeled nuclei is moved by diffusion to distant parts of the sample containing nuclei with different phases. After the 180-degree pulse, the second gradient pulse corrects the phase shifts induced by the first gradient; however, this occurs only in the nuclei, which are not diffused far from the original location. Dephasing due to diffusion loss causes the resulting signal. The higher diffusion coefficient or gradients (G) causes the lower signal. The pulse sequence described above is called Stejskalovo-Tanner scheme (Le Bihan D. 1995). The measurement is performed several times with different gradient sizes and following this the water diffusion coefficient, ADC_W, in tissue is obtained by fitting the equation:

$$S = S_0 \exp(-b \cdot ADC) \qquad [11]$$

$$b = \gamma^2 G^2 \delta^2 (\Delta - \delta/3) \qquad [12]$$

S is the integral of the signal that originates from water molecules during so called diffusion weighting, whose size is reflected by the b value; S_0 is the integral of the water signal without diffusion weighting.

3.3.3. Used magnetic resonance imaging methods

DW-MRI measurements were performed using an experimental MR spectrometer BIOSPEC 4.7 T system (Bruker, Germany) equipped with a 200 mT/m gradient system and a head surface coil. For DW measurements, four coronal slices were selected (thickness = 0.8 mm (mice), 1.0 mm (rats); interslice distance = 1.2 mm (mice) and 1.5 mm (rats); field of view (FOV) = 1.92 x 1.92 cm^2 (mice) and 3,2 x 3,2 cm^2 (rats), matrix size = 256 x 128. DW images were measured using the stimulated echo sequence and the following parameters: b-factors = 75 (rats) and 136 (mice), and 1732 (rats), 1825 s/mm^2 (mice), Δ= 30 ms, TE = 46 ms, TR = 1.2 s. The diffusion gradient direction pointed along the rostrocaudal direction. Maps of ADC_W were calculated using the linear least squares method. ADC_W was assumed to be zero in pixels where the acquired data did not fit well to theoretical dependence (correlation coefficient was less than 0.2). These zero-values were ignored for statistical evaluation if they occurred in the region of interest (ROI). ADC_W maps were analysed using ImageJ software (W. Rasband, NIH, USA). The evaluated ROIs were positioned using a mouse (Paxinos G. and Fraklin K. B. J. 2001) or rat (Paxinos G. and Watson C. 1998) brain atlas in both the left and right hemispheres. The minimal area of an individual ROI was 1.2 mm^2 in mice and 1.5 mm^2 in rats. ADC_W was measured in the same animals in which the TMA measurements were performed one week later. For MRI measurements, the animals were anesthetized with isoflurane (1.5 % in a gas mixture consisting of 35 % O_2 and 65 % N_2O) administered via a face mask. The animals were placed in a heated cradle and their heads fitted into a built-in head holder (Rapid Biomedical, Germany).

3.4. Microdialysis

The technique of microdialysis is based on sampling fluid via a double-lumen probe with an integrated semipermeable membrane; in which the equilibration of substances in the extracellular space and perfusion fluid takes place by diffusion according to the concentration gradient. We used a double-lumen microdialysis probe with a membrane length of 2 mm, an outer diameter of 0.5 mm and a cut-off at 20 kDa (CMA 12, 2 mm membrane length, CMA Microdialysis, Sweden). The inserted microdialysis catheter was connected by low-volume Fluorinated Ethylene Propylene (FEP)-tubing (1.2 µl/10 cm) to a precision infusion pump

(CMA 102, CMA Microdialysis, Sweden) in order to maintain a constant dialysate flow. The microdialysis catheter was continuously perfused with a dialysate containing 147 mmol/l NaCl, 2.7 mmol/l KCl, 1.2 mmol/l $CaCl_2$ and 0.85 mmol/l $MgCl_2$ (Perfusion fluid CNS, CMA Microdialysis, Sweden) at a flow rate of 2 µl/min. After a stabilization period of 60 min following insertion into the brain, microdialysate samples were collected over 10-min intervals and immediately frozen at −40°C until analysed. Thawed and centrifuged dialysate samples were analysed enzymatically with a CMA 600 Microdialysis Analyser (CMA/Microdialysis, Sweden) for lactate, pyruvate, glucose and glu^- concentrations.

The exchange of substances across the microdialysis membrane is limited by the total area of the membrane, the perfusion flow rate, the characteristics of the diffusing substance, and the diffusion constant in the tissue surrounding the probe (Ungerstedt U. 1991). The recovery rate expresses the relation between the concentration of the substance in the microdialysis probe effluent and the concentration in the medium (Muller M. 2002). Before and at the end of the experiments, the recovery rates for each probe were determined by continuing the perfusion at the same settings in a calibration solution containing known concentrations of the different analytes. The calibration solution contained 2.50 mmol/l lactate, 250 µmol/l pyruvate, 5.55 mmol/l glucose, 250 mmol/l glycerol, and 25 µmol/l glu^- (Calibrator, CMA Microdialysis, Sweden). The concentrations in the calibration solution were compared with the concentrations of the *in vitro* microdialysis samples to determine the relative recovery for each substance. The measured experimental values were weighted by the relative recovery to estimate the *in vivo* extracellular concentration of the substances in the immediate vicinity of the probes. *In vitro* recovery rates were 19.2 ± 0.69% for lactate, 20.4 ± 0.48% for pyruvate, 9.5 ± 0.30% for glu^-, and 10.1 ± 0.31% for glucose (mean ± standard error of the mean [S.E.M.]). All results are presented as weighted concentrations. The concentration of a metabolite in the extracellular fluid is clearly affected by changes in the extracellular space volume fraction. A decrease in α would, in the absence of any changes in metabolite supply or utilization, result in an increase in the measured metabolite concentration. Similarly, an increase in α would cause the measured metabolite concentration to decrease. To take into account the effects of changes in α, we have expressed our results as both the actual measured metabolite concentrations and also as the concentrations corrected for changes in α relative to its baseline values.

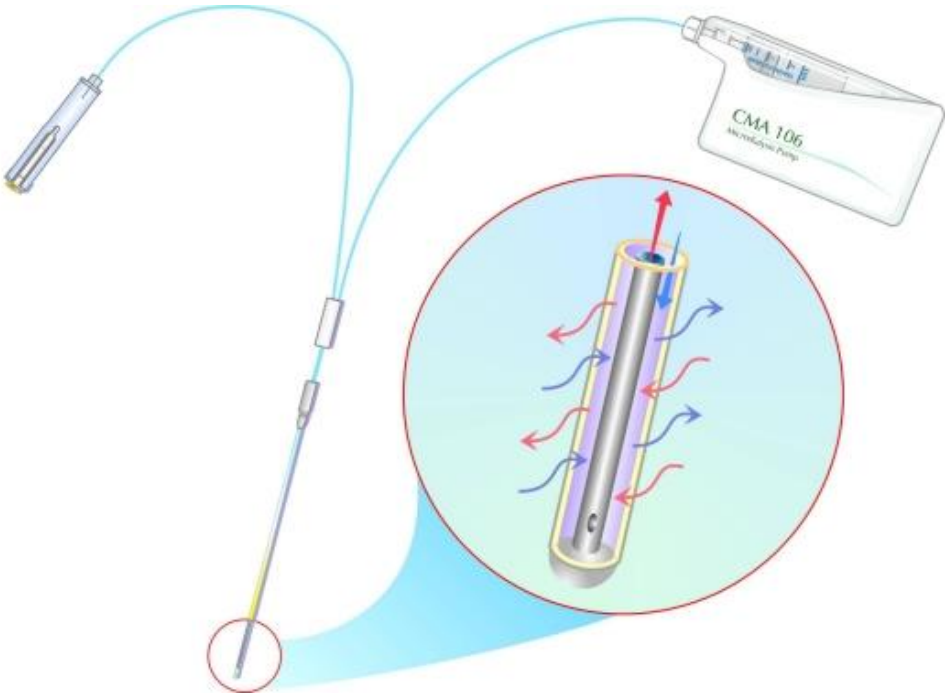

Fig. 21. Schematic representation of the microdialysis probe connected to a perfusion pump and sampler. The perfusion pump moves the perfusion solution via microdialysis probe. The tip of the microdialysis probe is provided with a semipermeable membrane, which allows the passage of substances in the direction of the concentration gradient. Permeability is limited by the size of pores in the membrane. The solution enriched with substances that are present in tissue is collected as dialysate in the sampler for further analysis of concentrations of monitored substances.

3.5. Local field potential recording

Local field potentials (FP) were recorded in all animals used for TMA^+ diffusion and extracellular K^+ measurements during measurements of pilocarpine-induced status epilepticus. For technical reasons, it was not possible to record neuronal activity in animals used for DW-MRI measurements. Local FPs were recorded on the reference barrel of a TMA^+- or K^+-sensitive microelectrode. The signal was amplified 10-fold and simultaneously displayed on a digital osciloscope and transferred to PC using a Lab-Trax acquisition system (World Precision Instruments, Inc., Sarasota, USA).

3.6. Immunohistochemistry

The 400 μm thick brain slices obtained prior to, after a 30 min incubation in -50 mOsmol/l, more severe -100 mOsmol/l hypotonic solutions or 10 mM K^+ and after a 60 min washout were post-fixed in 4% paraformaldehyde in 0.1 M phosphate buffer for 3 hours, then placed stepwise into solutions with gradually increasing sucrose concentrations (10%, 20%, 30%) for cryoprotection. The coronal slices (40 μm thick) were prepared using a microtome (HM 400, Microm Int. GmbH, Waldorf, Germany). The slices were first incubated in blocking solution, which contained 5% Chemiblocker (Millipore, MA) and 0.2% Triton in 0.01 M phosphate buffered-saline. This blocking solution was also used as the diluent for the antisera. The slices were then incubated with the primary mouse antibody against glial fibrillary acidic protein (anti-GFAP coupled to Alexa 488;1:800) at 4°C overnight (eBioscience, San Diego, CA, USA) and mounted using Vectashield mounting medium (Vector Laboratories, Burlingame, CA, USA). The tissue slices were then examined using an LSM 5 DUO spectral confocal microscope equipped with Arg/HeNe lasers and 40x or 63x oil objectives (Zeiss, Germany).

3.6.1. Quantification of GFAP staining in individual astrocytes

Changes in GFAP immunoreactivity in response to hypotonic stress or 10 mM K^+ were quantified using a previously described method (Chvatal A. et al. 2007). The GFAP staining was recorded as a set of two-dimensional (2D) sectional images with a resolution of 1024×1024 pixels using a Leica TCS SP system confocal microscope (Leica Germany). Alexa 488 was excited by an Ar laser set at 488 nm, and the emitted signal was recorded over the range of 510 – 552 nm using a TD488/543/633 filter. Each image was sectioned into 40 – 50 consecutive 2D images (at a uniform spacing of 0.5 μm), which were superimposed for further analyses. The parameters of the confocal microscope scanning, such as laser intensity, pinhole, gain and offset, were kept constant during the scanning of all samples. Image processing and morphometric measurements were performed using the program CellAnalyst developed at the Department of Cellular Neurophysiology, Institute of Experimental Medicine, Prague, Czech Republic (Benesova J. et al. 2012). The area corresponding to

GFAP immunoreactivity was estimated in individual cells (Fig. 22) in cortical slices prior to (control), during and after (washout) the application of hypotonic or 10 mM K^+ solutions.

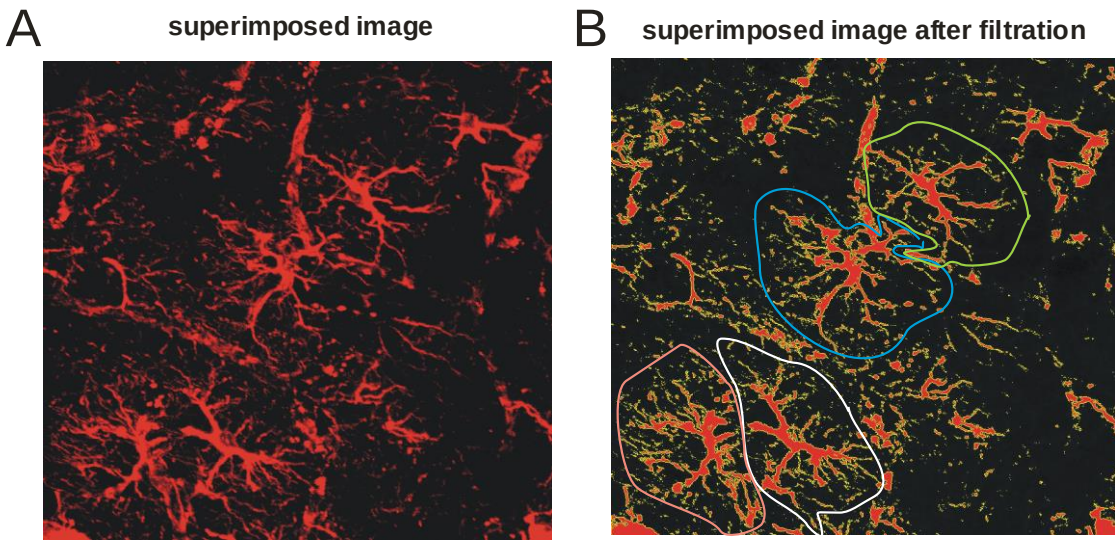

Fig. 22. (left) A superimposed image of GFAP staining in cortical astrocytes obtained by overlaying 20 individual confocal planes. **(right)** The superimposed image has been digitally filtered, and a red area (marked by yellow) was used for the quantification of GFAP staining. The area corresponding to the GFAP immunoreactivity of each astrocyte was calculated in clearly defined ROS. Here we show examples of such ROS that correspond to GFAP staining in individual astrocytes; individual ROS are highlighted by blue, green, pink and white colors.

3.7. Animals

For experiments involving models of pilocarpine-induced status epilepticus, adult male Wistar rats (300-350 g) were used. Animals were housed in cages with free access to food and water and maintained at a temperature of 22°C with a 12:12 h light-dark cycle (lights on at 08:00).

To study the role of α-syn protein on cell swelling, we used α-syn-deficient mouse line that was originally generated by Stan Froehner and Marv Adams (Department of Physiology and Biophysics, University of Washington, Seattle, 98195, USA). Both male and female 3-4-

month-old mice, homozygous for the targeted disruption of the gene encoding α-syntrophin, were used (α-syn -/- mice). This mouse line was kindly provided by Professor Ole P. Ottersen from the University of Oslo, Norway. Wild-type C57B/6 mice were used as controls.

For quantification of astrocyte volume changes transgenic GFAP/EGFP mice were used, in which the enhanced green fluorescent protein (EGFP) is expressed under the control of the promoter for human glial fibrillary acidic protein (GFAP) (Nolte C. et al. 2001). To elucidate the impact of the α-syntrophin knockout on astrocyte swelling double transgenic mice (GFAP/EGFP/α-syn -/- mice) were generated by Miroslava Anderova (Department of Cellular Neurophysiology, Institute of Experimental Medicine, Academy of Sciences of the Czech Republic, Prague, Czech Republic). This mouse line was generated by crossbreeding GFAP/EGFP mice and α-syn -/- mice. Diffusion measurements were performed *in vitro* as well as *in vivo* in the cortex of 3-4 month old transgenic mice.

All procedures involving the use of laboratory animals were performed in accordance with the European Communities Council Directive 24 November 1986 (86/609/EEC) and animal care guidelines were approved by the Institute of Experimental Medicine ASCR Animal Care Committee.

For *in vivo* experiments, rats were anesthetized by an intraperitoneal injection of urethane (1.2 g/kg; Sigma-Aldrich Chemie Gmbh, Steinheim, Germany), intubated and connected to a ventilator (CIV 101, Columbus Instruments, Columbus, Ohio, USA) and ventilated with air, while mice were anesthetized with isoflurane. Body temperature was maintained at 36-37 °C by a heating pad. The head of the animal was fixed into the stereotaxic holder. For TMA^+ and $[K^+]_e$ measurements, the somatosensory cortex of the animals was partially exposed by a burr hole 2-3 mm (rats) or 1.5 mm (mice) caudal from bregma and 2-3 mm (rats) or 1.5 mm (mice) lateral from the midline; the dura mater was then removed. The exposed cortex was washed in warm (37 ˚C) artificial CSF (aCSF) containing in mM: 117 NaCl, 3 KCl, 35 $NaHCO_3$, 1.25 Na_2HPO_4, 1.3 $MgCl_2$, 1.5 $CaCl_2$, 10 glucose, and 0.1 TMA^+ at a flow rate of 4 mL/min. The pH was adjusted to 7.4 by gassing the aCSF with 95% O_2 and 5% CO_2. Osmolality was confirmed to be 300 ± 5 mOsm/kg using a vapour pressure osmometer (Vapro 5520, Wescor Inc., Logan, USA).

For *in vitro* experiments, the mice were anesthetized by isofluran and decapitated. The brains were dissected out, and 400 μm thick coronal slices were prepared using a vibrating blade microtome (HM 400, Microm Int. GmbH) in ice-cold isolation solution containing in mM: 154.5 NaCl, 3 KCl, 35 $NaHCO_3$, 1.3 Na_2HPO_4, 0 $MgCl_2$, 1.5 $CaCl_2$ and 10

glucose. After cutting, the slices were maintained for 1-2 hours in aCSF with the same chemical composition as was used for *in vivo* experiments. Recordings were performed at room temperature in a chamber perfused with a continuously bubbled (95% O_2 and 5% CO_2) aCSF (pH 7.4, ~300mOsm/kg), at a flow rate of 10 mL/min.

3.8. Experimental models of acute pathological states

3.8.1. Pilocarpine-induced status epilepticus

In our study we induced status epilepticus by the administration of pilocarpine (Turski L. et al. 1989), a muscarinic cholinergic agonist. It was described (Treiman D. M. et al. 1990; Stringer J. L. and Sowell K. L. 1994) that intraperitoneal administration of high doses of pilocarpine (300-400 mg/kg), or lower doses of pilocarpine (30-40 mg/kg) after pretreatment with lithium, results in the stereotyped appearance of behavioral and electrographic seizures lasting for many hours. Behavioral and electroencephalographic alterations produced by pilocarpine application are similar to those of human temporal lobe epilepsy (Turski L. et al. 1989).

All measurements were recorded in the somatosensory cortex at a depth of 1000-1100 μm. For technical reasons, TMA^+ diffusion, $[K^+]_e$ and diffusion weighted magnetic resonance imaging measurements were performed separately using four groups of animals. To potentiate the subsequent action of pilocarpine (Ormandy G. C. and Jope R. S. 1991), lithium chloride (127 mg/kg, i.p.; Sigma-Aldrich) was given to the animals 14-18 h before each pilocarpine experiment. Methylscopolamine bromide (Sigma-Aldrich), an anticholinergic agent that does not cross the blood-brain barrier, was dissolved in normal saline at 1 mg/ml, and 1 mg/kg was given subcutaneously 20 min before the pilocarpine injection to block its peripheral activity. Pilocarpine hydrochloride (Sigma-Aldrich) was dissolved in normal saline at 100 mg/ml, and one dose of 300 mg/kg was administered i.p. Data obtained from recordings during the period prior to pilocarpine injection were used as control data. After the injection of pilocarpine, data was recorded over 10-min intervals for 4 h.

3.8.2. Acute cell swelling *in vivo*

Differences in cell swelling between α-syn-positive and α-syn-deficient mice during severe pathological states were examined in an experimental model of terminal ischemia/anoxia *in vivo*, evoked by cardiac arrest induced by the intraperitoneal administration of 1 ml saturated $MgCl_2$ (Vorisek I. and Sykova E. 1997).

3.8.3. Acute cell swelling *in vitro*

The changes in cell volume were evoked in the cortical slices (400 μm) by superfusion with either 10 mM K^+ or hypotonic solution. *Hypoosmotic solutions* (H-50 and H-100) were prepared by the reduction of NaCl concentration to 98.0 mM or to 58 mM, and their osmolarities were 250 and 205 mOsm/kg, respectively. The osmotic strength of the solutions was measured with a vapor pressure osmometer. Solution modeling *hyperkalemia* (+10 mM K^+) was prepared by the addition of 10 mM together with concurrent reduction of NaCl concentration. Its osmolality was confirmed to be 300 ± 5 mOsm/kg.

3.9. Statistical analysis

The results of the experiments were expressed as the mean ± S.E.M. Values of $p < 0.05$ were considered significant.

For the experiments with pilocarpine-induced SE, differences between different time intervals were evaluated using ANOVA for repeated measures test and Dunnett's post hoc test.

For the study on α-syn-positive and α-syn-deficient mice, statistical analysis of the differences within and between groups was performed using one-way ANOVA with the Tuckey post-test (Instat; GraphPad Software, San Diego, CA, USA). Repeated measures within a group of subjects were analyzed using repeated measures ANOVA (Statistica; Statsoft, Tulsa, OK, USA).

4. RESULTS

4.1. BRAIN METABOLSM AND DIFFUSION IN THE RAT CEREBRAL CORTEX DURING PILOCARPINE-INDUCED STATUS EPILEPTICUS

This study was performed *in vivo* in the somatosensory cortex of adult male Wistar rats. We correlated results obtained from DW-MRI, RTI-TMA method, measurements of local field potentials, extracellular potassium concentration, and microdialysis during pilocarpine-induced SE. Results of this work were published in *Experimental Neurology*, 2008 Jan; 209(1):145-54, IF = 4.156.

4.1.1. Extracellular field potentials

The amplitude of extracellular field potentials in the somatosensory cortex was 0.3-0.4 mV. Several minutes after the injection of pilocarpine, the amplitude decreased to 0.2-0.25 mV. The ictal activity in the neocortex began 25-40 min following the pilocarpine injection (average latency 30 min). The amplitude of the ictal discharges increased and reached a maximum of 2.0-2.5 mV about 80-100 min after the application of pilocarpine. The amplitude then started to diminish, but epileptiformic manifestations lasted up to the end of the experimental period. The typical records of a single experiment are presented in Fig. 23 and 24. Fig. 23 shows typical local field potential recordings of a urethane anesthetized pilocarpine injected rat. Before the injection of pilocarpine, local field potential was presented as the irregular baseline (Fig. 23A). Pilocarpine injection led to bursts of spike-wave activity (Fig. 23B), as well as episodes of high-frequency activity (Fig. 23C). Three hours after the pilocarpine injection, the amplitude of local field potential was normalizing. Fig. 24A shows an example of local field potential records before and 60, 120, 180 and 240 min after the injection of pilocarpine. No behavioral manifestations of seizures were observed during anaesthesia.

4.1.2. ECS diffusion parameters and extracellular K^+ concentration during status epilepticus

The mean values of extracellular volume fraction α and tortuosity λ before the application of pilocarpine were 0.19 ± 0.01 and 1.58 ± 0.01 (n = 7). Following pilocarpine application, there were no significant changes in tortuosity (Fig. 24B). The volume fraction started to decrease several minutes after the application of pilocarpine, reaching a minimum (0.13 ± 0.01) 80-100 min later. At 120 min, α started to increase and reached 0.18 ± 0.01 240 min after the application of pilocarpine (Fig. 24C).

$[K^+]_e$ in the brain somatosensory cortex at the beginning of the experiments was 3.07 ± 0.02 mM (n = 7). Following pilocarpine application, $[K^+]_e$ started to increase after several minutes, reaching a maximal concentration of 13.3 ± 1.04 mM 80 minutes later. Subsequently, $[K^+]_e$ returned to normal values, and at the end of the experiment (in the 240th minute) $[K^+]_e$ was 4.17 ± 0.21 mM (Fig. 24D).

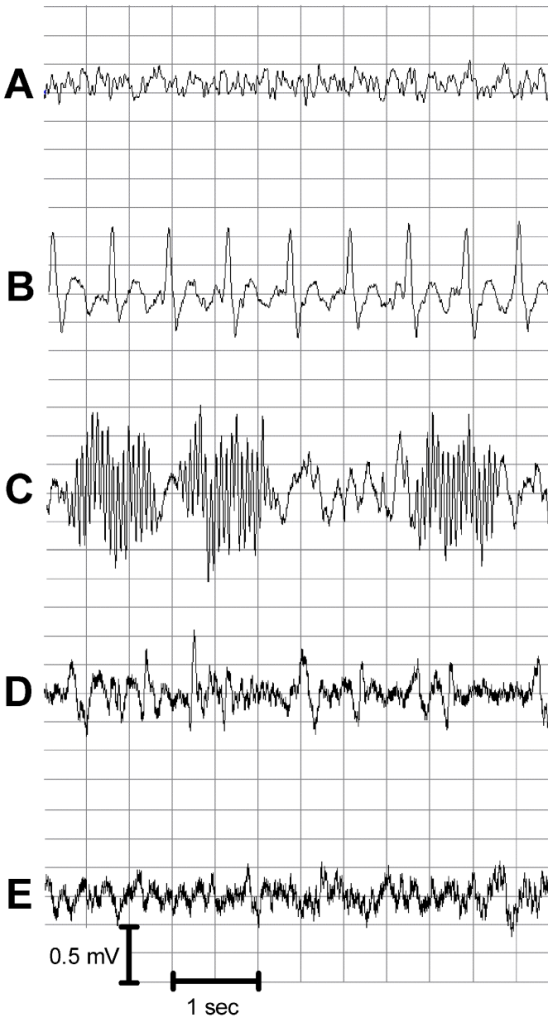

Fig. 23. Local field potential recordings of a urethane anesthetized pilocarpine injected rat. (**A**) Irregular baseline local field potential before pilocarpine injection. (**B**) Spike-wave complexes 60 min after pilocarpine injection. (**C**) Intervals of high-frequency activity 120 min after pilocarpine injection. (**D, E**) Local field potential records 180 and 240 min after pilocarpine injection, respectively.

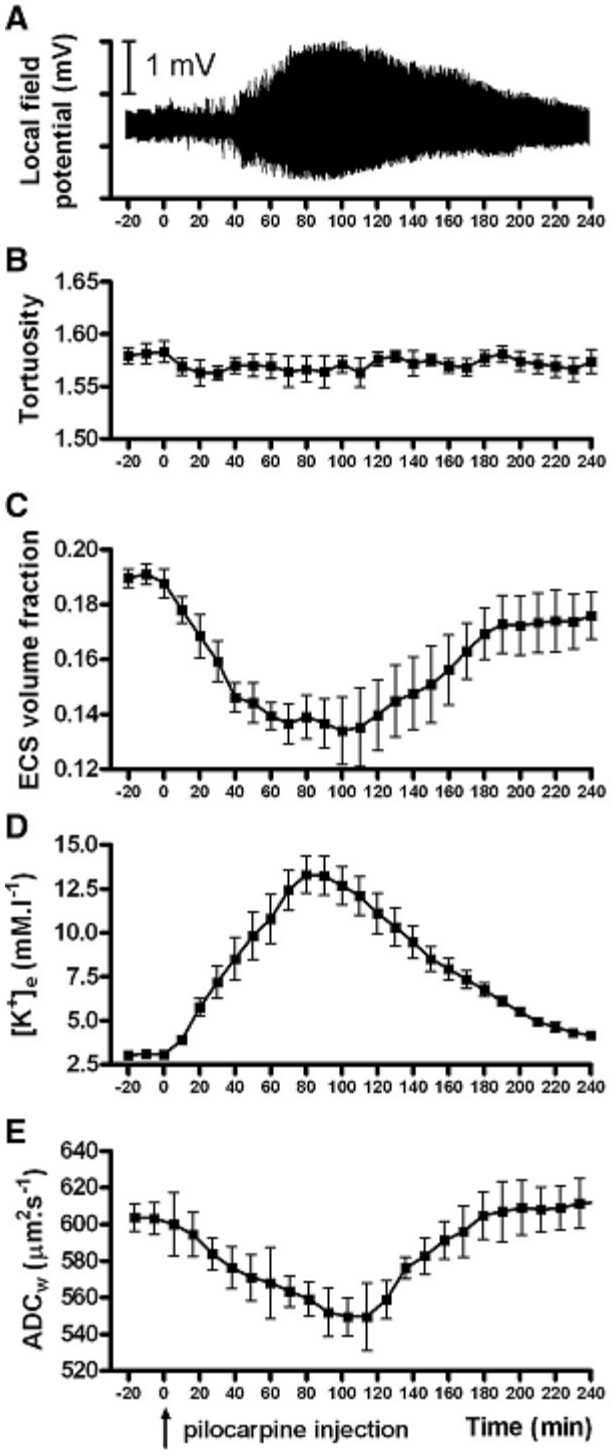

Fig. 24. Diffusion parameters and extracellular K^+ concentration after pilocarpine administration. The time course of potentials of electric field (**A**), tortuosity λ (**B**), ECS volume fraction α (**C**), the extracellular potassium concentration $[K^+]_e$ (**D**) and the apparent diffusion coefficient of water ADC_W (**E**). Pilocarpine was injected at time 0.

4.1.3. Apparent diffusion coefficient of water during status epilepticus

The mean value of ADC_W before the application of pilocarpine was 603.2 ± 8.6 μm^2 s^{-1} (n = 6, mean ± S.E.M.). Following pilocarpine application, ADC_W started to decrease, reaching a minimum of 549.5 ± 10.5 μm^2 s^{-1} 100 min later. At 120 min, ADC_W started to increase and reached 612.7 ± 14.7 μm^2 s^{-1} 240 min after the application of pilocarpine (Fig. 24D, 25).

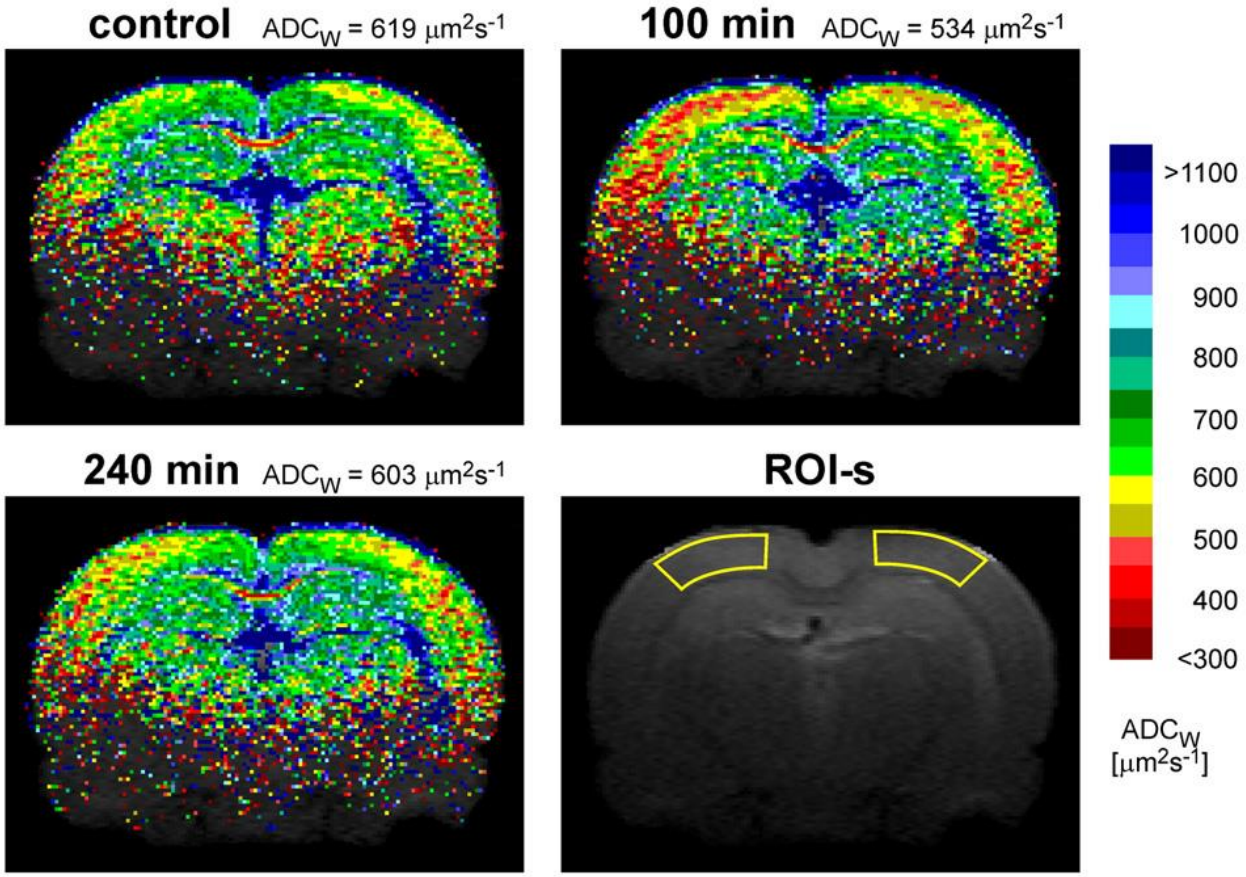

Fig. 25. Typical ADC_W maps in rat before and after pilocarpine injection in primary somatosensory cortex. The areas are outlined in T_2-weighted image (bottom-right panel). The image shows ADC_W maps taken from the identical coronal plane of the same animal. The scale at the right side of the figure shows the relation between the intervals of ADC_W values and the colors used for visualization. Note the significantly decreased ADC_W in the cerebral cortex 100 min after pilocarpine injection. ADC_W returned to the control values after 4 h. ROI-s indicate areas of measurement in the somatosensory cortex.

4.1.4. Microdialysis

After a stabilization period of 60 min following probe insertion, the basal cortical level of lactate and the lactate/ pyruvate ratio remained stable at 0.61 ± 0.05 mmol/l and 33.16 ± 4.26, respectively (n = 8). The application of pilocarpine led to a rise in lactate dialysate levels, reaching a plateau of 2.92 ± 0.60 mmol/l within 100 min (Fig. 26A). The lactate/pyruvate ratio showed a similar time course, reaching a plateau of 84.80 ± 11.72 (Fig. 26B). Subsequently, lactate levels and the lactate/pyruvate ratio decreased, reaching control values at the end of the experiment. Taking into account the effect of the decrease in ECS volume fraction, the calculated extracellular concentrations of lactate during hypoxia/ischemia would be as much as 30% lower than those actually measured (Fig. 26A). Basal glucose and glu^- levels were 2.42 ± 0.13 mmol/l and 6.55 ± 1.31 μmol/l, respectively (n = 8). Following pilocarpine application, glucose dialysate concentrations increased, reaching a maximum of 3.49 ± 0.24 mmol/l 40 min later. Thereafter, glucose concentrations decreased, reaching a value of 1.25 ± 0.40 mmol/l by the end of the experiment. The glucose concentrations during hypoxia/ischemia would be even lower if we take into account the accompanying decrease in ECS volume fraction (Fig. 26C). Extracellular glu^- levels started to increase 40 min after the application of pilocarpine and reached maximum values of 22.39 ± 5.85 μmol/l. Subsequently, the extracellular glu^- levels decreased, reaching control values by the end of the experiment. The concentrations of glu^- corrected for the increase in α would be therefore lower than the acquired concentrations (Fig. 26D).

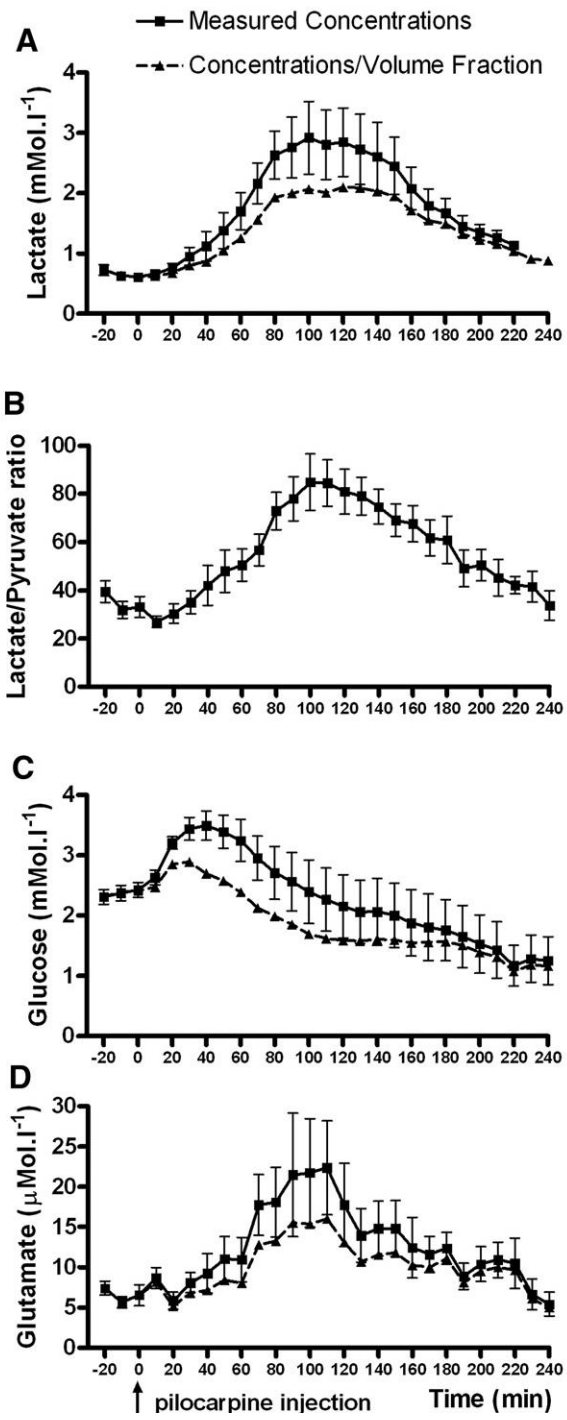

Fig. 26. The time course of extracellular lactate concentration (A), lactate/pyruvate ratio (B) and the concentrations of extracellular glucose (C) and glutamate (D). Pilocarpine was injected at time 0. The time courses of the concentrations of the evaluated metabolites corrected for changes in ECS volume are presented as dashed lines, and they show how much of the concentration change is due to the ECS volume change.

4.2. THE IMPACT OF ALPHA-SYNTROPHIN DELETION ON THE CHANGES IN TISSUE STRUCTURE AND EXTRACELLULAR DIFFUSION ASSOCIATED WITH CELL SWELLING IN EXPERIMENTAL MODELS

In this study, we established the ECS diffusion parameters in α-syn-positive and α-syn-deficient mice under resting conditions and during acute cell swelling in experimental models *in vivo* as well as *in vitro*. Values of ECS diffusion parameters were correlated with ADC_W values. To elucidate the impact of α-syntrophin deletion on astrocyte swelling and to reveal morphological changes during acute cell swelling, quantification of GFAP staining in individual astrocytes was performed. Results of this study were published in *PLoS ONE* 8(7):e68044, IF = 3.7.

4.2.1. ECS diffusion parameters and ADC_W in α-syn +/+ and α-syn -/- mice under resting conditions

The control values of the ECS volume fraction α measured on coronal slices *in vitro* were significantly higher in α-syn -/- compared with α-syn +/+ animals, while the tortuosity λ and non-specific uptake k' values did not significantly differ between α-syn +/+ and α-syn -/- mice (Fig. 27A; Table 2). Measurements carried out in the cortex *in vivo* confirmed the significantly higher control values of α in α-syn -/- in comparison with α-syn +/+ mice with no significant difference in λ and k' (Fig. 27E; Table 3). Additionally, significantly higher control values of ADC_W were detected in α-syn -/- mice using DW-MRI.

Significant differences in the control values of all three ECS diffusion parameters were found between *in vivo* and *in vitro* conditions in both α-syn +/+ and α-syn -/- mice: α and k' values were higher *in vivo*, while λ was higher *in vitro* (Table 2 and 3).

4.2.2. Effects of hypotonic stress *in vitro*

To reveal changes in cell volume associated with physiological or pathological cell swelling, slices were superfused with -50 mOsmol/l (H-50) or more severe -100 mOsmol/l (H-100) hypotonic solution.

A 30 min superfusion of brain slices with mild hypotonic solution (H-50) led to a significant decrease in α and no increase in λ in α-syn +/+ and α-syn -/- mice (Fig. 28A, B; Table 2). The maximum decrease of the ECS volume reached during the application was larger in α-syn +/+ animals than in α-syn -/- mice (Fig. 27B; Fig. 28A; Table 2). Since there was a significant difference in the control values of the ECS volume between α-syn +/+ and α-syn -/- mice, we set the control values of all experiments to 100% in order to determine the relative changes in ECS volume fraction during perfusion. This analysis revealed that the relative decrease in extracellular volume in α-syn +/+ and α-syn -/- mice during the application of a mild hypotonic stress (of 30.53% ± 2.16% and 25.94% ± 3.80%, respectively) was not significantly different.

In contrast, the application of a more severe hypotonic solution (H-100) evoked a significantly smaller decrease in α in α-syn -/- mice than in α-syn +/+ in both absolute and relative values (Fig. 27C; 28C; 29B; Table 2; a relative decrease of 36.79 % ± 6.05% and 61.58% ± 7.53%, respectively). During washout, the values of α overshot the control values in α-syn -/- mice but not in α-syn +/+ animals (Fig 28C; Table 2). The increase in λ and k' evoked by mild or severe hypotonic stress was similar in both animal groups (Fig. 27B, C; 28B, D; Table 2) and fully recovered to control values during washout.

4.2.3. Effects of elevated K^+ *in vitro*

The decrease in α observed during a 30 min superfusion with 10 mM K^+ was significantly smaller in α-syn -/- mice than in α-syn +/+ animals in both absolute as well as relative values (Fig. 27D; 28E; 29C; Table 2; a relative decrease of 27.36% ± 1.21% and 44.74% ± 5.38%, respectively). The increase in λ evoked by 10 mM K^+ was similar in both animal groups (Fig. 27D; Fig. 28F; Table 2); however, in contrast to α-syn -/- mice, tortuosity remained elevated even after washout in the α-syn +/+ animals (Fig. 28F; Table 2), indicating the creation of additional diffusion barriers, presumably due to structural changes of the fine astrocytic processes. The increase in k' during application was similar in both animal groups (Table 2) and fully recovered to control values during washout.

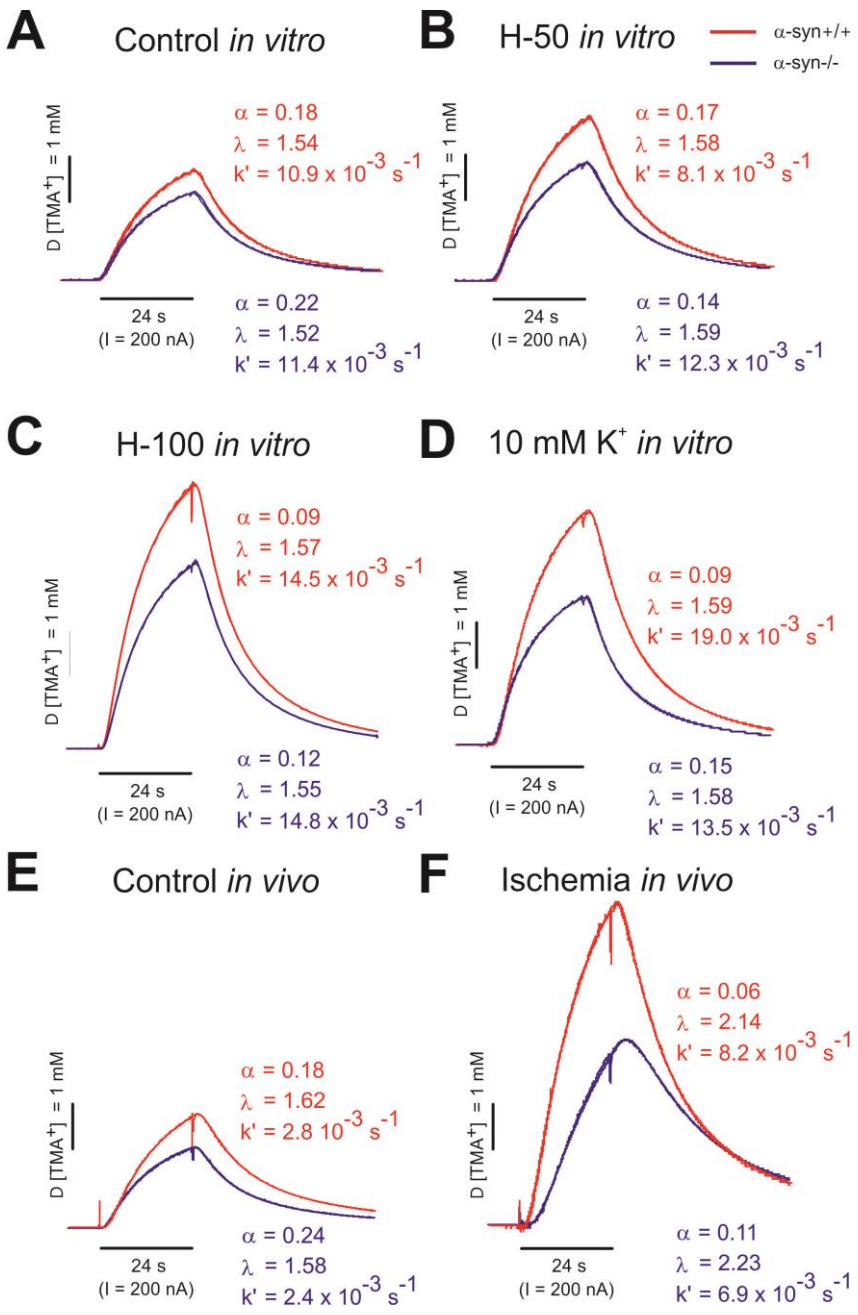

Fig. 27. Representative TMA^+-diffusion curves under resting conditions and during cell swelling. TMA^+-diffusion curves with the corresponding values of the extracellular volume fraction (α), tortuosity (λ) and non-specific uptake (k') obtained in the cortex of α-syn +/+ and α-syn -/- mice under resting conditions **(A, E)** as well as during acute cell swelling evoked by the application of hypotonic solutions H-50 **(B)**, H-100 **(C)** or increased potassium **(D)** *in vitro* or by ischemia/anoxia *in vivo* **(F)**. The values of the ECS diffusion parameters were determined by a non-linear curve fitting algorithm operating on the diffusion curve. The amplitude of the curves is inversely proportional to the ECS volume fraction while the shape of the curves reflects tortuosity.

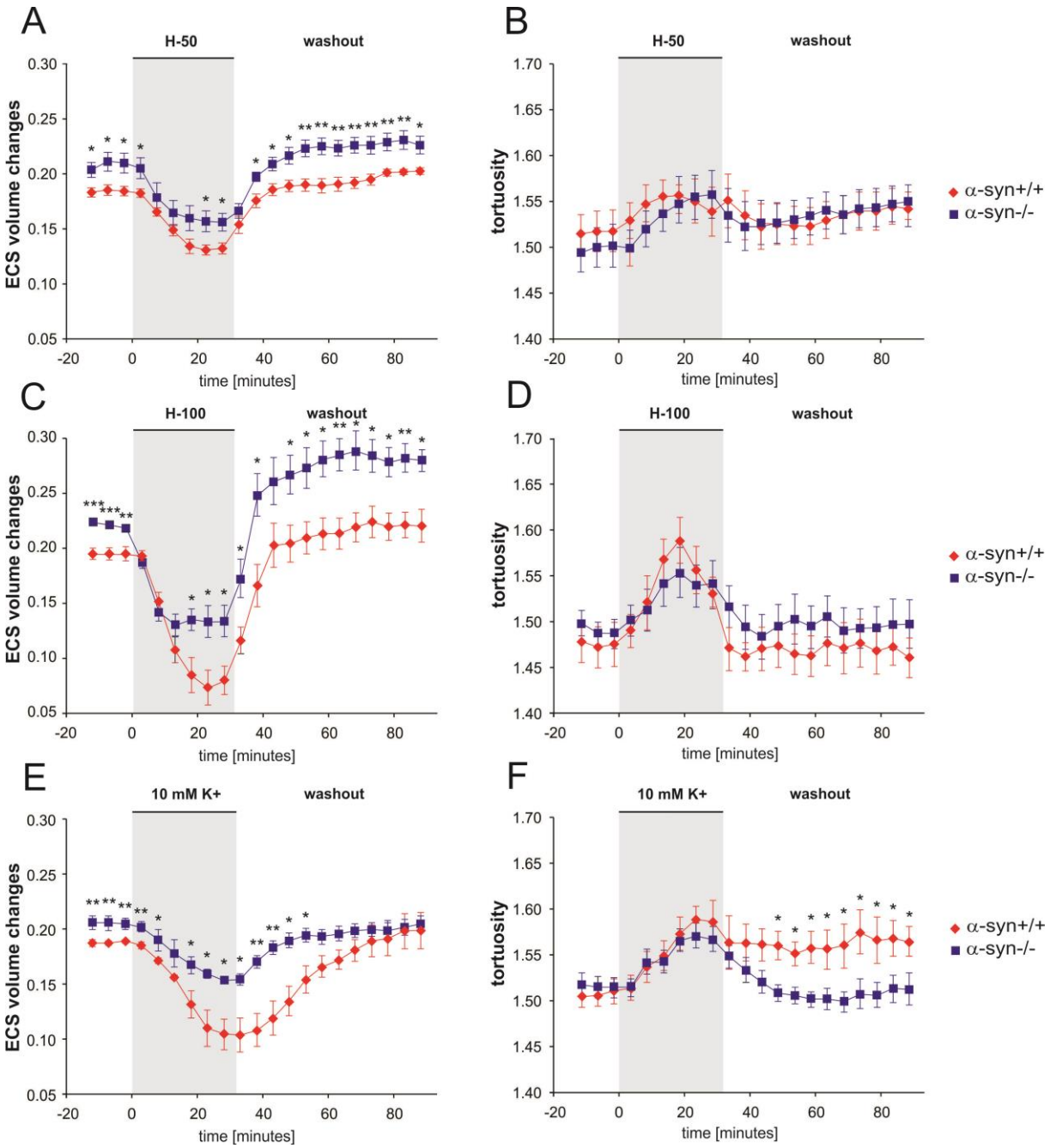

Fig. 28. The effect of hypotonic solutions or 10 mM K^+ on ECS diffusion parameters *in vitro* in α-syn +/+ and α-syn -/- mice. The absolute values of the extracellular volume fraction (α) and tortuosity (λ) were measured in cortical slices from the somatosensory cortex of α-syn +/+ and α-syn -/- mice during a 30 min application of hypotonic solution H-50 (-50 mOsmol/l) **(A, B)** and H-100 (-100 mOsmol/l) **(C, D)** or 10 mM K^+ **(E, F)**, as well as during washout. Each data point represents mean ± S.E.M. Asterisks (*- $p < 0.05$; **- $p < 0.01$; ***- $p < 0.001$) indicate significant differences between the values in α-syn +/+ and α-syn -/- animals.

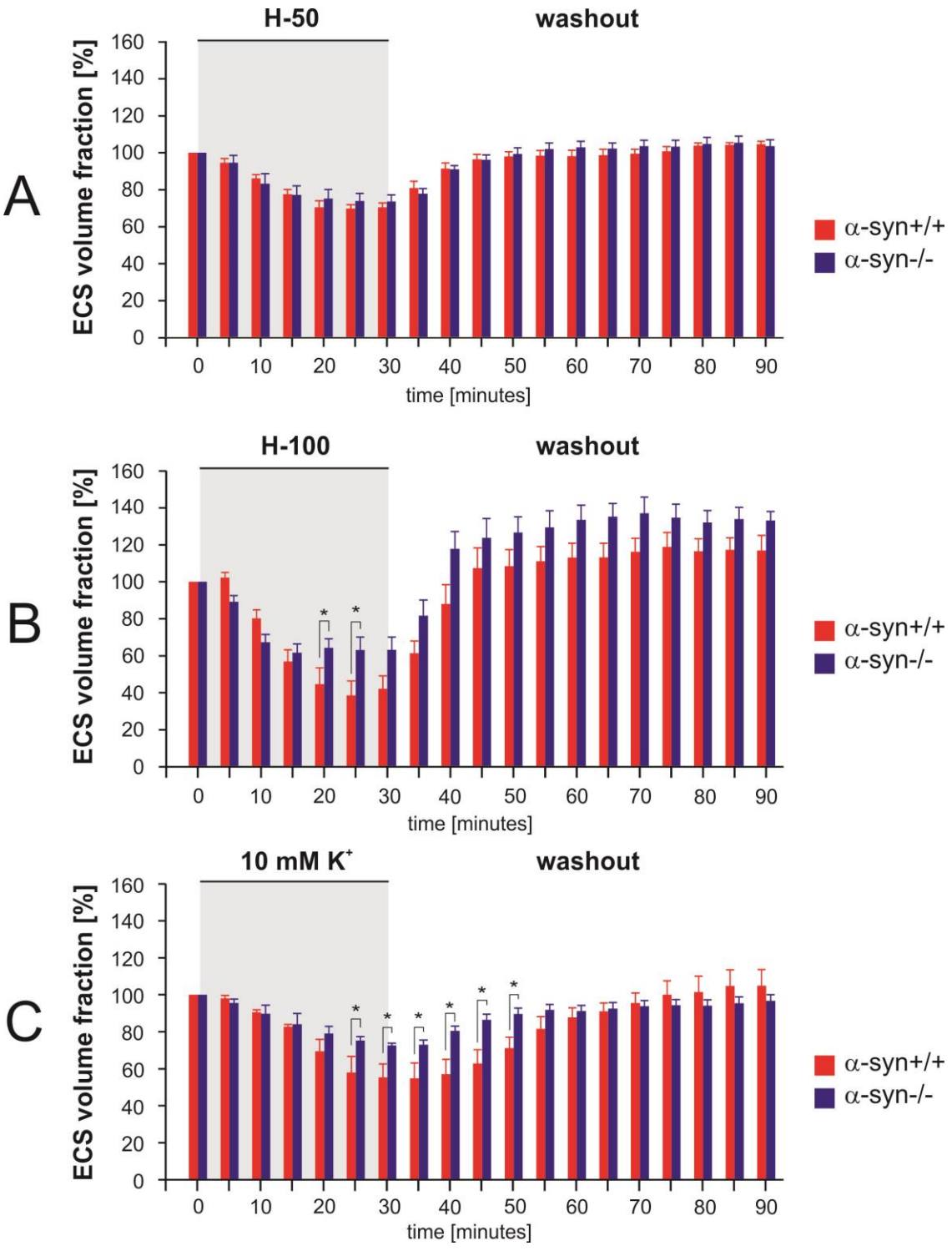

Fig. 29. The effect of hypotonic stress or elevated K^+ on the relative changes in the ECS volume *in vitro* in α-syn +/+ and α-syn -/- mice. The control values of all experiments were set to 100% and the relative changes of values of the extracellular volume fraction α were calculated in 5 min intervals during 30 min application and subsequent 60 min washout of mild (**A**) or severe (**B**) hypotonic stress or 10 mM K^+ (**C**). Each data point represents mean ± S.E.M. Asterisks indicate significant (*- $p < 0.05$) differences between α-syn +/+ and α-syn -/- mice.

Table 2. Effect of hypotonic stress and elevated K^+ on the ECS diffusion parameters in α-syn +/+ and α-syn -/- mice *in vitro*.

	α-syn +/+				**α-syn -/-**			
	α	***λ***	***k´* x $10^{-3}s^{-1}$**	**n/N**	***α***	***λ***	***k´* x $10^{-3}s^{-1}$**	**n/N**
control values	0.190 ± 0.002	1.502 ± 0.011	9.504 ± 0.700	26/17	0.212 ± 0.003**	1.499 ± 0.008	11.716 ± 1.220	21/13
H-50	0.132 ± 0.004$^{\#\#\#}$	1.565 ± 0.023$^{\#}$	13.990 ± 1.400	9/6	0.157 ± 0.008$^{**\#\#\#}$	1.554 ± 0.018$^{\#}$	13.664 ± 1.679	7/4
wash-out	0.198 ± 0.003	1.542 ± 0.019	9.331 ± 1.301		0.220 ± 0.007*	1.549 ± 0.021	9.735 ± 1.251	
H-100	0.073 ± 0.016$^{\#\#\#}$	1.589 ± 0.025$^{\#}$	23.819 ± 3.335$^{\#\#\#}$	7/4	0.134 ± 0.015$^{***\#\#\#}$	1.554 ± 0.025	20.923 ± 1.652$^{\#\#}$	10/5
wash-out	0.222 ± 0.015$^{\#}$	1.460 ± 0.022$^{\#}$	8.878 ± 2.196		0.283 ± 0.010$^{***\#\#\#}$	1.512 ± 0.028	14.000 ± 3.044	
10 mM K^+	0.105 ± 0.014$^{\#\#\#}$	1.588 ± 0.022$^{\#\#\#}$	20.579 ± 2.914$^{\#\#\#}$	10/7	0.154 ± 0.003$^{*\#\#\#}$	1.569 ± 0.013$^{\#}$	15.462 ± 2.884	7/4
wash-out	0.199 ± 0.017	1.566 ± 0.017$^{\#}$	9.260 ± 0.797$^{\#}$		0.205 ± 0.007	1.515 ± 0.017	13.003 ± 3.763	

The values are presented as mean ± S.E.M. Asterisks (*- $p < 0.05$; **- $p < 0.01$; ***- $p < 0.001$) indicate significant differences between the values in α-syn +/+ and α-syn -/- animals; crosshatches (#- $p < 0.05$; ##- $p < 0.01$; ###- $p < 0.001$) indicate significant differences between control values and those obtained under experimental conditions in the same group of animals. The control values of the ECS diffusion parameters from each individual experiment were calculated as the average values extracted from three diffusion curves before application. The mean control value presented in the table is the average of the control values from all *in vitro* experiments. The mean values of the maximum change during application correspond to the time-point of the maximum decrease of α (i.e., the 25th min in H-50 and H-100 and the 30th min in 10 mM K^+); the values for washout correspond to the data point at the 90th min. Abbreviations: extracellular space volume fraction (α), tortuosity (λ), non-specific uptake (k'), number of animals (N), number of slices (n), hypotonic solutions (H-50 and H-100).

4.2.4. Effect of cardiac arrest *in vivo*

The minimal values of the ECS volume fraction reached after cardiac arrest, due to the administration of $MgCl_2$, were larger in α-syn -/- mice compared to α-syn +/+ mice, suggesting diminished cell swelling in the α-syn -/- animals (Fig. 30A; Table 3). The maximum decrease of ADC_W was also smaller in α-syn -/- mice; in addition, the time course of changes in α-syn -/- animals was slowed down in comparison with α-syn +/+ animals (Fig. 32, Table 3).

Shortly after the administration of $MgCl_2$, the values of λ in α-syn -/- mice reached higher levels than in α-syn +/+ animals (Fig 30B), reflecting a more rapid increase in the number of obstacles for diffusion in the ECS of the α-syn -/- mice. However, the final values of λ 35-45 min after the induction of cardiac arrest were not significantly different between the two types of animals (Fig. 30B; Table 3).

The increase of $[K^+]_e$ in α-syn +/+ and α-syn -/- mice immediately after terminal cardiac arrest displayed a steep rise, which was faster and reached its maximum in α-syn -/- animals about 4 min after cardiac arrest. In α-syn +/+ animals, $[K^+]_e$ increased more slowly and reached maximum values 9 min after $MgCl_2$ administration (Fig. 30C). There were no significant differences between these two animal groups in the final values of $[K^+]_e$ (Fig. 30C; Table 3).

Table 3. Effect of terminal ischemia/anoxia on the ECS diffusion parameters, ADC_W and extracellular K^+ concentration in α-syn +/+ and α-syn -/- mice *in vivo*.

	α-syn +/+				α-syn -/-			
	control values	**N**	**terminal ischemia/anoxia**	**N**	**control values**	**N**	**terminal ischemia/anoxia**	**N**
α	0.204 ± 0.003†††	14	0.101 ± 0.006$^{\#\#\#}$	6	0.227 ± 0.003**††	11	0.143 ± 0.008$^{***\#\#\#}$	7
λ	1.596 ± 0.010†††	14	2.073 ± 0.057$^{\#\#\#}$	6	1.598 ± 0.010†††	11	2.245 ± 0.045$^{*\#\#\#}$	7
k' x10^{-3} s^{-1}	3.622 ± 2.421	14	2.102 ± 2.651	6	2.623 ± 2.480	11	5.410 ± 4.270	7
$[K^+]_e$ (mM)	2.858 ± 0.218†	6	52.370 ± 2.644$^{\#\#\#}$	6	2.859 ± 0.256††	5	53.750 ± 2.635$^{\#\#\#}$	5
ADC_W (μm^{2}s^{-1})	590 ± 6	6	374 ± 8$^{\#\#\#}$	6	627 ± 6*	6	413 ± 11$^{*\#\#\#}$	6

The values are presented as mean ± S.E.M. Asterisks (*- p < 0.05; **- p < 0.01; ***- p < 0.001) indicate significant differences between the values in α-syn +/+ and α-syn -/- animals; crosshatches (#- p < 0.05; ##- p < 0.01; ###- p < 0.001) indicate significant differences between control values and those obtained under experimental conditions in the same group of animals and crosses (†- p < 0.05; ††- p < 0.01; †††- p < 0.001) indicate significant difference between values *in vitro* and *in vivo*. The mean values of the maximum change during terminal ischemia/anoxia correspond to the 30th minute after cardiac arrest. Abbreviations: extracellular space volume fraction (α), tortuosity (λ), non-specific uptake (k'), extracellular potassium concentration ($[K^+]_e$), apparent diffusion coefficient (ADC_W) number of animals (N).

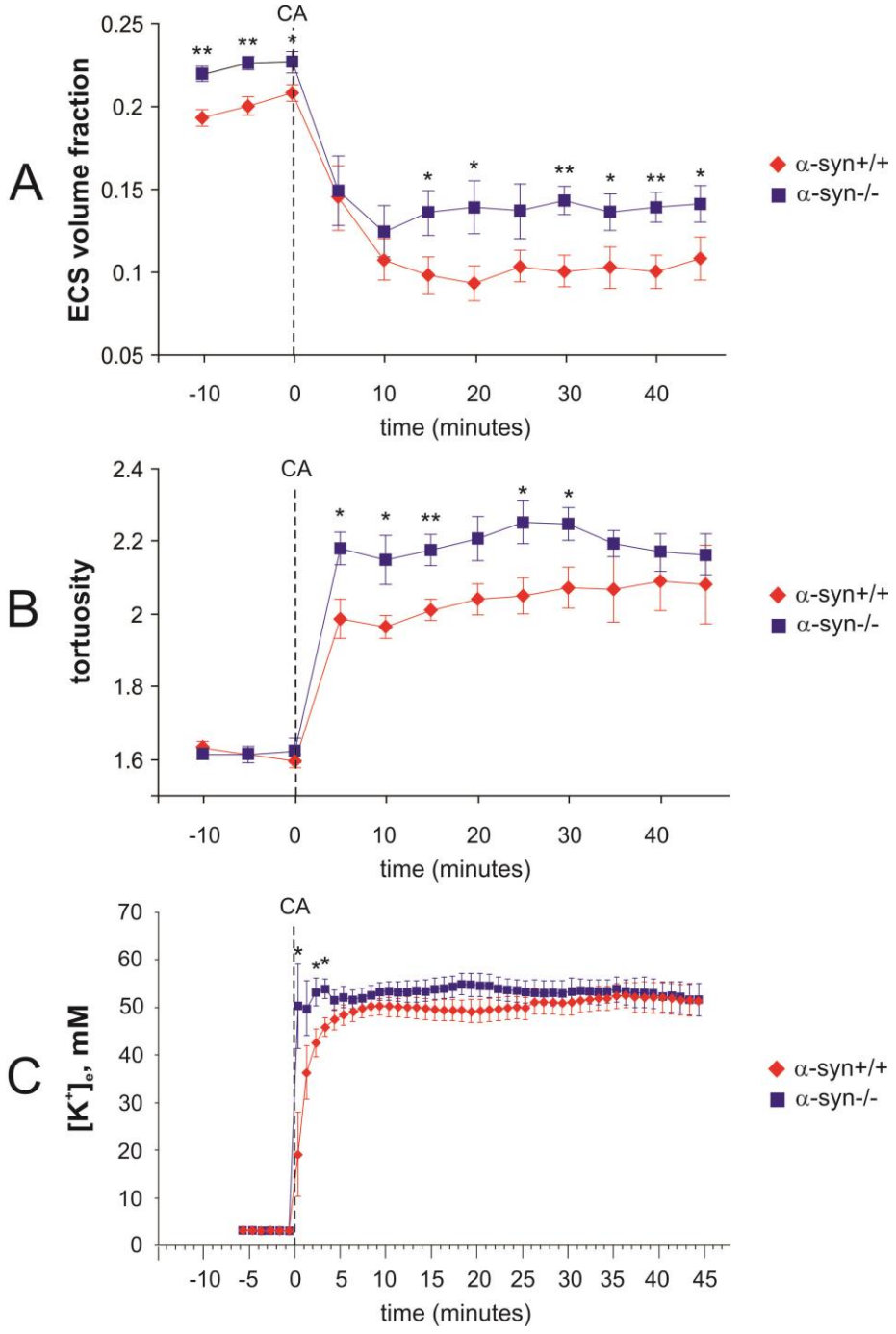

Fig. 30. Changes in the ECS diffusion parameters and $[K^+]_e$ evoked by terminal ischemia/anoxia *in vivo* in α-syn +/+ and α-syn -/- mice. Each data point represents mean ± S.E.M. The control values as well as the final values of the ECS volume fraction α **(A)** reached during terminal ischemia/anoxia evoked by cardiac arrest (CA) were significantly smaller in α-syn +/+ mice than in α-syn -/- animals. There was no significant difference in the control values of λ between α-syn +/+ and α-syn -/- mice **(B)**. After the onset of terminal ischemia/anoxia, tortuosity **(B)** as well as $[K^+]_e$ **(C)** were significantly higher in α-syn -/- mice compared to α-syn +/+ animals, but the final values did not differ. Asterisks (*- $p < 0.05$; **- $p < 0.01$) indicate significant differences between the values in α-syn +/+ and α-syn -/- animals.

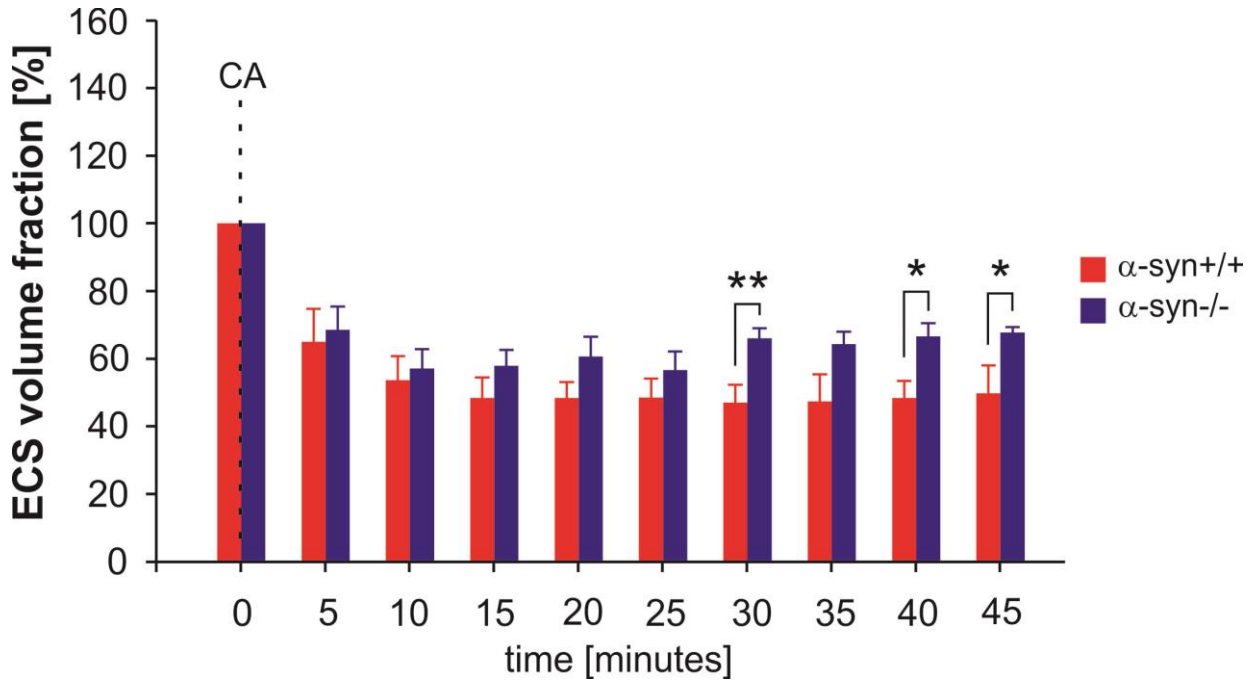

Fig. 31. Relative changes in the ECS volume fraction evoked by terminal ischemia/anoxia *in vivo* in α-syn +/+ and α-syn -/- mice. Each data point represents mean ± S.E.M, calculated in 5 min intervals for ECS volume changes and each minute for $[K^+]_o$ changes. Dashed line indicates the cardiac arrest. Asterisks indicate significant (*- $p < 0.05$) and very significant (**- $p < 0.01$) differences between α-syn +/+ and α-syn -/- mice.

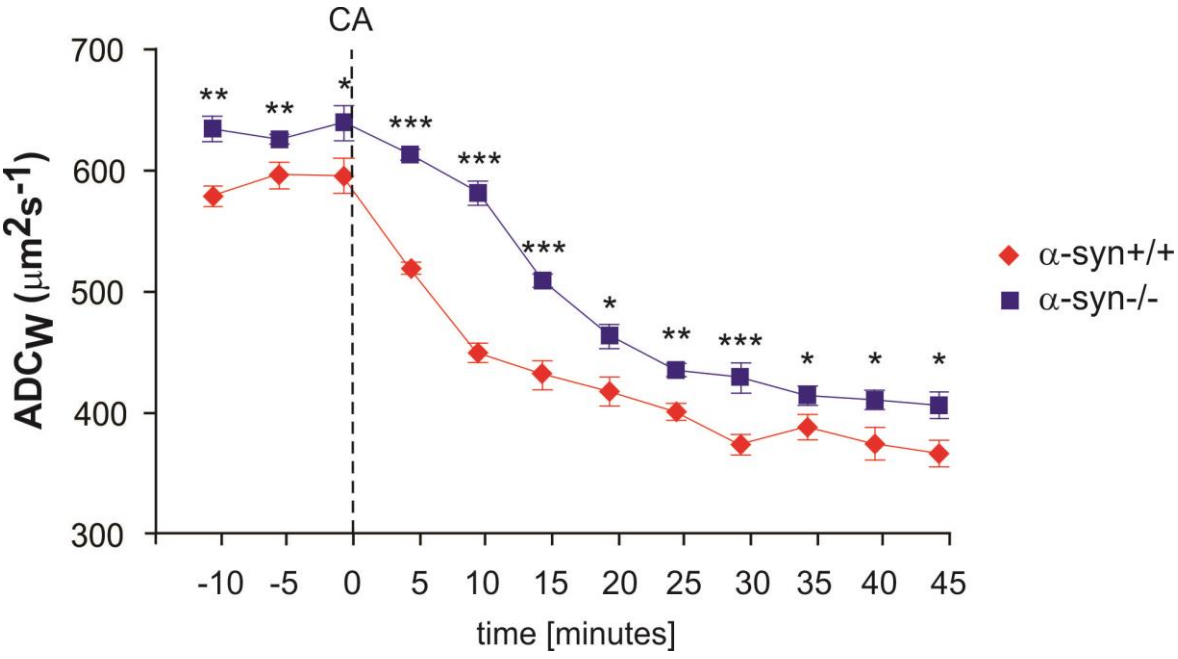

Fig. 32. Changes in ADC_W evoked by terminal ischemia/anoxia in α-syn +/+ and α-syn -/- mice. Each data point represents mean ± S.E.M. Asterisks (*- $p < 0.05$; **- $p < 0.01$; ***- $p < 0.001$) indicate significant differences between the values in α-syn +/+ and α-syn -/- animals.

4.2.5. Immunohistochemical analysis of astrocytes

Morphological differences between α-syn +/+ and α-syn -/- cortical astrocytes were analysed prior to, after a 30 min incubation in H-50, H-100 or 10 mM K^+, and after a 60 min washout. Immunohistochemical staining for GFAP showed no distinct differences in astrocytes in either group prior to incubation (Fig. 33).

The impact of α-syntrophin deficiency on astrocytic swelling was estimated by quantifying GFAP immunoreactivity in individual astrocytes from α-syn +/+ and α-syn -/- mice. We found that the swelling of α-syn -/- and α-syn +/+ astrocytes was comparable when exposed to hypotonic solution (H-50) (Fig. 33A); however, the swelling of α-syn -/- astrocytes was smaller during their exposure to a more severe hypotonic solution (H-100) or 10 mM K^+ (Fig. 33B and 33C, respectively). In each model of cell swelling, the analysis showed only a partial recovery of astrocytic volume during washout.

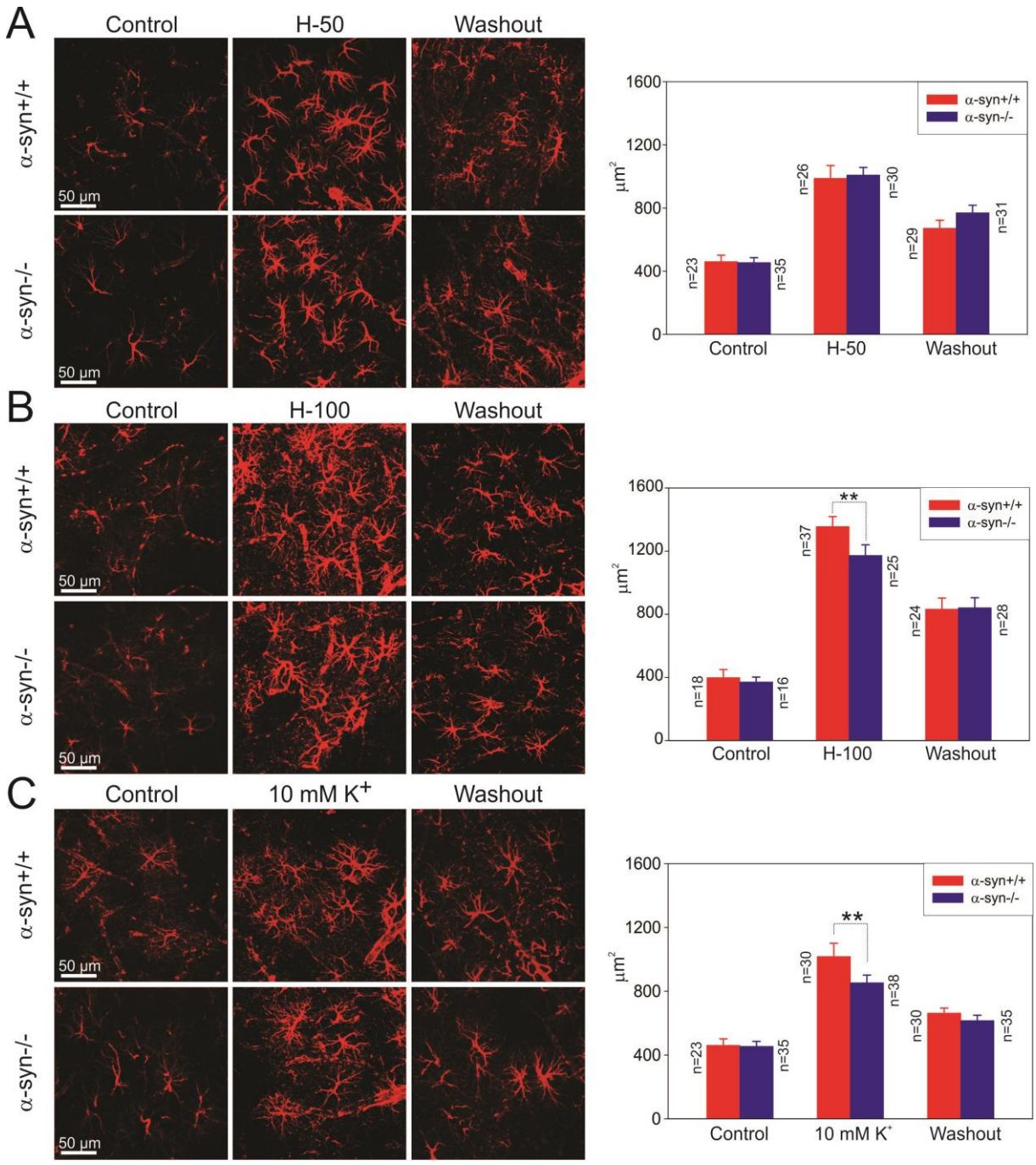

Fig. 33. Changes in astrocyte morphology evoked by hypotonic stress and elevated extracellular K^+ in α-syn +/+ and α-syn -/- mice. Changes in astrocyte morphology, based on changes in glial fibrillary acidic protein immunoreactivity, were determined in the cortex (layers III-IV) of α-syn +/+ and α-syn -/- mice: 1) prior to (control), 2) after a 30 minute application of hypotonic solutions (H-50 and H-100) or 10 mM K^+ and 3) following a 60 minute washout. The bar graphs on the right side indicate cell volume changes expressed as changes in the area corresponding to GFAP immunoreactivity.

4.3. ALTERED CELL SWELLING IN THE CORTEX OF ALPHA-SYNTROPHIN-NEGATIVE GFAP/EGFP MICE

Quantification of astrocytic swelling using GFAP staining is only approximate as these intermediate filaments do not fill the entire cell volume. Transgenic GFAP/EGFP mice, in which the enhanced green fluorescent protein (EGFP) is expressed under the control of the promoter for human glial fibrillary acidic protein (GFAP) (Nolte C. et al. 2001), allows for more detailed volume morphometry when using 3D confocal microscopy. To elucidate the impact of alpha-syntrophin deletion on astrocyte swelling, double transgenic mice (GFAP/EGFP/α-syn -/- mice) were generated by crossbreeding GFAP/EGFP mice and mice with a genetic deletion of α-syntrophin (α-syn -/-) (Vargova L. et al. 2013; Anděrová M. et al. submitted to Glia). We used RTI method to determine ECS diffusion parameter values in these animals and confirm their similar characteristic with α-syn -/- mice during resting conditions and experimental models of cell swelling. The results are a part of a study currently prepared for publication.

4.3.1. Control values of diffusion parameters in GFAP/EGFP/α-syn -/- and GFAP/EGFP *in vivo* and *in vitro*

We have employed RTI method with TMA^+ to show that the cortex of our newly generated transgenic mice displays similar characteristics with respect to changes in diffusion parameters observed in cortical slices of α-syn -/- mice during their exposure to pathological stimuli.

In agreement with our previous study comparing wild type and α-syn -/- mice, diffusion measurements in coronal slices *in vitro* as well as in the somatosensory cortex *in vivo* revealed significantly lower basal values of the ECS volume fraction α in GFAP/EGFP mice in comparison with GFAP/EGFP/α-syn -/- animals. There was no significant difference between these animal groups in the basal values of tortuosity λ or non-specific uptake k' (Table 4, 5).

4.3.2. Effects of hypotonic stress and elevated K^+ on ECS diffusion parameters in GFAP/EGFP and GFAP/EGFP/α-syn -/- *in vitro*

A 30 min application of mild (H-50) or severe (H-100) hypotonic solutions resulted in a significant decrease in ECS volume fraction α due to cell swelling in both GFAP/EGFP and GFAP/EGFP/α-syn -/- mice (Table 4). Since the basal values of α in GFAP/EGFP and GFAP/EGFP/α-syn -/- mice differed; we evaluated both absolute as well as relative changes of the ECS volume fraction. For a relative change analysis, the control values of all experiments were set to 100% and the relative changes in α during perfusion were calculated. During superfusion with H-50, we did not find any significant differences between GFAP/EGFP/α-syn -/- and GFAP/EGFP mice either in the absolute values of α or in its relative change (Table 4, Fig. 34A). However, the exposure to more severe hypotonic stress revealed that deletion of α-syntrophin attenuates cell swelling-induced decrease in α in both absolute as well as relative values (Table 4, Fig. 34A; 35A). During washout following H-50 or H-100 perfusion, the absolute and relative values of α returned to their control values or even slightly overshot them in both GFAP/EGFP and GFAP/EGFP/α-syn -/- animals (Fig. 34A, C, Table 4). Changes in λ or k' evoked by H-50 or H-100 application were insignificant in both animal groups (Table 4).

A decrease in α observed during a 30 min superfusion with 10 mM K^+ was significantly smaller in GFAP/EGFP/α-syn -/- mice than in GFAP/EGFP animals in both absolute as well as relative values (Table 4, Fig. 34E; 35C). During washout, the values of α overshot the control values in GFAP/EGFP mice, but not in GFAP/EGFP/α-syn -/- animals (Fig. 34E). Relative ECS volume changes during washout showed larger and faster recovery in GFAP/EGFP than in GFAP/EGFP/α-syn -/- mice (Fig. 35C). A small increase in λ evoked by 10 mM K^+ did not differ between both animal groups; the changes in k' were not significant (Table 4).

Table 4. Effect of hypotonic stress and elevated K^+ on the ECS diffusion parameters in GFAP/EGFP and GFAP/EGFP/α-syn -/- mice *in vitro*.

	GFAP/EGFP				**GFAP/EGFP/α-syn -/-**			
	α	λ	k' x $10^{-3}s^{-1}$	**n/N**	α	λ	k' x $10^{-3}s^{-1}$	**n/N**
control values	0.189 ± 0.002	1.514 ± 0.011	11.115 ± 1.004	26/16	0.217 ± 0.003***	1.523 ± 0.010	9.023 ± 0.731	32/22
H-50	0.149 ± 0.007###	1.553 ± 0.031	10.465 ± 1.756	6/4	0.168 ± 0.012###	1.582 ± 0.033	12.242 ± 0.939	5/4
wash-out	0.215 ± 0.011	1.558 ± 0.023	9.318 ± 1.186		0.211 ± 0.026	1.601 ± 0.029	10.452 ± 1.025	
H-100	0.089 ± 0.012###	1.559 ± 0.068	13.955 ± 2.581	7/4	0.156 ± 0.009***###	1.557 ± 0.059	9.795 ± 1.795	7/7
wash-out	0.205 ± 0.005	1.565 ± 0.072	10.449 ± 1.655		0.274 ± 0.019***###	1.532 ± 0.043	8.191 ± 1.631	
10 mM K^+	0.087 ± 0.018###	1.582 ± 0.034#	14.316 ± 2.493	7/5	0.161 ± 0.012***###	1.590 ± 0.027	10.620 ± 1.766	7/6
wash-out	0.218 ± 0.012#	1.583 ± 0.050	10.972 ± 1.649		0.205 ± 0.011	1.558 ± 0.023	8.943 ± 1.222	

The values are presented as mean ± S.E.M. Asterisks (*- $p < 0.05$; **- $p < 0.01$; ***- $p < 0.001$) indicate significant differences between the values in GFAP/EGFP and GFAP/EGFP/α-syn -/- animals; crosshatches (#- $p < 0.05$; ##- $p < 0.01$; ###- $p < 0.001$) indicate significant differences between control values and those obtained under experimental conditions in the same group of animals. The control values of the ECS diffusion parameters from each individual experiment were calculated as the average values extracted from three diffusion curves before application. The mean control value presented in the table is the average of the control values from all *in vitro* experiments. The mean values of the maximum change during application correspond to the 30th minute of application; the values for washout correspond to the data point at the 90th min. Abbreviations: extracellular space volume fraction (α), tortuosity (λ), non-specific uptake (k'), number of animals (N), number of slices (n), hypotonic solutions (H-50 and H-100).

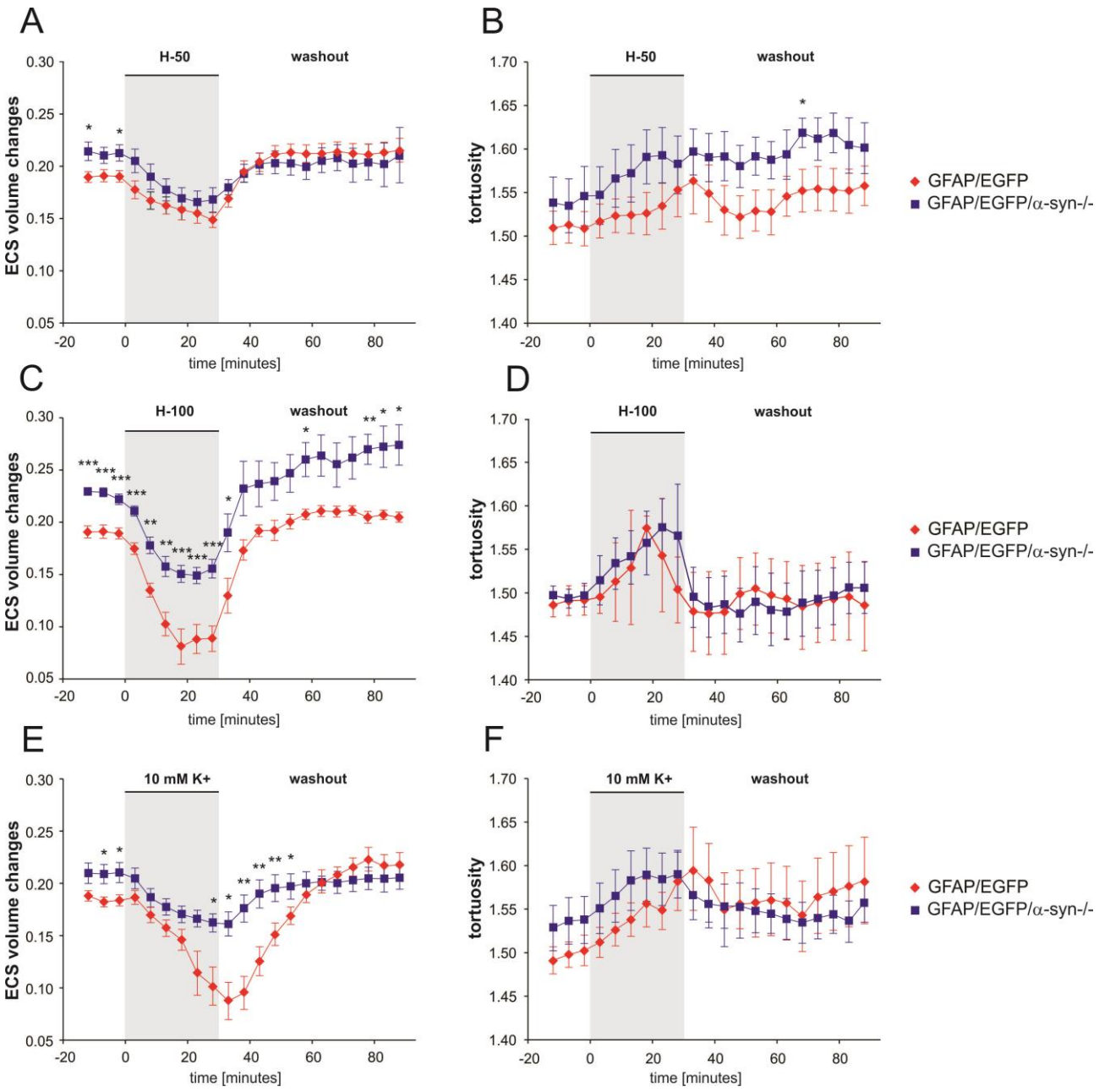

Fig. 34. The effect of hypotonic solutions and 10 mM K^+ on ECS diffusion parameters *in vitro* in GFAP/EGFP and GFAP/EGFP/α-syn -/- mice. The absolute values of the extracellular volume fraction (α) and tortuosity (λ) were measured in cortical slices from the somatosensory cortex of GFAP/EGFP and GFAP/EGFP/α-syn -/- mice during a 30 min application of hypotonic solution H-50 (-50 mOsmol/l) **(A, B)** and H-100 (-100 mOsmol/l) **(C, D)** or 10 mM K^+ **(E, F)** and during washout. Each data point represents mean ± S.E.M. Asterisks (*- $p < 0.05$; **- $p < 0.01$; ***- $p < 0.001$) indicate significant differences between the values in GFAP/EGFP and GFAP/EGFP/α-syn -/- animals.

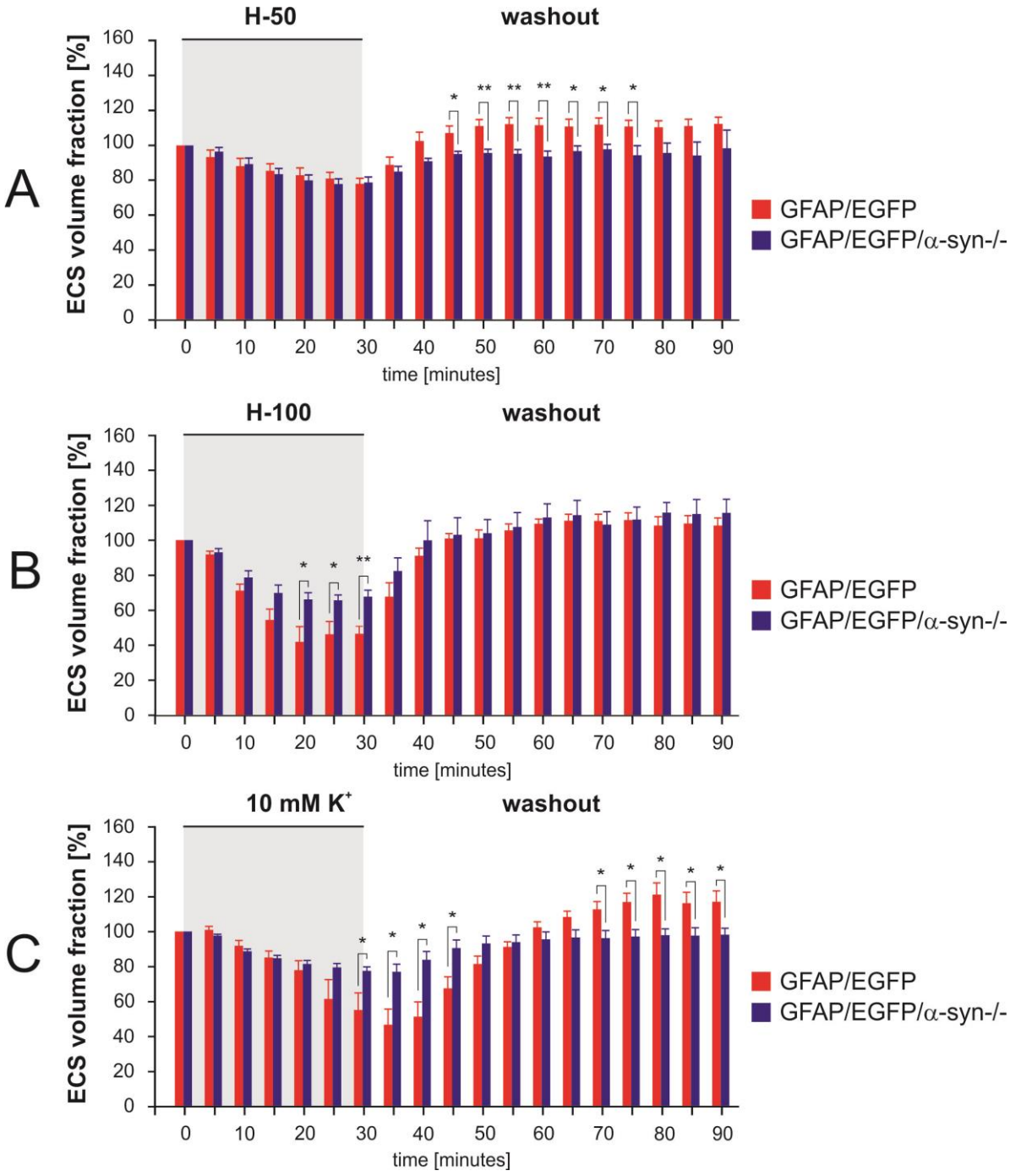

Fig. 35. The effect of hypotonic stress or elevated K^+ on the relative changes of the ECS volume *in vitro* in GFAP/EGFP and GFAP/EGFP/α-syn -/- mice. The control values of all experiments were set to 100% and the relative changes of values of the extracellular volume fraction α were calculated in 5 min intervals during 30 min application and subsequent 60 min washout of mild (**A**) or severe (**B**) hypotonic stress or 10 mM K^+ (**C**). Each data point represents mean ± S.E.M. Asterisks indicate significant (*- $p < 0.05$) and very significant (**- $p < 0.01$) differences between GFAP/EGFP and GFAP/EGFP/α-syn -/- mice.

4.3.3. Effect of ischemia/anoxia on ECS diffusion parameters in GFAP/EGFP and GFAP/EGFP/α-syn -/- mice

Terminal ischemia/anoxia due to cardiac arrest evoked by administration of $MgCl_2$ resulted in dramatic changes in both ECS volume fraction α and tortuosity λ. The minimal absolute values of α reached after cardiac arrest were larger in GFAP/EGFP/α-syn -/- mice than in GFAP/EGFP animals and the time course of relative changes of α indicated slower and smaller changes in GFAP/EGFP/α-syn -/- animals compared to GFAP/EGFP animals (Table 5; Fig. 36A; 37). In contrast, λ in GFAP/EGFP/α-syn -/- mice reached higher maximum than in GFAP/EGFP animals (Table 5, Fig. 36B), suggesting larger/faster formation of additional diffusion barriers.

A steep rise of $[K^+]_e$ immediately after the onset of terminal ischemia/anoxia was faster and reached its maximum in α-syn -/- animals at about 3 min after cardiac arrest. In GFAP/EGFP animals, the $[K^+]_e$ increase was gradual and slower, reaching the highest point at the 9th minute, with the maximum value significantly lower than in GFAP/EGFP/α-syn -/- animals (Table 5; Fig. 36C).

Table 5. Effect of terminal ischemia/anoxia on the ECS diffusion parameters and extracellular K^+ concentration in GFAP/EGFP and GFAP/EGFP/α-syn -/- mice *in vivo*.

	GFAP/EGFP				**GFAP/EGFP/α-syn -/-**			
	control values	**N**	**terminal ischemia/anoxia**	**N**	**control values**	**N**	**terminal ischemia/anoxia**	**N**
α	0.193 ± 0.002	6	0.122 ± 0.010$^{\#\#\#}$	6	0.224 ± 0.004***	6	0.164 ± 0.006$^{*\#\#\#}$	6
λ	1.600 ± 0.014††	6	1.893 ± 0.026$^{\#\#\#}$	6	1.640 ± 0.012†††	6	2.262 ± 0.086$^{*\#\#\#}$	6
k' **x10^{-3} s^{-1}**	4.309 ± 0.295†	6	6.607 ± 3.018	6	3.522 ± 0.447††	6	5.779 ± 1.570	6
$[K^+]_e$ (mM)	2.847 ± 0.052	6	57.180 ± 2.426$^{\#\#\#}$	5	2.877 ± 0.116	6	71.210 ± 1.879$^{\#\#\#}$	5

The values are presented as mean ± S.E.M. Asterisks (*- p < 0.05; **- p < 0.01; ***- p < 0.001) indicate significant differences between the values in GFAP/EGFP and GFAP/EGFP/α-syn -/- mice; crosshatches (#- p < 0.05; ##- p < 0.01; ###- p < 0.001) indicate significant differences between control values and those obtained under experimental conditions in the same group of animals and crosses (†- p < 0.05; ††- p < 0.01; †††- p < 0.001) indicate significant difference between values *in vitro* and *in vivo*.

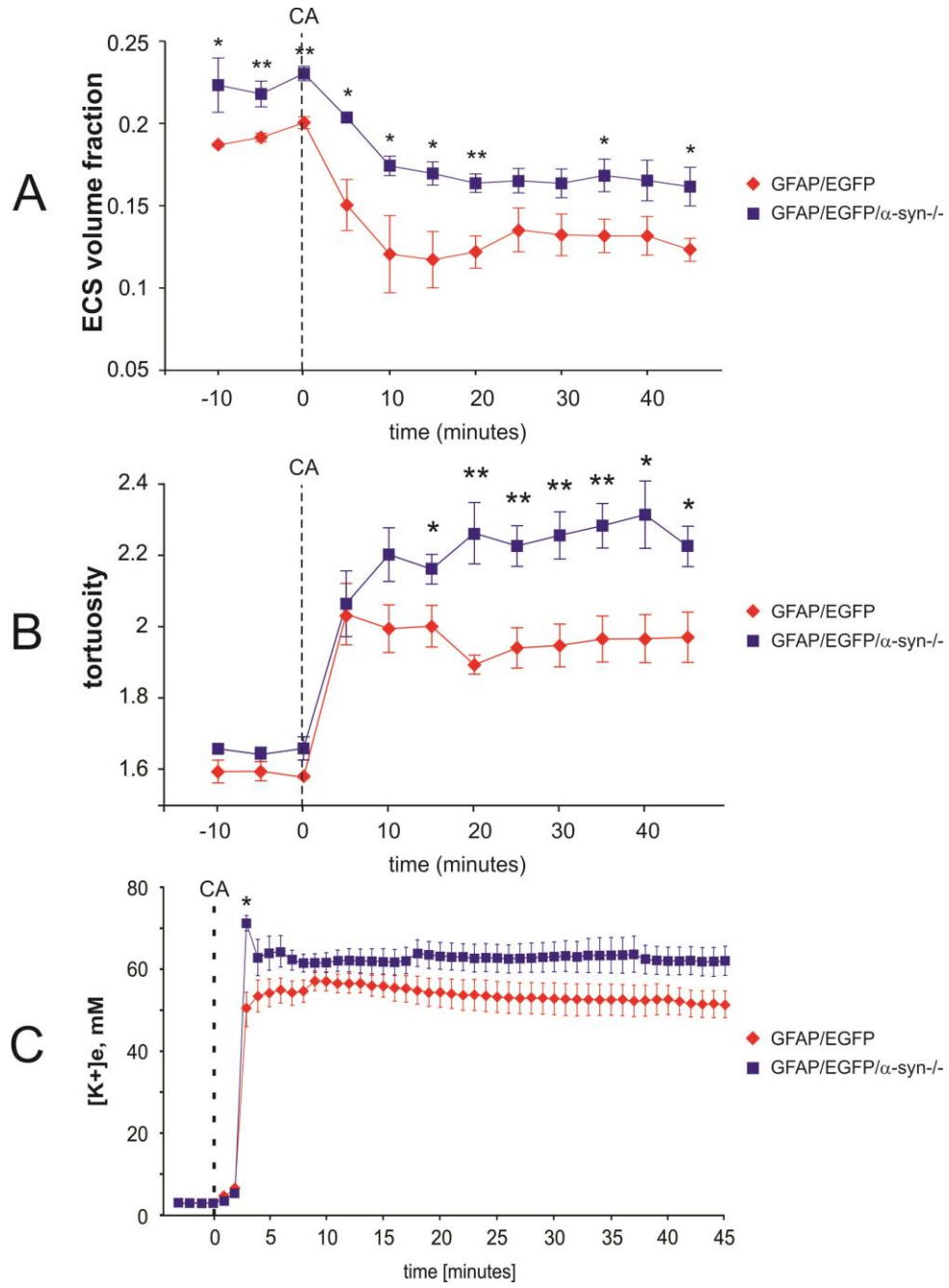

Fig. 36. Changes in the ECS volume fraction and $[K^+]_o$ evoked by terminal ischemia/anoxia *in vivo* in GFAP/EGFP and GFAP/EGFP/α-syn -/- mice. Each data point represents mean ± S.E.M. The control values as well as the final values of the ECS volume fraction α **(A)** reached during terminal ischemia/anoxia evoked by cardiac arrest (CA) were significantly smaller in GFAP/EGFP mice than in GFAP/EGFP/α-syn -/- animals. There was no significant difference in the control values of λ between GFAP/EGFP and GFAP/EGFP/α-syn -/- **(B)**. A steep rise in $[K^+]_e$ level (**C**) was higher and faster in GFAP/EGFP/α-syn -/- mice compared to GFAP/EGFP animals, with no difference in the final values. Asterisks (*- $p < 0.05$; **- $p < 0.01$; ***- $p < 0.001$) indicate significant differences between the values in GFAP/EGFP and GFAP/EGFP/α-syn -/- mice.

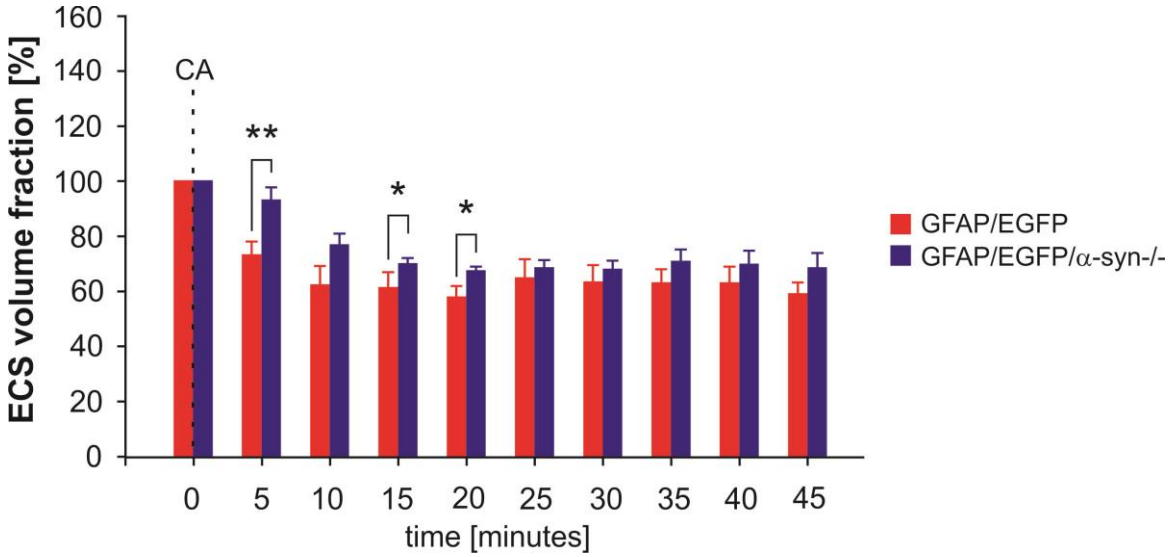

Fig. 37. Relative changes in the ECS volume fraction evoked by terminal ischemia/anoxia *in vivo* in GFAP/EGFP and GFAP/EGFP/α-syn -/- mice. Each data point represents mean ± S.E.M, calculated at 5 min intervals for ECS volume changes. The relative changes in the values of the ECS volume fraction α after the onset of terminal ischemia/anoxia were significantly smaller and slower in GFAP/EGFP/α-syn -/- mice than in GFAP/EGFP controls, but the final values did not differ. Dashed line indicates the cardiac arrest. Asterisks indicate significant (*- $p < 0.05$) and very significant (**- $p < 0.01$) differences between GFAP/EGFP and GFAP/EGFP/α-syn -/- mice.

5. DISCUSSION

The aims of this investigative work have been to study the effect of acute cell swelling on the ECS diffusion parameters on *in vivo* models of pilocarpine-induced status epilepticus and terminal ischemia/anoxia induced by cardiac arrest. Moreover, the influence of the α-syn deletion on the ECS diffusion parameters was investigated on *in vitro* models of hypotonic and hyperkalemic stress.

5.1. Pilocarpine-induced status epilepticus

The initiation and early expression of seizures induced by pilocarpine are a cholinergic phenomenon; anticholinergics readily terminate seizures at this stage and no neuropathology is evident. Following the toxicity induced by an initial cholinergic phase, a distinct noncholinergic phase occurs, in which excessive glu^- release induces SE in this epilepsy model (McDonough J. H., Jr. and Shih T. M. 1997).

To induce SE in urethane anesthetized animals, we used a high dose of pilocarpine in combination with lithium chloride pre-treatment (Stringer J. L. and Sowell K. L. 1994). Although it is difficult to induce status epilepticus under anaesthesia, records of local field potentials showed epileptiform neuronal activity, and the levels of K^+ reached were (Stringer J. L. and Lothman E. W. 1996) comparable to values measured during status epilepticus. We believe that our model, with some limitation due to the use of anaesthesia, is comparable with SE in awake animals.

Changes in cerebral energy metabolism during status epilepticus

To monitor changes in cerebral energy metabolism during SE, we used microdialysis. During the initial stadium of SE, our results show that glucose levels in the extracellular space increase (Fig. 25C). These results are supported by another microdialysis study of Darbin and co-authors (Darbin O. et al. 2005), who showed an increase in extracellular glucose concentration in the rat striatum after maximal electroshock. The decrease of ECS space volume is possibly a factor contributing to the transient increase of glucose concentration.

However, as seizures continue high cerebral metabolic rates (Fernandes M. J. et al. 1999), caused by increased uptake and glycolysis during increased neuronal activity in SE (Fray A. E. et al. 1997), could be the cause of the subsequent decrease in glucose concentration starting 1 h after pilocarpine administration and continuing until the end of the experiments.

Increased glycolysis resulted in the consumption of glucose and production of lactate, which is transported into the extracellular space. This is supported by our results, in which a decrease in glucose is accompanied by an increase in lactate levels. Such an increase in lactate levels in selected brain regions during seizures was also seen previously (Darbin O. et al. 2005; During M. J. et al. 1994; Fornai F. et al. 2000; Kuhr W. G. and Korf J. 1988; 1988). These studies demonstrated that epileptic activity increases the levels of lactic acid in those areas that are recruited during seizure propagation. This is in agreement with our results, which show an increase in lactate concentrations during SE. We also found that with decreasing amplitude of the ictal discharges, elevated lactate levels recovered to initial values. In activated brain areas the increase in energy demands exceeds the glucose supply (Adachi K. et al. 1995). Under these conditions the increased lactate levels might be utilized by neurons as an alternative energy supply (Schurr A. et al. 1999; Schurr A. et al. 1997; Schurr A. et al. 1988). This normalization must represent the uptake and utilization of lactate by neurons and astrocytes, because no significant transport of lactate across the blood–brain barrier has been found (Kuhr W. G. et al. 1988). The increase of ECS volume in the last 2 h of our experiments is another possible contribution to the normalization of extracellular lactate concentrations during the same time period.

In addition to lactate levels as a marker for anaerobic metabolism, the tissue-specific Lactate/Pyruvate ratio is an excellent indicator of cellular hypoxia, since it is closely correlated with the redox potential (Kuhr W. G. et al. 1988; Zoremba N. et al. 2007). In this study, we have found an increase in the Lactate/Pyruvate ratio during SE (Fig. 26B), indicating an increase in anaerobic glycolysis. The extracellular space volume did not affect the changes that were seen in the Lactate/Pyruvate ratio in any way, since the ratio between two extracellular substances that are subject to the same correction coefficient clearly remains unaffected by the value of that coefficient, and the diffusion coefficients of these substances are nearly equal.

Increased glutamatergic transmission is regarded as one of the possible causes of seizure origination (Bradford H. F. 1995). *In vivo* microdialysis data have shown increases in extracellular glu^- concentrations during epileptic seizures in the hippocampus (Pena F. and Tapia R. 1999; Slezia A. et al. 2004) and striatum (Kovacs A. et al. 2003) of 4-

aminopyridine-treated rats and in the hippocampus of kainic acid- (Liu Z. et al. 1997) and pilocarpine- (Khan G. M. et al. 1999; Smolders I. et al. 1997) treated rats. Many experiments have supported the view that the extent of glu^- release during epileptic seizures is so great that uptake is not able to re-establish the normal glutamate concentration and the excess of glu^- spreads by diffusion, activating neurons via extra-synaptic receptors (Bradford H. F. 1995). Most of the damage induced by seizure activity is generated by glutamatergic neurotransmission-driven excitotoxicity (Whetsell W. O., Jr. 1996). 10–100 μM glu^- is toxic to neurons grown in culture (Choi D. W. 1988), but neurons *in vivo* are less vulnerable due to the presence of highly effective uptake carriers (Bruhn T. et al. 1992). Elevation of the extracellular levels of endogenous glu^- *per se* is not sufficient for the induction of neuronal degradation. Other factors that facilitate the overactivation of excitatory amino-acid receptors, for instance hyperexcitation present during seizures, seem to be necessary to induce neuronal damage. Sustained activation of the NMDA receptor as a result of excess extracellular glu^- would allow the additional entry of Ca^{2+} into the neuron which, in conjunction with the sustained repetitive depolarization of neurons by the seizure, could allow free Ca^{2+} levels in the neuron to build up to toxic amounts and produce the subsequent neuropathology. The maximum increase in extracellular glu^- levels was observed over the same time interval as the maximum decrease in ECS volume fraction. Thus, we suggest that a substantial amount of this increase in glu^- was caused by the shrinkage of the ECS.

Changes in the ECS diffusion parameters and in $[K^+]_e$

Acute experimental convulsions increase $[K^+]_e$ and the extracellular concentrations of various transmitter substances due to prolonged neuronal depolarization (Macias W. et al. 2001). With SE, the metabolism is markedly increased, resulting in the depletion of adenosine triphosphate and energy reserves at its later stage. Consequently, this results in impaired ion exchange pump functions and increased membrane ion permeability of the cells, resulting in an increase in $[K^+]_e$ and the accumulation of intracellular Ca^{2+} (Wasterlain C. G. et al. 1993). The increase in $[K^+]_e$ and changes in pH_e is followed by cell swelling and compensatory shrinkage of the ECS (Sykova E. et al. 1994; Sykova E. et al. 1999). The dependence of changes in α caused by cellular swelling on changes in $[K^+]_e$ is also demonstrated in our results. The increase of $[K^+]_e$ and the decrease of α start in the first minutes after the pilocarpine injection as a consequence of increased neuronal activity after cholinergic

activation (McDonough J. H., Jr. and Shih T. M. 1997), while normalization of elevated $[K^+]_e$ leads to a quick normalization of α to the control values. The onset of the first ictal discharges comes later, about 30 min after pilocarpine injection. A more pronounced increase in the discharge amplitude follows 40–50 min after pilocarpine application, when the ECS volume is about 30% smaller than its initial value, showing the possible contribution of ECS volume reduction to the initiation of SE (Kilb W. et al. 2006).

5.2. The effect of α-syntrophin deletion on ECS diffusion parameters

Using the real-time iontophoretic method both *in vivo* and *in vitro*, we have demonstrated that the ECS volume fraction under resting conditions is higher in mice lacking the α-syntrophin protein, while there was no difference in tortuosity between wild-type and α-syntrophin-deficient mice, which is in agreement with another TMA study performed on AQP4-deficient mice *in vivo* (Yao X. et al. 2008). Studies using electron microscopy have revealed that perivascular and subpial astroglial end-feet are swollen in the brains of α-syn -/- mice in the basal state, compared to α-syn +/+ animals, indicating the compensatory shrinkage of the surrounding ECS (Amiry-Moghaddam M. et al. 2003). Thus, it was suggested that α-syn-deficient mice have a reduced clearance of the water generated by brain metabolism and that AQP4 channels facilitate the release of water from astrocytes into the brain capillaries under resting conditions. It may seem controversial that our study shows a higher ECS volume fraction in α-syn -/- mice, but the RTI-TMA method describes the average properties of the ECS over a range of about 0.5 mm^3, including the extracellular volume around the somata and processes. Interestingly, Zeynalov and colleagues (Zeynalov E. et al. 2008) have found reduced brain water content in α-syn -/- animals with no differences in the baseline level of serum osmolality. However, a recent study by Haj-Yasein and co-authors (Haj-Yasein N. N. et al. 2011) on glial-conditional AQP4-deficient animals showed increased brain water content and delayed postnatal water resorption, which may be associated with an increased ECS volume.

Moreover, our measurements in coronal slices have also revealed higher control values of α and k', but smaller control values of λ than those found under *in vivo* conditions. Small differences between the ECS diffusion parameters measured *in vitro* and *in vivo* have been

reported previously (Sykova E. and Nicholson C. 2008) and may result from increased water accumulation in the tissue (increased α and k') and from cut cell processes and/or washing out of the extracellular matrix (decreased λ) in slices.

Mild and severe hypotonic stress

As revealed by a previous study in α-syn -/- mice, most of the AQP4 channels disappeared from the astrocytic end-feet that face blood vessels with unchanged total number of brain AQP4 channels, suggesting that α-syntrophin protein regulates AQP4 localization in the astrocytic end-feet (Amiry-Moghaddam M. et al. 2004). The redistribution of AQP4 channels without any decrease in their total number may explain the fact that we did not detect a significant difference in the relative ECS volume decrease between α-syn +/+ and α-syn -/- mice during mild hypotonic stress. However, since mice with α-syn deletion have a larger ECS volume fraction under control conditions, the absolute values of α during hypotonic stress do not decrease as much as in α-syn +/+ mice; this means that neuroactive substances might reach a neurotoxic concentration more slowly. The differences between α-syn +/+ and α-syn -/-, and between GFAP/EGFP and GFAP/EGFP/α-syn -/- mice, in terms of relative decrease in α, were revealed only by the more severe hypotonicity of the perfusing solution (H-100); indicating that water transport through aquaporin channels becomes more important during pathological conditions then during physiological states. This hypothesis is supported by the fact that an increase in non-specific uptake during either severe hypotonic stress, increased potassium concentration, or ischemic conditions, which reflects changes in the permeability of the cell membranes and/or capillaries and might be an additional factor affecting transmembrane ion and water movement and thus cell swelling, did not differ between α-syn +/+ and α-syn -/- mice.

Hyperkalemic stress

The application of 10 mM K^+ evoked more pronounced changes in ECS volume than did mild hypotonic stress and highlighted the differences between α-syn +/+ and α-syn -/- mice, as well as between GFAP/EGFP and GFAP/EGFP/α-syn -/- animals. This may be due to the

more complex mechanisms occurring in the tissue during $[K^+]_e$ elevation, which involve KCl uptake through Na^+-K^+-$2Cl^-$ co-transporters; creating a driving force for the influx of water (Kimelberg H. K. et al. 1995) and the release of excitatory amino acids (EAA) from astrocytes, which is mediated by volume-sensitive organic anion channels (Su G. et al. 2002) or the different proportion of swelling between the cell soma and the processes.

Terminal ischemia/anoxia

Global or terminal ischemia/anoxia represents a severe pathological condition with massive cell swelling and a dramatic increase in extracellular potassium (Vorisek I. and Sykova E. 1997). It leads to the activation of many volume regulatory mechanisms, such as the increased release of glu^-, aspartate, chloride and taurine, which help reduce the intracellular water volume (Kimelberg H. K. et al. 1995).

Our *in vivo* results show that 30 min after the induction of terminal ischemia/anoxia, the ECS volume fraction was larger in α-syn-deficient mice, indicating less cell swelling. These results correspond to our *in vitro* measurements and to recent studies showing that in α-syn -/- mice brain edema is reduced and attenuated during transient cerebral ischemia (Amiry-Moghaddam M. et al. 2003) and during acute water intoxication (Manley G. T. et al. 2000). Despite the larger ECS volume fraction in α-syn-deficient animals, the tortuosity values during the early phase (up to 35 min) of terminal ischemia/anoxia were higher in both strains of α-syn-deficient mice in comparison to their α-syn-positive controls. Final values of tortuosity between α-syn +/+ and α-syn -/- did not significantly differ, while final values of tortuosity in GFAP/EGFP/α-syn -/- were higher compared to those of GFAP/EGFP animals. This suggests the appearance of additional diffusion barriers in the ECS due to structural changes probably associated with the higher extracellular K^+ concentration under ischemic conditions in mice lacking α-syntrophin. Indeed, our current data as well as our previous studies have shown that increased K^+ induces morphological changes, especially in fine astrocytic processes, that are associated with a large increase in tortuosity (Sykova E. et al. 1999).

Moreover, it was also shown that pre-exposure to high K^+ concentrations, an early event leading to astrogliosis, causes not only morphological changes in astrocytes, but also changes in their membrane properties and cell volume regulation (Neprasova H. et al. 2007). The

smaller degree of astrocyte swelling after high potassium pre-exposure may thus contribute to the smaller decrease in ECS volume found in the α-syn-deficient cortex after the induction of terminal ischemia/anoxia.

Our *in vivo* data shows that the onset of the steep rise in $[K^+]_e$ directly after terminal ischemia/anoxia induction is faster and reaches higher values in α-syn-deficient mice, compared to α-syn-positive animals. This fast, steep rise of $[K^+]_e$ in α-syn-deficient mice reflects the inability of astrocytes to distribute K^+ in the extracellular space by spatial buffering; a finding that is in agreement with previous studies showing altered K^+ clearance in AQP4 knock-out mice (Amiry-Moghaddam M. et al. 2003; Strohschein S. et al. 2011). These results support the finding that AQP4 channels have a functional relationship with inwardly rectifying K^+ channel subunit 4.1 (Kir4.1), which is involved in spatial buffering (Nagelhus E. A. et al. 1999). Biochemical data also indicates that AQP4 and Kir4.1 proteins might be part of the same complex (Guadagno E. and Moukhles H. 2004). However, a recent study performed using glia-specific conditional Kir4.1 knockout mice (cKir4.1 -/-) showed altered spatial buffering of K^+ with an unchanged distribution of AQP4 channels in these animals (Guadagno E. and Moukhles H. 2004), indicating that the exact relationship between Kir4.1 and AQP4 has not yet been fully clarified (Haj-Yasein N. N. et al. 2011).

Quantification of the changes in GFAP immunoreactivity

Quantifying the changes in GFAP immunoreactivity disclosed that the knockout of α-syn alters astrocyte swelling when exposed to H-100 hypoosmotic solution or 10 mM K^+. The finding, that the application of H-50 hypotonic solution was not sufficient to reveal such alterations in astrocyte swelling, further supports the hypothesis that AQP4 channels play a role mostly during intensive stimuli.

Nevertheless, it should be considered that as the intermediate filaments do not fill the entire cell volume, quantification of GFAP staining only reveals an approximate estimation of astrocytic volume changes in general. Thus, the supposed control cell volume in our morphometry analysis may be underestimated and the real relative change during cell swelling might be smaller.

It is evident from our study that changes in astrocytic volume estimated from GFAP immunoreactivity and changes in ECS volume are not in direct relationship. While GFAP

analysis showed only a partial recovery of astrocytic volume after experimentally evoked cell swelling, the RTI method detected a full recovery or even an overshoot in the values of the ECS volume fraction α. A possible explanation of these observations is that the ECS volume changes, measured by the RTI method, reflect reciprocally the volume changes in all cellular elements of the tissue, including neurons, oligodendrocytes, polydendrocytes, microglia, pericytes, and endothelial cells. As a result, it can be hypothesized that intense volume regulation of some of these cell types may compensate for the insufficient recovery of astrocytes. Moreover, it is important to realize that staining for GFAP is rather limited to the primary and secondary processes. Thus, a rebuilding of the tertiary or quaternary processes, which might be associated with the formation of additional diffusion barriers and a persistent increase in tortuosity after increased K^+ application, cannot be detected. A more detailed evaluation of the possible fine structural changes in the finest astrocytic processes is required, which would bring additional information about astrocyte swelling/volume recovery in the cortex of α-syn -/- mice, e.g., using 3D confocal morphometry to analyze astrocytes expressing enhanced green fluorescent protein under the control of the human GFAP promoter (Benesova J. et al. 2009; Pivonkova H. et al. 2010). Therefore, double transgenic mice (GFAP/EGFP/α-syn -/- mice) were generated by crossbreeding GFAP/EGFP mice and mice with a genetic deletion of α-syntrophin (α-syn -/-). ECS diffusion parameter measurements were performed in double transgenic animals to confirm their similar characteristic with α-syn -/- mice during resting conditions and cell swelling.

The obtained results indicate that the responds of GFAP/EGFP/α-syn -/- and GFAP/EGFP animals to selected experimental models of cell swelling is similar to that of α-syn -/- and α-syn +/+ mice, respectively. We can therefore assume that GFAP/EGFP/α-syn -/- mice display similar characteristic as α-syn -/- animals and the results of further analysis of astrocytic volume subtle morphological changes using 3D confocal microscopy can be valid for both groups.

5.3. Correlation between ECS diffusion parameters and ADC_W changes during acute cell swelling

The first report of the use of DW-MRI in epilepsy is from Zhong and colleagues (Zhong J. et al. 1993), who documented early ADC_W decrease in a model of bicuculline-induced SE in

rats. By using the experimental model of kainic acid-induced SE in rats, it has been shown that postictal ADC_W decreased in the piriform cortex, hippocampus, and amygdala within 24 h with subsequent normalization (Righini A. et al. 1994; Wang Y. et al. 1996). Using pilocarpine induced seizures, van Eijsden et al. (van Eijsden P. et al. 2004) and Wall et al. (Wall C. J. et al. 2000) observed an ADC_W decrease in the amygdala and the piriform cortex within the first hours after pilocarpine application in rats. Also, a recent study by Fabene et al. (Fabene P. F. et al. 2006) showed a decrease of ADC_W throughout the brain 2 h after a 4-aminopyridine injection in rats. Our DW-MRI results are in agreement with previous works and show, as we know, for the first time in detail the entire time course of the start, maximal decrease and renormalization of ADC_W in somatosensory cortex during SE.

To the best of our knowledge, the results of our extracellular diffusion parameter measurements represent the first time the absolute values of the cortical diffusion parameters have been determined *in vivo* during SE. In our previous studies we demonstrated (Sykova E. et al. 2005) that changes in extracellular volume fraction correlate with changes in ADC_W, as we confirmed also in this study. Correlating the RTI and DW-MRI methods is not simple. While the RTI method measures the geometrical and viscosity parameters of the extracellular space, DW-MRI measures the overall diffusion coefficient in the tissue. Changes in ADC_W usually correlate well with changes in the ECS parameters during physiological states as well as in various pathologies (Vorisek I. and Sykova E. 2009). This is because geometrical changes in the ECS are related to water movement between compartments with different diffusion coefficients (i.e., the extracellular and intracellular space). On the other hand, ADC_W also reflects diffusion in the intracellular space and so-called dead spaces that cannot be reached by diffusing TMA^+ molecules. Moreover, since ADC_W reflects both α and λ changes, the correlation between ADC_W and the ECS diffusion parameters is valid only for acute cell swelling such as ischemia/anoxia and not for chronic states with the formation of additional diffusion barriers (Vorisek I. and Sykova E. 2009). The ECS diffusion parameters provide important information for experimental and clinical neuroscience research. However, the methods employed for the direct measurement of these parameters, such as RTI, fluorescence recovery after photobleaching or integrative optical imaging, are less suitable for clinical use because of their invasiveness. On the other hand, the non-invasiveness, good spatial resolution and widespread availability of suitable scanners have made DW-MRI an important tool for studying diffusion parameters in the brain in clinical research. Although DW-MRI does not provide complete information about the diffusion parameters in the ECS, changes in

ADC_W can be better interpreted when correlated with the ECS diffusion parameters measured by the RTI method.

The changes seen in diffusion-weighted images in cases of epilepsy are similar to those observed in cerebral ischemia. Our results show that the decrease in ADC_W during SE is caused by a decrease in the volume fraction, without significant changes in tortuosity. This is in contrast to findings during ischemia of α-syn +/+ and α-syn -/- mice, where a decrease in ADC_W is associated by both a decrease in volume fraction and an increase in tortuosity. Possible explanations why tortuosity values did not increased during SE concomitantly with an α decrease is a slower time course of changes in α and the fact that the decrease in α during SE is only moderate (about 30%) compared to the 65–70% reduction in α seen in experimental models of ischemia (Homola A. et al. 2006; van der Toorn A. et al. 1996; Vorisek I. and Sykova E. 1997). Our previous data showed that a pronounced increase in tortuosity occurs during the experimental application of K^+ or glu^- agonists if the concentration of K^+ exceeds 20 mM. This evokes dramatic alterations in glial cell morphology, especially in the cell processes, which form diffusion barriers (Sykova E. et al. 1999; Vargova L. et al. 2001). $[K^+]_e$ during SE reached about 13 mM, which may not be sufficient to evoke an increase in diffusion barriers formed by glial processes and, thus, lead to an increase in a large tortuosity, whereas during terminal ischemia/anoxia $[K^+]_e$ has reached ~50-60 mM.

Altogether, we can say that in both severe pathological states, SE and/or terminal ischemia/anoxia, the huge transmembrane ionic shifts are accompanied by corresponding redistribution of water, in order to maintain the same osmolality inside and outside cells, leading to the cell swelling, reflecting the intensity and extent of the stimulus. Our data indicates that the removal of the perivascular pool of AQP4, due to α-syntrophin deletion, reduces edema formation, especially under pathological conditions and during states associated with elevated K^+, which may be related to altered K^+ transport in these animals. A larger initial extracellular volume could also serve as a protective factor that buffers any increase in the concentration of potentially neurotoxic substances and slows down the process of cell swelling. On the other hand, impaired water movement across cell membranes may delay the recovery and normalization of the volume conditions.

6. SUMMARY

The diffusion properties of the ECS, which govern the movement of neuroactive substances through its volume and, therefore, extracynaptic transmission, is profoundly affected in states associated with cell swelling. In this work we compared ECS diffusion parameter changes during acute cell swelling *in vivo* in models of pilocarpine-induced status epilepticus and ischemia/anoxia evoked by cardiac arrest. To elucidate mechanisms involving the AQP4 water channel during pathological cell swelling, we used models of hypotonic stress and elevated K^+ *in vitro.*

In both models *in vivo*, ECS volume fraction and ADC_W decreased (to 0.13 ± 0.01 in SE and to 0.10 ± 0.01 in terminal ischemia/anoxia); the time course of these change was slower in the SE model compared to that during terminal ischemia/anoxia. The shrunken ECS volume fraction in the initial phase of epileptiform activity further increased $[K^+]_e$, which influenced neuronal activity and triggered the onset of the first ictal discharges 30 min after pilocarpine injection. A more pronounced increase in the discharge amplitude started when the ECS volume was about 30% smaller than its initial value, showing the possible contribution of ECS volume reduction to the initiation of SE. The reduced ECS also affected the extracellular concentration of tissue metabolites such as glucose, lactate and glu^-. A massive increase in extracellular K^+ concentration during terminal ischemia/anoxia (to 52.37 ± 2.64 mM) was accompanied by a dramatic increase in tortuosity values (to 2.07 ± 0.06), but not during SE, when the maximum increase in K^+ was 13.3 ± 1.04 mM.

Our data indicates that the removal of the perivascular pool of AQP4 due to α-syntrophin deletion reduces edema formation, especially under severe pathological conditions and during states associated with elevated K^+, which may be related to altered K^+ transport in these animals. A larger initial extracellular volume could also serve as a protective factor that buffers any increase in the concentration of potentially neurotoxic substances and slows down the process of cell swelling. On the other hand, impaired water movement across cell membranes may delay the recovery and normalization of the ECS volume.

Changes in tortuosity, reflecting the number and extent of diffusion barriers, and in the extracellular volume fraction affect the movement of neuroactive substances as well as trophic factors and may therefore modulate the extent of the damaged area, the process of healing and/or drug distribution. Understanding the detailed mechanisms underlying the movement of water and ions (especially K^+) across the cell membrane could reveal new

targets for potential therapeutic intervention during serious human pathologies associated with cell swelling, such as stroke or blood-brain barrier damage.

7. CONCLUSIONS

From our results we can conclude:

1) Overall brain diffusivity is hindered during acute pathological states such as ischemia or status epilepticus. This is reflected by a decrease in ADC_W and ECS volume fraction and an increase in tortuosity. The extent of these changes correlates with the increase in $[K^+]_e$ and the extent of the stimuli.

2) Reduction of the ECS during epileptiform activity is associated with an increase in extracellular K^+ concentration. The onset of status epilepticus is triggered by a profoundly shrunken ECS volume fraction that further increases $[K^+]_e$ and affects concentration of metabolites, which may reach toxic levels leading to brain tissue damage.

3) Water transport through AQP4 channels plays an important role especially during pathological conditions, when it enhances and accelerates astrocyte swelling. The substantially altered ECS diffusion parameters will likely affect the movement of neuroactive substances and trophic factors, which in turn may modulate the extent of tissue damage, recovery processes and possible drug distribution.

Altogether, we can say that in both models of severe pathological states (SE and/or terminal ischemia/anoxia) huge transmembrane ionic shifts are accompanied by corresponding redistributions of water, in order to maintain the same osmolality inside and outside cells. Water influx leads to the cell swelling, which reflects the intensity and extent of the stimulus. Our data indicates that the removal of the perivascular pool of AQP4, due to α-syntrophin deletion, reduces edema formation. This is especially true under pathological conditions and during states associated with elevated K^+, which may be related to altered K^+ transport in these animals. A larger initial extracellular volume could also serve as a protective factor that buffers any increase in the concentration of potentially neurotoxic substances and slows down the process of cell swelling. On the other hand, impaired water movement across cell membranes may delay the recovery and normalization of the volume conditions.

Abstracts related to the thesis:

1. **L. Dmytrenko**, K. Šlais, I. Voříšek, E. Syková (2007) Diffusion parameters during pilocarpine-induced seizures in the rat cerebral cortex. *6th International Symposium on Cell Volume Regulation in Health and Disease, Salzburg, Austria.*

2. **L. Dmytrenko**, K. Šlais, I. Voříšek, E. Syková (2008) Diffusion parameters in the rat cerebral cortex during pilocarpine-induced seizures. *6th FENS Forum of European Neuroscience, Geneva, Switzerland.*

3. **L. Dmytrenko**, K. Šlais, L. Vargová, O. P. Ottersen. E. Syková (2008) Mice lacking perivascular aquaporin-4 channels are protected from vasogenic edema after water intoxication. *Society for Neuroscience 38th Annual Meeting, Washington DC, USA.*

4. **L. Dmytrenko**, K. Šlais, L. Vargová, E. Syková (2010) Extracellular volume in aquaporin-4 knock-out mice before and during terminal anoxia/ischemia *Society for Neuroscience 40th Annual Meeting, San Diego CA, USA.*

5. **L. Dmytrenko**, L. Vargová, E. Syková (2011) Effect of terminal anoxia/ischemia on cell swelling and extracellular potassium concentration in α-syntrophin knock-out mice *IBRO world congress of neuroscience, Florence, Italy.*

6. **L. Dmytrenko**, L. Vargová, E. Syková (2011) Extracellular diffusion parameters and potassium concentration in α-syntrophin knock-out mice before and during terminal anoxia/ischemia 10th European Meeting on Glial Cells in Health and Disease, *Prague, Czech Republic.*

7. **L. Dmytrenko**, M. Cicanič, J. Benešová, M. Anděrová, L.Vargová, E. Syková (2012) Diffusion parameters of the extracellular space in GFAP-EGFP-α-syn+/+ and GFAP-EGFP-α-syn-/- mice in models of cell swelling. *6th FENS Forum of European Neuroscience, Barcelona, Spain.*

8. **L. Dmytrenko**, M. Cicanič, J. Benešová, M. Anděrová, L. Vargová, E. Syková (2012) Extracellular diffusion parameters and potassium concentration in GFAP-EGFP-α-syn+/+ and GFAP-EGFP-α-syn-/- mice in models of cell swelling. *Society for Neuroscience 42th Annual Meeting, New Orleans LA, USA.*

9. **L. Dmytrenko**, M. Cicanič, M. Anděrová, I. Voříšek, E. Syková, L. Vargová (2013) Extracellular diffusion parameters in alpha-syntrophin knock-out mice during physiological and pathological states *in vivo* and *in vitro*. *FENS Featured Regional Meeting, Prague, Czech Republic.*

Other author's abstracts:

1. **L. Dmytrenko**, L. Vargová, I. Voříšek, E., Bekku Y., Oohashi T., Syková (2009) Facilitated extracellular diffusion in the corpus callosum of Bral1-deficient mice. *9th Integral congress of Polish Neuroscience Society, First FENS Featured Regional Meeting, Warsaw, Poland.*
2. **L. Dmytrenko**, L. Vargová, I. Voříšek, Syková (2009) Bral1 deficient mice have facilitated extracellular diffusion in the corpus callosum. *Vědecká konference 2. lékařské fakulty, 22.4-23.4.2009, Praha, Česká republika.*
3. **L. Dmytrenko**, L. Vargová, I. Voříšek, Syková (2009) Role of link protein Bral1 in diffusion barrier formation in mice corpus callosum. *Joint Conference of the Czech and Slovak Neuroscience Societies together with 7th International Stem Cell School in Regenerative Medicine, 1-4.11.2009, Prague, Czech Republic.*

8. REFERENCES

Abbott, N. J. (2004). "Evidence for bulk flow of brain interstitial fluid: significance for physiology and pathology." Neurochem Int 45(4): 545-552.

Adachi, K., Cruz, N. F., Sokoloff, L. and Dienel, G. A. (1995). "Labeling of metabolic pools by [6-14C]glucose during K(+)-induced stimulation of glucose utilization in rat brain." J Cereb Blood Flow Metab 15(1): 97-110.

Adams, M. E., Mueller, H. A. and Froehner, S. C. (2001). "In vivo requirement of the alpha-syntrophin PDZ domain for the sarcolemmal localization of nNOS and aquaporin-4." J Cell Biol 155(1): 113-122.

Agnati, L. F., Zoli, M., Stromberg, I. and Fuxe, K. (1995). "Intercellular communication in the brain: Wiring versus volume transmission." Neuroscience 69: 711-726.

Agre, P., King, L. S., Yasui, M., Guggino, W. B., Ottersen, O. P., Fujiyoshi, Y., Engel, A. and Nielsen, S. (2002). "Aquaporin water channels--from atomic structure to clinical medicine." J Physiol 542(Pt 1): 3-16.

Amiry-Moghaddam, M., Frydenlund, D. S. and Ottersen, O. P. (2004). "Anchoring of aquaporin-4 in brain: molecular mechanisms and implications for the physiology and pathophysiology of water transport." Neuroscience 129(4): 999-1010.

Amiry-Moghaddam, M., Otsuka, T., Hurn, P. D., Traystman, R. J., Haug, F. M., Froehner, S. C., Adams, M. E., Neely, J. D., Agre, P., Ottersen, O. P. and Bhardwaj, A. (2003). "An alpha-syntrophin-dependent pool of AQP4 in astroglial end-feet confers bidirectional water flow between blood and brain." Proc Natl Acad Sci U S A 100(4): 2106-2111.

Amiry-Moghaddam, M. and Ottersen, O. P. (2003). "The molecular basis of water transport in the brain." Nat Rev Neurosci 4(12): 991-1001.

Amiry-Moghaddam, M., Xue, R., Haug, F. M., Neely, J. D., Bhardwaj, A., Agre, P., Adams, M. E., Froehner, S. C., Mori, S. and Ottersen, O. P. (2004). "Alpha-syntrophin deletion removes the perivascular but not endothelial pool of aquaporin-4 at the blood-brain barrier and delays the development of brain edema in an experimental model of acute hyponatremia." FASEB J 18(3): 542-544.

Anděrová, M., Benešová, J., Mikešová, M., Dzamba, D., Honsa, P., Kriška, J., Butenko, O., Rusnaková, V., Valihrach, L., Kubista, M., Dmytrenko, L., Cicanič, M. and Vargová, L. (submitted to Glia). "Altered astrocytic swelling in the cortex of alpha-syntrophin-negative GFAP/EGFP mice.".

Anderova, M., Kubinova, S., Mazel, T., Chvatal, A., Eliasson, C., Pekny, M. and Sykova, E. (2001). "Effect of elevated K(+), hypotonic stress, and cortical spreading depression on astrocyte swelling in GFAP-deficient mice." Glia 35(3): 189-203.

Anderova, M., Vorisek, I., Pivonkova, H., Benesova, J., Vargova, L., Cicanic, M., Chvatal, A. and Sykova, E. (2011). "Cell death/proliferation and alterations in glial morphology contribute to changes in diffusivity in the rat hippocampus after hypoxia-ischemia." J Cereb Blood Flow Metab 31(3): 894-907.

Anderson, W. W., Lewis, D. V., Swartzwelder, H. S. and Wilson, W. A. (1986). "Magnesium-free medium activates seizure-like events in the rat hippocampal slice." Brain Res 398(1): 215-219.

Araque, A. and Navarrete, M. (2010). "Glial cells in neuronal network function." Philos Trans R Soc Lond B Biol Sci 365(1551): 2375-2381.

Araque, A., Parpura, V., Sanzgiri, R. P. and Haydon, P. G. (1999). "Tripartite synapses: glia, the unacknowledged partner." Trends Neurosci 22(5): 208-215.

Asztely, F., Erdemli, G. and Kullmann, D. M. (1997). "Extrasynaptic glutamate spillover in the hippocampus: dependence on temperature and the role of active glutamate uptake." Neuron 18: 281-293.

Bandtlow, C. E. and Zimmermann, D. R. (2000). "Proteoglycans in the developing brain: new conceptual insights for old proteins." Physiol Rev 80(4): 1267-1290.

Barres, B. A. (2008). "The mystery and magic of glia: a perspective on their roles in health and disease." Neuron 60(3): 430-440.

Batter, D. K., Corpina, R. A., Roy, C., Spray, D. C., Hertzberg, E. L. and Kessler, J. A. (1992). "Heterogeneity in gap junction expression in astrocytes cultured from different brain regions." Glia 6(3): 213-221.

Bekku, Y., Rauch, U., Ninomiya, Y. and Oohashi, T. (2009). "Brevican distinctively assembles extracellular components at the large diameter nodes of Ranvier in the CNS." J Neurochem 108(5): 1266-1276.

Bekku, Y., Su, W. D., Hirakawa, S., Fassler, R., Ohtsuka, A., Kang, J. S., Sanders, J., Murakami, T., Ninomiya, Y. and Oohashi, T. (2003). "Molecular cloning of Bral2, a novel brain-specific link protein, and immunohistochemical colocalization with brevican in perineuronal nets." Mol Cell Neurosci 24(1): 148-159.

Bekku, Y., Vargova, L., Goto, Y., Vorisek, I., Dmytrenko, L., Narasaki, M., Ohtsuka, A., Fassler, R., Ninomiya, Y., Sykova, E. and Oohashi, T. (2010). "Bral1: its role in

diffusion barrier formation and conduction velocity in the CNS." J Neurosci 30(8): 3113-3123.

Benesova, J., Hock, M., Butenko, O., Prajerova, I., Anderova, M. and Chvatal, A. (2009). "Quantification of astrocyte volume changes during ischemia in situ reveals two populations of astrocytes in the cortex of GFAP/EGFP mice." J Neurosci Res 87(1): 96-111.

Benesova, J., Rusnakova, V., Honsa, P., Pivonkova, H., Dzamba, D., Kubista, M. and Anderova, M. (2012). "Distinct expression/function of potassium and chloride channels contributes to the diverse volume regulation in cortical astrocytes of GFAP/EGFP mice." PLoS One 7(1): e29725.

Benfenati, V. and Ferroni, S. (2010). "Water transport between CNS compartments: functional and molecular interactions between aquaporins and ion channels." Neuroscience 168(4): 926-940.

Benveniste, H., Hedlund, L. W. and Johnson, G. A. (1992). "Mechanism of detection of acute cerebral ischemia in rats by diffusion-weighted magnetic resonance microscopy." Stroke 23(5): 746-754.

Besnard, F., Brenner, M., Nakatani, Y., Chao, R., Purohit, H. J. and Freese, E. (1991). "Multiple interacting sites regulate astrocyte-specific transcription of the human gene for glial fibrillary acidic protein." J Biol Chem 266(28): 18877-18883.

Bezzi, P., Gundersen, V., Galbete, J. L., Seifert, G., Steinhauser, C., Pilati, E. and Volterra, A. (2004). "Astrocytes contain a vesicular compartment that is competent for regulated exocytosis of glutamate." Nat Neurosci 7(6): 613-620.

Binder, D. K., Nagelhus, E. A. and Ottersen, O. P. (2012). "Aquaporin-4 and epilepsy." Glia 60(8): 1203-1214.

Binder, D. K., Papadopoulos, M. C., Haggie, P. M. and Verkman, A. S. (2004). "In vivo measurement of brain extracellular space diffusion by cortical surface photobleaching." J Neurosci 24(37): 8049-8056.

Binder, D. K. and Steinhauser, C. (2006). "Functional changes in astroglial cells in epilepsy." Glia 54(5): 358-368.

Binder, D. K., Yao, X., Zador, Z., Sick, T. J., Verkman, A. S. and Manley, G. T. (2006). "Increased seizure duration and slowed potassium kinetics in mice lacking aquaporin-4 water channels." Glia 53(6): 631-636.

Bloch, O., Auguste, K. I., Manley, G. T. and Verkman, A. S. (2006). "Accelerated progression of kaolin-induced hydrocephalus in aquaporin-4-deficient mice." J Cereb Blood Flow Metab 26(12): 1527-1537.

Blumcke, I., Beck, H., Suter, B., Hoffmann, D., Fodisch, H. J., Wolf, H. K., Schramm, J., Elger, C. E. and Wiestler, O. D. (1999). "An increase of hippocampal calretinin-immunoreactive neurons correlates with early febrile seizures in temporal lobe epilepsy." Acta Neuropathol 97(1): 31-39.

Bradford, H. F. (1995). "Glutamate, GABA and epilepsy." Prog Neurobiol 47(6): 477-511.

Bruckner, G., Grosche, J., Schmidt, S., Hartig, W., Margolis, R. U., Delpech, B., Seidenbecher, C. I., Czaniera, R. and Schachner, M. (2000). "Postnatal development of perineuronal nets in wild-type mice and in a mutant deficient in tenascin-R." J Comp Neurol 428(4): 616-629.

Bruhn, T., Cobo, M., Berg, M. and Diemer, N. H. (1992). "Limbic seizure-induced changes in extracellular amino acid levels in the hippocampal formation: a microdialysis study of freely moving rats." Acta Neurol Scand 86(5): 455-461.

Cavazzin, C., Ferrari, D., Facchetti, F., Russignan, A., Vescovi, A. L., La Porta, C. A. and Gritti, A. (2006). "Unique expression and localization of aquaporin-4 and aquaporin-9 in murine and human neural stem cells and in their glial progeny." Glia 53(2): 167-181.

Cavus, I., Kasoff, W. S., Cassaday, M. P., Jacob, R., Gueorguieva, R., Sherwin, R. S., Krystal, J. H., Spencer, D. D. and Abi-Saab, W. M. (2005). "Extracellular metabolites in the cortex and hippocampus of epileptic patients." Ann Neurol 57(2): 226-235.

Coles, J. A. and Orkand, R. K. (1983). "Modification of potassium movement through the retina of the drone (Apis mellifera male) by glial uptake." J Physiol 340: 157-174.

Connors, N. C., Adams, M. E., Froehner, S. C. and Kofuji, P. (2004). "The potassium channel Kir4.1 associates with the dystrophin-glycoprotein complex via alpha-syntrophin in glia." J Biol Chem 279(27): 28387-28392.

Connors, N. C. and Kofuji, P. (2006). "Potassium channel Kir4.1 macromolecular complex in retinal glial cells." Glia 53(2): 124-131.

Cornell-Bell, A. H., Finkbeiner, S. M., Cooper, M. S. and Smith, S. J. (1990). "Glutamate induces calcium waves in cultured astrocytes: long-range glial signaling." Science 247(4941): 470-473.

Darbin, O., Risso, J. J., Carre, E., Lonjon, M. and Naritoku, D. K. (2005). "Metabolic changes in rat striatum following convulsive seizures." Brain Res 1050(1-2): 124-129.

David, Y., Cacheaux, L. P., Ivens, S., Lapilover, E., Heinemann, U., Kaufer, D. and Friedman, A. (2009). "Astrocytic dysfunction in epileptogenesis: consequence of altered potassium and glutamate homeostasis?" J Neurosci 29(34): 10588-10599.

Davies, D. C. (2002). "Blood-brain barrier breakdown in septic encephalopathy and brain tumours." J Anat 200(6): 639-646.

De Pina-Benabou, M. H., Srinivas, M., Spray, D. C. and Scemes, E. (2001). "Calmodulin kinase pathway mediates the K+-induced increase in Gap junctional communication between mouse spinal cord astrocytes." J Neurosci 21(17): 6635-6643.

Dermietzel, R., Hertberg, E. L., Kessler, J. A. and Spray, D. C. (1991). "Gap junctions between cultured astrocytes: immunocytochemical, molecular, and electrophysiological analysis." J Neurosci 11(5): 1421-1432.

Dibaj, P., Kaiser, M., Hirrlinger, J., Kirchhoff, F. and Neusch, C. (2007). "Kir4.1 channels regulate swelling of astroglial processes in experimental spinal cord edema." J Neurochem 103(6): 2620-2628.

Dijkhuizen, R. M., Knollema, S., van der Worp, H. B., Ter Horst, G. J., De Wildt, D. J., Berkelbach van der Sprenkel, J. W., Tulleken, K. A. and Nicolay, K. (1998). "Dynamics of cerebral tissue injury and perfusion after temporary hypoxia-ischemia in the rat: evidence for region-specific sensitivity and delayed damage." Stroke 29(3): 695-704.

Ding, S., Fellin, T., Zhu, Y., Lee, S. Y., Auberson, Y. P., Meaney, D. F., Coulter, D. A., Carmignoto, G. and Haydon, P. G. (2007). "Enhanced astrocytic Ca2+ signals contribute to neuronal excitotoxicity after status epilepticus." J Neurosci 27(40): 10674-10684.

Doetsch, F., Caille, I., Lim, D. A., Garcia-Verdugo, J. M. and Alvarez-Buylla, A. (1999). "Subventricular zone astrocytes are neural stem cells in the adult mammalian brain." Cell 97(6): 703-716.

During, M. J., Fried, I., Leone, P., Katz, A. and Spencer, D. D. (1994). "Direct measurement of extracellular lactate in the human hippocampus during spontaneous seizures." J Neurochem 62(6): 2356-2361.

Eclancher, F., Perraud, F., Faltin, J., Labourdette, G. and Sensenbrenner, M. (1990). "Reactive astrogliosis after basic fibroblast growth factor (bFGF) injection in injured neonatal rat brain." Glia 3(6): 502-509.

Edwards, M. A., Yamamoto, M. and Caviness, V. S., Jr. (1990). "Organization of radial glia and related cells in the developing murine CNS. An analysis based upon a new monoclonal antibody marker." Neuroscience 36(1): 121-144.

Eid, T., Lee, T. S., Thomas, M. J., Amiry-Moghaddam, M., Bjornsen, L. P., Spencer, D. D., Agre, P., Ottersen, O. P. and de Lanerolle, N. C. (2005). "Loss of perivascular aquaporin 4 may underlie deficient water and K+ homeostasis in the human epileptogenic hippocampus." Proc Natl Acad Sci U S A 102(4): 1193-1198.

Eid, T., Williamson, A., Lee, T. S., Petroff, O. A. and de Lanerolle, N. C. (2008). "Glutamate and astrocytes--key players in human mesial temporal lobe epilepsy?" Epilepsia 49 Suppl 2: 42-52.

Eng, L. F., Ghirnikar, R. S. and Lee, Y. L. (2000). "Glial fibrillary acidic protein: GFAP-thirty-one years (1969-2000)." Neurochem Res 25(9-10): 1439-1451.

Eriksson, J. E., Dechat, T., Grin, B., Helfand, B., Mendez, M., Pallari, H. M. and Goldman, R. D. (2009). "Introducing intermediate filaments: from discovery to disease." J Clin Invest 119(7): 1763-1771.

Fabene, P. F., Weiczner, R., Marzola, P., Nicolato, E., Calderan, L., Andrioli, A., Farkas, E., Sule, Z., Mihaly, A. and Sbarbati, A. (2006). "Structural and functional MRI following 4-aminopyridine-induced seizures: a comparative imaging and anatomical study." Neurobiol Dis 21(1): 80-89.

Feng, L., Hatten, M. E. and Heintz, N. (1994). "Brain lipid-binding protein (BLBP): a novel signaling system in the developing mammalian CNS." Neuron 12(4): 895-908.

Feng, Z. and Durand, D. M. (2006). "Effects of potassium concentration on firing patterns of low-calcium epileptiform activity in anesthetized rat hippocampus: inducing of persistent spike activity." Epilepsia 47(4): 727-736.

Fernandes, M. J., Dube, C., Boyet, S., Marescaux, C. and Nehlig, A. (1999). "Correlation between hypermetabolism and neuronal damage during status epilepticus induced by lithium and pilocarpine in immature and adult rats." J Cereb Blood Flow Metab 19(2): 195-209.

Fiacco, T. A., Agulhon, C., Taves, S. R., Petravicz, J., Casper, K. B., Dong, X., Chen, J. and McCarthy, K. D. (2007). "Selective stimulation of astrocyte calcium in situ does not affect neuronal excitatory synaptic activity." Neuron 54(4): 611-626.

Fornai, F., Bassi, L., Gesi, M., Giorgi, F. S., Guerrini, R., Bonaccorsi, I. and Alessandri, M. G. (2000). "Similar increases in extracellular lactic acid in the limbic system during epileptic and/or olfactory stimulation." Neuroscience 97(3): 447-458.

Fray, A. E., Boutelle, M. and Fillenz, M. (1997). "Extracellular glucose turnover in the striatum of unanaesthetized rats measured by quantitative microdialysis." J Physiol 504 (Pt 3): 721-726.

Frigeri, A., Gropper, M. A., Turck, C. W. and Verkman, A. S. (1995). "Immunolocalization of the mercurial-insensitive water channel and glycerol intrinsic protein in epithelial cell plasma membranes." Proc Natl Acad Sci U S A 92(10): 4328-4331.

Furman, C. S., Gorelick-Feldman, D. A., Davidson, K. G., Yasumura, T., Neely, J. D., Agre, P. and Rash, J. E. (2003). "Aquaporin-4 square array assembly: opposing actions of M1 and M23 isoforms." Proc Natl Acad Sci U S A 100(23): 13609-13614.

Gabriel, S., Njunting, M., Pomper, J. K., Merschhemke, M., Sanabria, E. R., Eilers, A., Kivi, A., Zeller, M., Meencke, H. J., Cavalheiro, E. A., Heinemann, U. and Lehmann, T. N. (2004). "Stimulus and potassium-induced epileptiform activity in the human dentate gyrus from patients with and without hippocampal sclerosis." J Neurosci 24(46): 10416-10430.

Galvan, M., Grafe, P. and ten Bruggencate, G. (1982). "Convulsant actions of 4-aminopyridine on the guinea-pig olfactory cortex slice." Brain Res 241(1): 75-86.

Giaume, C., Koulakoff, A., Roux, L., Holcman, D. and Rouach, N. (2010). "Astroglial networks: a step further in neuroglial and gliovascular interactions." Nat Rev Neurosci 11(2): 87-99.

Gomi, H., Yokoyama, T., Fujimoto, K., Ikeda, T., Katoh, A., Itoh, T. and Itohara, S. (1995). "Mice devoid of the glial fibrillary acidic protein develop normally and are susceptible to scrapie prions." Neuron 14(1): 29-41.

Goncalves, C. A., Leite, M. C. and Nardin, P. (2008). "Biological and methodological features of the measurement of S100B, a putative marker of brain injury." Clin Biochem 41(10-11): 755-763.

Gordon, G. R., Mulligan, S. J. and MacVicar, B. A. (2007). "Astrocyte control of the cerebrovasculature." Glia 55(12): 1214-1221.

Guadagno, E. and Moukhles, H. (2004). "Laminin-induced aggregation of the inwardly rectifying potassium channel, Kir4.1, and the water-permeable channel, AQP4, via a dystroglycan-containing complex in astrocytes." Glia 47(2): 138-149.

Hablitz, J. J. (1987). "Spontaneous ictal-like discharges and sustained potential shifts in the developing rat neocortex." J Neurophysiol 58(5): 1052-1065.

Haj-Yasein, N. N., Jensen, V., Vindedal, G. F., Gundersen, G. A., Klungland, A., Ottersen, O. P., Hvalby, O. and Nagelhus, E. A. (2011). "Evidence that compromised K+ spatial

buffering contributes to the epileptogenic effect of mutations in the human Kir4.1 gene (KCNJ10)." Glia 59(11): 1635-1642.

Haj-Yasein, N. N., Vindedal, G. F., Eilert-Olsen, M., Gundersen, G. A., Skare, O., Laake, P., Klungland, A., Thoren, A. E., Burkhardt, J. M., Ottersen, O. P. and Nagelhus, E. A. (2011). "Glial-conditional deletion of aquaporin-4 (Aqp4) reduces blood-brain water uptake and confers barrier function on perivascular astrocyte endfeet." Proc Natl Acad Sci U S A 108(43): 17815-17820.

Halassa, M. M., Fellin, T. and Haydon, P. G. (2007). "The tripartite synapse: roles for gliotransmission in health and disease." Trends Mol Med 13(2): 54-63.

Halassa, M. M., Fellin, T. and Haydon, P. G. (2009). "Tripartite synapses: roles for astrocytic purines in the control of synaptic physiology and behavior." Neuropharmacology 57(4): 343-346.

Harukuni, I. and Bhardwaj, A. (2006). "Mechanisms of brain injury after global cerebral ischemia." Neurol Clin 24(1): 1-21.

Hasegawa, H., Ma, T., Skach, W., Matthay, M. A. and Verkman, A. S. (1994). "Molecular cloning of a mercurial-insensitive water channel expressed in selected water-transporting tissues." J Biol Chem 269(8): 5497-5500.

Haydon, P. G. (2001). "GLIA: listening and talking to the synapse." Nat Rev Neurosci 2(3): 185-193.

Hazama, A., Kozono, D., Guggino, W. B., Agre, P. and Yasui, M. (2002). "Ion permeation of AQP6 water channel protein. Single channel recordings after Hg2+ activation." J Biol Chem 277(32): 29224-29230.

Helpern, J. A., Dereski, M. O., Knight, R. A., Ordidge, R. J., Chopp, M. and Qing, Z. X. (1993). "Histopathological correlations of nuclear magnetic resonance imaging parameters in experimental cerebral ischemia." Magn Reson Imaging 11(2): 241-246.

Hertz, L. (2008). "Bioenergetics of cerebral ischemia: a cellular perspective." Neuropharmacology 55(3): 289-309.

Hertz, L., Chen, Y. and Spatz, M. (2000). "Involvement of non-neuronal brain cells in AVP-mediated regulation of water space at the cellular, organ, and whole-body level." J Neurosci Res 62(4): 480-490.

Hibino, H., Fujita, A., Iwai, K., Yamada, M. and Kurachi, Y. (2004). "Differential assembly of inwardly rectifying K+ channel subunits, Kir4.1 and Kir5.1, in brain astrocytes." J Biol Chem 279(42): 44065-44073.

Hirakawa, S., Oohashi, T., Su, W. D., Yoshioka, H., Murakami, T., Arata, J. and Ninomiya, Y. (2000). "The brain link protein-1 (BRAL1): cDNA cloning, genomic structure, and characterization as a novel link protein expressed in adult brain." Biochem Biophys Res Commun 276(3): 982-989.

Hirt, L., Ternon, B., Price, M., Mastour, N., Brunet, J. F. and Badaut, J. (2009). "Protective role of early aquaporin 4 induction against postischemic edema formation." J Cereb Blood Flow Metab 29(2): 423-433.

Hofer, A. and Dermietzel, R. (1998). "Visualization and functional blocking of gap junction hemichannels (connexons) with antibodies against external loop domains in astrocytes." Glia 24(1): 141-154.

Hoffmann, E. K., Lambert, I. H. and Pedersen, S. F. (2009). "Physiology of cell volume regulation in vertebrates." Physiol Rev 89(1): 193-277.

Homola, A., Zoremba, N., Slais, K., Kuhlen, R. and Sykova, E. (2006). "Changes in diffusion parameters, energy-related metabolites and glutamate in the rat cortex after transient hypoxia/ischemia." Neurosci Lett 404(1-2): 137-142.

Horio, Y. (2001). "Potassium channels of glial cells: distribution and function." Jpn J Pharmacol 87(1): 1-6.

Hrabe, J., Hrabetova, S. and Segeth, K. (2004). "A model of effective diffusion and tortuosity in the extracellular space of the brain." Biophys J 87(3): 1606-1617.

Hrabetova, S., Hrabe, J. and Nicholson, C. (2003). "Dead-space microdomains hinder extracellular diffusion in rat neocortex during ischemia." J Neurosci 23(23): 8351-8359.

Hrabetova, S., Masri, D., Tao, L., Xiao, F. and Nicholson, C. (2009). "Calcium diffusion enhanced after cleavage of negatively charged components of brain extracellular matrix by chondroitinase ABC." J Physiol 587(Pt 16): 4029-4049.

Chan, P. H., Yang, G. Y., Chen, S. F., Carlson, E. and Epstein, C. J. (1991). "Cold-induced brain edema and infarction are reduced in transgenic mice overexpressing CuZn-superoxide dismutase." Ann Neurol 29(5): 482-486.

Chang, B. S. and Lowenstein, D. H. (2003). "Epilepsy." N Engl J Med 349(13): 1257-1266.

Chaudhry, F. A., Lehre, K. P., van Lookeren Campagne, M., Ottersen, O. P., Danbolt, N. C. and Storm-Mathisen, J. (1995). "Glutamate transporters in glial plasma membranes: highly differentiated localizations revealed by quantitative ultrastructural immunocytochemistry." Neuron 15(3): 711-720.

Chen, H. and Sun, D. (2005). "The role of Na-K-Cl co-transporter in cerebral ischemia." Neurol Res 27(3): 280-286.

Chesler, M. (1990). "The regulation and modulation of pH in the nervous system." Prog Neurobiol 34(5): 401-427.

Choi, D. W. (1988). "Glutamate neurotoxicity and diseases of the nervous system." Neuron 1(8): 623-634.

Christopherson, K. S., Ullian, E. M., Stokes, C. C., Mullowney, C. E., Hell, J. W., Agah, A., Lawler, J., Mosher, D. F., Bornstein, P. and Barres, B. A. (2005). "Thrombospondins are astrocyte-secreted proteins that promote CNS synaptogenesis." Cell 120(3): 421-433.

Chvatal, A., Anderova, M. and Kirchhoff, F. (2007). "Three-dimensional confocal morphometry - a new approach for studying dynamic changes in cell morphology in brain slices." J Anat 210(6): 671-683.

Chvatal, A., Berger, T., Vorisek, I., Orkand, R. K., Kettenmann, H. and Sykova, E. (1997). "Changes in glial K+ currents with decreased extracellular volume in developing rat white matter." Journal of Neuroscience Research 49(1): 98-106.

Illarionova, N. B., Gunnarson, E., Li, Y., Brismar, H., Bondar, A., Zelenin, S. and Aperia, A. (2010). "Functional and molecular interactions between aquaporins and Na,K-ATPase." Neuroscience 168(4): 915-925.

Ishii, M., Horio, Y., Tada, Y., Hibino, H., Inanobe, A., Ito, M., Yamada, M., Gotow, T., Uchiyama, Y. and Kurachi, Y. (1997). "Expression and clustered distribution of an inwardly rectifying potassium channel, KAB-2/Kir4.1, on mammalian retinal Muller cell membrane: their regulation by insulin and laminin signals." J Neurosci 17(20): 7725-7735.

Jayakumar, A. R. and Norenberg, M. D. (2010). "The Na-K-Cl Co-transporter in astrocyte swelling." Metab Brain Dis 25(1): 31-38.

Jefferys, J. G. and Haas, H. L. (1982). "Synchronized bursting of CA1 hippocampal pyramidal cells in the absence of synaptic transmission." Nature 300(5891): 448-450.

Jessen, K. R. and Mirsky, R. (1985). "Glial fibrillary acidic polypeptides in peripheral glia. Molecular weight, heterogeneity and distribution." J Neuroimmunol 8(4-6): 377-393.

Jessen, K. R., Morgan, L., Stewart, H. J. and Mirsky, R. (1990). "Three markers of adult non-myelin-forming Schwann cells, 217c(Ran-1), A5E3 and GFAP: development and regulation by neuron-Schwann cell interactions." Development 109(1): 91-103.

Joester, A. and Faissner, A. (2001). "The structure and function of tenascins in the nervous system." Matrix Biol 20(1): 13-22.

Johansson, C. B., Momma, S., Clarke, D. L., Risling, M., Lendahl, U. and Frisen, J. (1999). "Identification of a neural stem cell in the adult mammalian central nervous system." Cell 96(1): 25-34.

Jung, J. S., Bhat, R. V., Preston, G. M., Guggino, W. B., Baraban, J. M. and Agre, P. (1994). "Molecular characterization of an aquaporin cDNA from brain: candidate osmoreceptor and regulator of water balance." Proc Natl Acad Sci U S A 91(26): 13052-13056.

Kahlert, S. and Reiser, G. (2004). "Glial perspectives of metabolic states during cerebral hypoxia--calcium regulation and metabolic energy." Cell Calcium 36(3-4): 295-302.

Kachinsky, A. M., Froehner, S. C. and Milgram, S. L. (1999). "A PDZ-containing scaffold related to the dystrophin complex at the basolateral membrane of epithelial cells." J Cell Biol 145(2): 391-402.

Kalman, M. and Ajtai, B. M. (2000). "Lesions do not provoke GFAP-expression in the GFAP-immunonegative areas of the teleost brain." Ann Anat 182(5): 459-463.

Ke, C., Poon, W. S., Ng, H. K., Pang, J. C. and Chan, Y. (2001). "Heterogeneous responses of aquaporin-4 in oedema formation in a replicated severe traumatic brain injury model in rats." Neurosci Lett 301(1): 21-24.

Khan, G. M., Smolders, I., Lindekens, H., Manil, J., Ebinger, G. and Michotte, Y. (1999). "Effects of diazepam on extracellular brain neurotransmitters in pilocarpine-induced seizures in rats." Eur J Pharmacol 373(2-3): 153-161.

Kilb, W., Dierkes, P. W., Sykova, E., Vargova, L. and Luhmann, H. J. (2006). "Hypoosmolar conditions reduce extracellular volume fraction and enhance epileptiform activity in the CA3 region of the immature rat hippocampus." J Neurosci Res 84(1): 119-129.

Kimelberg, H. K. (1995). "Current concepts of brain edema. Review of laboratory investigations." J Neurosurg 83(6): 1051-1059.

Kimelberg, H. K., Goderie, S. K., Higman, S., Pang, S. and Waniewski, R. A. (1990). "Swelling-induced release of glutamate, aspartate, and taurine from astrocyte cultures." J Neurosci 10(5): 1583-1591.

Kimelberg, H. K. and Nedergaard, M. (2010). "Functions of astrocytes and their potential as therapeutic targets." Neurotherapeutics 7(4): 338-353.

Kimelberg, H. K., Rutledge, E., Goderie, S. and Charniga, C. (1995). "Astrocytic swelling due to hypotonic or high K+ medium causes inhibition of glutamate and aspartate uptake and increases their release." J Cereb Blood Flow Metab 15(3): 409-416.

Kiss, J. P., Zsilla, G. and Vizi, E. S. (2004). "Inhibitory effect of nitric oxide on dopamine transporters: interneuronal communication without receptors." Neurochem Int 45(4): 485-489.

Klatzo, I. (1994). "Evolution of brain edema concepts." Acta Neurochir Suppl (Wien) 60: 3-6.

Knight, R. A., Ordidge, R. J., Helpern, J. A., Chopp, M., Rodolosi, L. C. and Peck, D. (1991). "Temporal evolution of ischemic damage in rat brain measured by proton nuclear magnetic resonance imaging." Stroke 22(6): 802-808.

Kofuji, P., Biedermann, B., Siddharthan, V., Raap, M., Iandiev, I., Milenkovic, I., Thomzig, A., Veh, R. W., Bringmann, A. and Reichenbach, A. (2002). "Kir potassium channel subunit expression in retinal glial cells: implications for spatial potassium buffering." Glia 39(3): 292-303.

Kofuji, P. and Newman, E. A. (2004). "Potassium buffering in the central nervous system." Neuroscience 129(4): 1045-1056.

Kovacs, A., Mihaly, A., Komaromi, A., Gyengesi, E., Szente, M., Weiczner, R., Krisztin-Peva, B., Szabo, G. and Telegdy, G. (2003). "Seizure, neurotransmitter release, and gene expression are closely related in the striatum of 4-aminopyridine-treated rats." Epilepsy Res 55(1-2): 117-129.

Kreisman, N. R. and Olson, J. E. (2003). "Taurine enhances volume regulation in hippocampal slices swollen osmotically." Neuroscience 120(3): 635-642.

Kriz, N., Sykova, E., Ujec, E. and Vyklicky, L. (1974). "Changes of extracellular potassium concentration induced by neuronal activity in the sinal cord of the cat." J Physiol 238(1): 1-15.

Kuhr, W. G. and Korf, J. (1988). "Extracellular lactic acid as an indicator of brain metabolism: continuous on-line measurement in conscious, freely moving rats with intrastriatal dialysis." J Cereb Blood Flow Metab 8(1): 130-137.

Kuhr, W. G. and Korf, J. (1988). "N-methyl-D-aspartate receptor involvement in lactate production following ischemia or convulsion in rats." Eur J Pharmacol 155(1-2): 145-149.

Kuhr, W. G., van den Berg, C. J. and Korf, J. (1988). "In vivo identification and quantitative evaluation of carrier-mediated transport of lactate at the cellular level in the striatum of conscious, freely moving rats." J Cereb Blood Flow Metab 8(6): 848-856.

Kullmann, D. M., Erdemli, G. and Asztely, F. (1996). "LTP of AMPA and NMDA receptor-mediated signals: evidence for presynaptic expression and extrasynaptic glutamate spill-over." Neuron 17: 461-474.

Kunzelmann, P., Schroder, W., Traub, O., Steinhauser, C., Dermietzel, R. and Willecke, K. (1999). "Late onset and increasing expression of the gap junction protein connexin30 in adult murine brain and long-term cultured astrocytes." Glia 25(2): 111-119.

Lakhan, S. E., Kirchgessner, A. and Hofer, M. (2009). "Inflammatory mechanisms in ischemic stroke: therapeutic approaches." J Transl Med 7: 97.

Lang, F. (2007). "Mechanisms and significance of cell volume regulation." J Am Coll Nutr 26(5 Suppl): 613S-623S.

Le Bihan, D. (1995). Molecular diffusion and nuclear magnetic resonance. . Diffusion and Perfusion Magnetic Resonance Imaging: Applications to Functional Mri New York, Raven Press: 5-17.

Lee, T. S., Eid, T., Mane, S., Kim, J. H., Spencer, D. D., Ottersen, O. P. and de Lanerolle, N. C. (2004). "Aquaporin-4 is increased in the sclerotic hippocampus in human temporal lobe epilepsy." Acta Neuropathol 108(6): 493-502.

Lehmenkuhler, A., Sykova, E., Svoboda, J., Zilles, K. and Nicholson, C. (1993). "Extracellular space parameters in the rat neocortex and subcortical white matter during postnatal development determined by diffusion analysis." Neuroscience 55(2): 339-351.

Leis, J. A., Bekar, L. K. and Walz, W. (2005). "Potassium homeostasis in the ischemic brain." Glia 50(4): 407-416.

Liedtke, W., Edelmann, W., Bieri, P. L., Chiu, F. C., Cowan, N. J., Kucherlapati, R. and Raine, C. S. (1996). "GFAP is necessary for the integrity of CNS white matter architecture and long-term maintenance of myelination." Neuron 17(4): 607-615.

Lichter-Konecki, U., Mangin, J. M., Gordish-Dressman, H., Hoffman, E. P. and Gallo, V. (2008). "Gene expression profiling of astrocytes from hyperammonemic mice reveals altered pathways for water and potassium homeostasis in vivo." Glia 56(4): 365-377.

Liu, Z., Stafstrom, C. E., Sarkisian, M. R., Yang, Y., Hori, A., Tandon, P. and Holmes, G. L. (1997). "Seizure-induced glutamate release in mature and immature animals: an in vivo microdialysis study." Neuroreport 8(8): 2019-2023.

Losi, G., Cammarota, M. and Carmignoto, G. (2012). "The role of astroglia in the epileptic brain." Front Pharmacol 3: 132.

Macias, W., Carlson, R., Rajadhyaksha, A., Barczak, A. and Konradi, C. (2001). "Potassium chloride depolarization mediates CREB phosphorylation in striatal neurons in an NMDA receptor-dependent manner." Brain Res 890(2): 222-232.

MacVicar, B. A. (1984). "Voltage-dependent calcium channels in glial cells." Science 226(4680): 1345-1347.

Makara, J. K., Petheo, G. L., Toth, A. and Spat, A. (2001). "pH-sensitive inwardly rectifying chloride current in cultured rat cortical astrocytes." Glia 34(1): 52-58.

Manley, G. T., Binder, D. K., Papadopoulos, M. C. and Verkman, A. S. (2004). "New insights into water transport and edema in the central nervous system from phenotype analysis of aquaporin-4 null mice." Neuroscience 129(4): 983-991.

Manley, G. T., Fujimura, M., Ma, T., Noshita, N., Filiz, F., Bollen, A. W., Chan, P. and Verkman, A. S. (2000). "Aquaporin-4 deletion in mice reduces brain edema after acute water intoxication and ischemic stroke." Nat Med 6(2): 159-163.

Masood, K., Besnard, F., Su, Y. and Brenner, M. (1993). "Analysis of a segment of the human glial fibrillary acidic protein gene that directs astrocyte-specific transcription." J Neurochem 61(1): 160-166.

Mazel, T., Simonova, Z. and Sykova, E. (1998). "Diffusion heterogeneity and anisotropy in rat hippocampus." Neuroreport 9(7): 1299-1304.

McCall, M. A., Gregg, R. G., Behringer, R. R., Brenner, M., Delaney, C. L., Galbreath, E. J., Zhang, C. L., Pearce, R. A., Chiu, S. Y. and Messing, A. (1996). "Targeted deletion in astrocyte intermediate filament (Gfap) alters neuronal physiology." Proc Natl Acad Sci U S A 93(13): 6361-6366.

McDonough, J. H., Jr. and Shih, T. M. (1997). "Neuropharmacological mechanisms of nerve agent-induced seizure and neuropathology." Neurosci Biobehav Rev 21(5): 559-579.

Miller, R. H. and Raff, M. C. (1984). "Fibrous and protoplasmic astrocytes are biochemically and developmentally distinct." J Neurosci 4(2): 585-592.

Moe, S. E., Sorbo, J. G., Sogaard, R., Zeuthen, T., Petter Ottersen, O. and Holen, T. (2008). "New isoforms of rat Aquaporin-4." Genomics 91(4): 367-377.

Montgomery, D. L. (1994). "Astrocytes: form, functions, and roles in disease." Vet Pathol 31(2): 145-167.

Moonen, C. T., Pekar, J., de Vleeschouwer, M. H., van Gelderen, P., van Zijl, P. C. and DesPres, D. (1991). "Restricted and anisotropic displacement of water in healthy cat brain and in stroke studied by NMR diffusion imaging." Magn Reson Med 19(2): 327-332.

Muller, M. (2002). "Science, medicine, and the future: Microdialysis." BMJ 324(7337): 588-591.

Nagelhus, E. A., Horio, Y., Inanobe, A., Fujita, A., Haug, F. M., Nielsen, S., Kurachi, Y. and Ottersen, O. P. (1999). "Immunogold evidence suggests that coupling of K+ siphoning and water transport in rat retinal Muller cells is mediated by a coenrichment of Kir4.1 and AQP4 in specific membrane domains." Glia 26(1): 47-54.

Nagelhus, E. A., Mathiisen, T. M. and Ottersen, O. P. (2004). "Aquaporin-4 in the central nervous system: cellular and subcellular distribution and coexpression with KIR4.1." Neuroscience 129(4): 905-913.

Nagy, J. I., Patel, D., Ochalski, P. A. and Stelmack, G. L. (1999). "Connexin30 in rodent, cat and human brain: selective expression in gray matter astrocytes, co-localization with connexin43 at gap junctions and late developmental appearance." Neuroscience 88(2): 447-468.

Nakane, M., Tamura, A., Miyasaka, N., Nagaoka, T. and Kuroiwa, T. (2001). "Astrocytic swelling in the ipsilateral substantia nigra after occlusion of the middle cerebral artery in rats." AJNR Am J Neuroradiol 22(4): 660-663.

Nawashiro, H., Messing, A., Azzam, N. and Brenner, M. (1998). "Mice lacking GFAP are hypersensitive to traumatic cerebrospinal injury." Neuroreport 9(8): 1691-1696.

Nedergaard, M. and Dirnagl, U. (2005). "Role of glial cells in cerebral ischemia." Glia 50(4): 281-286.

Nedergaard, M., Ransom, B. and Goldman, S. A. (2003). "New roles for astrocytes: redefining the functional architecture of the brain." Trends Neurosci 26(10): 523-530.

Neely, J. D., Amiry-Moghaddam, M., Ottersen, O. P., Froehner, S. C., Agre, P. and Adams, M. E. (2001). "Syntrophin-dependent expression and localization of Aquaporin-4 water channel protein." Proc Natl Acad Sci U S A 98(24): 14108-14113.

Neely, J. D., Christensen, B. M., Nielsen, S. and Agre, P. (1999). "Heterotetrameric composition of aquaporin-4 water channels." Biochemistry 38(34): 11156-11163.

Neprasova, H., Anderova, M., Petrik, D., Vargova, L., Kubinova, S., Chvatal, A. and Sykova, E. (2007). "High extracellular K(+) evokes changes in voltage-dependent K(+) and Na (+) currents and volume regulation in astrocytes." Pflugers Arch 453(6): 839-849.

Newey, S. E., Benson, M. A., Ponting, C. P., Davies, K. E. and Blake, D. J. (2000). "Alternative splicing of dystrobrevin regulates the stoichiometry of syntrophin binding to the dystrophin protein complex." Curr Biol 10(20): 1295-1298.

Nicchia, G. P., Srinivas, M., Li, W., Brosnan, C. F., Frigeri, A. and Spray, D. C. (2005). "New possible roles for aquaporin-4 in astrocytes: cell cytoskeleton and functional relationship with connexin43." FASEB J 19(12): 1674-1676.

Nielsen, S., Nagelhus, E. A., Amiry-Moghaddam, M., Bourque, C., Agre, P. and Ottersen, O. P. (1997). "Specialized membrane domains for water transport in glial cells: high-resolution immunogold cytochemistry of aquaporin-4 in rat brain." J Neurosci 17(1): 171-180.

Nicholson, C. and Phillips, J. M. (1981). "Ion diffusion modified by tortuosity and volume fraction in the extracellular microenvironment of the rat cerebellum." Journal of Physiology (London) 321: 225-257.

Nicholson, C. and Sykova, E. (1998). "Extracellular space structure revealed by diffusion analysis." Trends in Neuroscience 21(5): 207-215.

Noel, G., Belda, M., Guadagno, E., Micoud, J., Klocker, N. and Moukhles, H. (2005). "Dystroglycan and Kir4.1 coclustering in retinal Muller glia is regulated by laminin-1 and requires the PDZ-ligand domain of Kir4.1." J Neurochem 94(3): 691-702.

Nolte, C., Matyash, M., Pivneva, T., Schipke, C. G., Ohlemeyer, C., Hanisch, U. K., Kirchhoff, F. and Kettenmann, H. (2001). "GFAP promoter-controlled EGFP-expressing transgenic mice: a tool to visualize astrocytes and astrogliosis in living brain tissue." Glia 33(1): 72-86.

Oliet, S. H., Piet, R. and Poulain, D. A. (2001). "Control of glutamate clearance and synaptic efficacy by glial coverage of neurons." Science 292(5518): 923-926.

Oohashi, T. and Bekku, Y. (2007). Brain Link Proteins: Neuromodulators for scaffolding the specialized hyaluronan-binding extracellular milieu in the brain. Neural Proteoglycans. M. N. Kerala, Research Signpost 37/661 (2): 67-83.

Oohashi, T., Hirakawa, S., Bekku, Y., Rauch, U., Zimmermann, D. R., Su, W. D., Ohtsuka, A., Murakami, T. and Ninomiya, Y. (2002). "Bral1, a brain-specific link protein, colocalizing with the versican V2 isoform at the nodes of Ranvier in developing and adult mouse central nervous systems." Mol Cell Neurosci 19(1): 43-57.

Ordaz, B., Tuz, K., Ochoa, L. D., Lezama, R., Pena-Segura, C. and Franco, R. (2004). "Osmolytes and mechanisms involved in regulatory volume decrease under conditions of sudden or gradual osmolarity decrease." Neurochem Res 29(1): 65-72.

Orkand, R. K., Nicholls, J. G. and Kuffler, S. W. (1966). "Effect of nerve impulses on the membrane potential of glial cells in the central nervous system of amphibia." J Neurophysiol 29(4): 788-806.

Ormandy, G. C. and Jope, R. S. (1991). "Pertussis toxin potentiates seizures induced by pilocarpine, kainic acid and N-methyl-D-aspartate." Brain Res 553(1): 51-57.

Oshio, K., Binder, D. K., Yang, B., Schecter, S., Verkman, A. S. and Manley, G. T. (2004). "Expression of aquaporin water channels in mouse spinal cord." Neuroscience 127(3): 685-693.

Pannasch, U., Derangeon, M., Chever, O. and Rouach, N. (2012). "Astroglial gap junctions shape neuronal network activity." Commun Integr Biol 5(3): 248-254.

Pannasch, U., Vargova, L., Reingruber, J., Ezan, P., Holcman, D., Giaume, C., Sykova, E. and Rouach, N. (2011). "Astroglial networks scale synaptic activity and plasticity." Proc Natl Acad Sci U S A 108(20): 8467-8472.

Park, D., Xiang, A. P., Zhang, L., Mao, F. F., Walton, N. M., Choi, S. S. and Lahn, B. T. (2009). "The radial glia antibody RC2 recognizes a protein encoded by Nestin." Biochem Biophys Res Commun 382(3): 588-592.

Parpura, V., Heneka, M. T., Montana, V., Oliet, S. H., Schousboe, A., Haydon, P. G., Stout, R. F., Jr., Spray, D. C., Reichenbach, A., Pannicke, T., Pekny, M., Pekna, M., Zorec, R. and Verkhratsky, A. (2012). "Glial cells in (patho)physiology." J Neurochem 121(1): 4-27.

Parpura, V., Scemes, E. and Spray, D. C. (2004). "Mechanisms of glutamate release from astrocytes: gap junction "hemichannels", purinergic receptors and exocytotic release." Neurochem Int 45(2-3): 259-264.

Patterson, G. H., Knobel, S. M., Sharif, W. D., Kain, S. R. and Piston, D. W. (1997). "Use of the green fluorescent protein and its mutants in quantitative fluorescence microscopy." Biophys J 73(5): 2782-2790.

Paxinos, G. and Fraklin, K. B. J. (2001). The Mouse Brain in Stereotaxic Coordinates, Academic Press.

Paxinos, G. and Watson, C. (1998). The rat brain in stereotaxic coordinates, Academic Press.

Pekny, M., Leveen, P., Pekna, M., Eliasson, C., Berthold, C. H., Westermark, B. and Betsholtz, C. (1995). "Mice lacking glial fibrillary acidic protein display astrocytes devoid of intermediate filaments but develop and reproduce normally." EMBO J 14(8): 1590-1598.

Pekny, M. and Pekna, M. (2004). "Astrocyte intermediate filaments in CNS pathologies and regeneration." J Pathol 204(4): 428-437.

Pellerin, L. and Magistretti, P. J. (2004). "Neuroenergetics: calling upon astrocytes to satisfy hungry neurons." Neuroscientist 10(1): 53-62.

Pena, F. and Tapia, R. (1999). "Relationships among seizures, extracellular amino acid changes, and neurodegeneration induced by 4-aminopyridine in rat hippocampus: a microdialysis and electroencephalographic study." J Neurochem 72(5): 2006-2014.

Perea, G. and Araque, A. (2010). "GLIA modulates synaptic transmission." Brain Res Rev 63(1-2): 93-102.

Perea, G., Navarrete, M. and Araque, A. (2009). "Tripartite synapses: astrocytes process and control synaptic information." Trends Neurosci 32(8): 421-431.

Perillan, P. R., Li, X., Potts, E. A., Chen, M., Bredt, D. S. and Simard, J. M. (2000). "Inward rectifier K(+) channel Kir2.3 (IRK3) in reactive astrocytes from adult rat brain." Glia 31(2): 181-192.

Perillan, P. R., Li, X. and Simard, J. M. (1999). "K(+) inward rectifier currents in reactive astrocytes from adult rat brain." Glia 27(3): 213-225.

Peters, M. F., Adams, M. E. and Froehner, S. C. (1997). "Differential association of syntrophin pairs with the dystrophin complex." J Cell Biol 138(1): 81-93.

Peters, M. F., O'Brien, K. F., Sadoulet-Puccio, H. M., Kunkel, L. M., Adams, M. E. and Froehner, S. C. (1997). "beta-dystrobrevin, a new member of the dystrophin family. Identification, cloning, and protein associations." J Biol Chem 272(50): 31561-31569.

Piet, R., Vargova, L., Sykova, E., Poulain, D. A. and Oliet, S. H. (2004). "Physiological contribution of the astrocytic environment of neurons to intersynaptic crosstalk." Proc Natl Acad Sci U S A 101(7): 2151-2155.

Pivonkova, H., Benesova, J., Butenko, O., Chvatal, A. and Anderova, M. (2010). "Impact of global cerebral ischemia on K+ channel expression and membrane properties of glial cells in the rat hippocampus." Neurochem Int 57(7): 783-794.

Preston, G. M. and Agre, P. (1991). "Isolation of the cDNA for erythrocyte integral membrane protein of 28 kilodaltons: member of an ancient channel family." Proc Natl Acad Sci U S A 88(24): 11110-11114.

Preston, G. M., Smith, B. L., Zeidel, M. L., Moulds, J. J. and Agre, P. (1994). "Mutations in aquaporin-1 in phenotypically normal humans without functional CHIP water channels." Science 265(5178): 1585-1587.

Prokopova, S., Vargova, L. and Sykova, E. (1997). "Heterogeneous and anisotropic diffusion in the developing rat spinal cord." Neuroreport 8(16): 3527-3532.

Rash, J. E. and Yasumura, T. (1999). "Direct immunogold labeling of connexins and aquaporin-4 in freeze-fracture replicas of liver, brain, and spinal cord: factors limiting quantitative analysis." Cell Tissue Res 296(2): 307-321.

Rash, J. E., Yasumura, T. and Dudek, F. E. (1998). "Ultrastructure, histological distribution, and freeze-fracture immunocytochemistry of gap junctions in rat brain and spinal cord." Cell Biol Int 22(11-12): 731-749.

Rash, J. E., Yasumura, T., Hudson, C. S., Agre, P. and Nielsen, S. (1998). "Direct immunogold labeling of aquaporin-4 in square arrays of astrocyte and ependymocyte plasma membranes in rat brain and spinal cord." Proc Natl Acad Sci U S A 95(20): 11981-11986.

Ribeiro Mde, C., Hirt, L., Bogousslavsky, J., Regli, L. and Badaut, J. (2006). "Time course of aquaporin expression after transient focal cerebral ischemia in mice." J Neurosci Res 83(7): 1231-1240.

Rice, M. E., Okada, Y. C. and Nicholson, C. (1993). "Anisotropic and heterogeneous diffusion in the turtle cerebellum: implications for volume transmission." J Neurophysiol 70(5): 2035-2044.

Righini, A., Pierpaoli, C., Alger, J. R. and Di Chiro, G. (1994). "Brain parenchyma apparent diffusion coefficient alterations associated with experimental complex partial status epilepticus." Magn Reson Imaging 12(6): 865-871.

Roitbak, T. and Sykova, E. (1999). "Diffusion barriers evoked in the rat cortex by reactive astrogliosis." Glia 28(1): 40-48.

Rojek, A., Praetorius, J., Frokiaer, J., Nielsen, S. and Fenton, R. A. (2008). "A current view of the mammalian aquaglyceroporins." Annu Rev Physiol 70: 301-327.

Ron, N. P., Kazianis, J. A., Padbury, J. F., Brown, C. M., McGonnigal, B. G., Sysyn, G. D., Sadowska, G. B. and Stonestreet, B. S. (2005). "Ontogeny and the effects of corticosteroid pretreatment on aquaporin water channels in the ovine cerebral cortex." Reprod Fertil Dev 17(5): 535-542.

Rossi, D. J., Oshima, T. and Attwell, D. (2000). "Glutamate release in severe brain ischaemia is mainly by reversed uptake." Nature 403(6767): 316-321.

Rouach, N., Koulakoff, A., Abudara, V., Willecke, K. and Giaume, C. (2008). "Astroglial metabolic networks sustain hippocampal synaptic transmission." Science 322(5907): 1551-1555.

Russell, J. M. (2000). "Sodium-potassium-chloride cotransport." Physiol Rev 80(1): 211-276.

Saghyan, A., Lewis, D. P., Hrabe, J. and Hrabetova, S. (2012). "Extracellular diffusion in laminar brain structures exemplified by hippocampus." J Neurosci Methods 205(1): 110-118.

Seifert, G., Carmignoto, G. and Steinhauser, C. (2010). "Astrocyte dysfunction in epilepsy." Brain Res Rev 63(1-2): 212-221.

Seifert, G., Schilling, K. and Steinhauser, C. (2006). "Astrocyte dysfunction in neurological disorders: a molecular perspective." Nat Rev Neurosci 7(3): 194-206.

Shibuki, K., Gomi, H., Chen, L., Bao, S., Kim, J. J., Wakatsuki, H., Fujisaki, T., Fujimoto, K., Katoh, A., Ikeda, T., Chen, C., Thompson, R. F. and Itohara, S. (1996). "Deficient cerebellar long-term depression, impaired eyeblink conditioning, and normal motor coordination in GFAP mutant mice." Neuron 16(3): 587-599.

Shneker, B. F. and Fountain, N. B. (2003). "Epilepsy." Dis Mon 49(7): 426-478.

Schousboe, A., Sickmann, H. M., Walls, A. B., Bak, L. K. and Waagepetersen, H. S. (2010). "Functional importance of the astrocytic glycogen-shunt and glycolysis for maintenance of an intact intra/extracellular glutamate gradient." Neurotox Res 18(1): 94-99.

Schurr, A., Miller, J. J., Payne, R. S. and Rigor, B. M. (1999). "An increase in lactate output by brain tissue serves to meet the energy needs of glutamate-activated neurons." J Neurosci 19(1): 34-39.

Schurr, A., Payne, R. S., Miller, J. J. and Rigor, B. M. (1997). "Brain lactate, not glucose, fuels the recovery of synaptic function from hypoxia upon reoxygenation: an in vitro study." Brain Res 744(1): 105-111.

Schurr, A., West, C. A. and Rigor, B. M. (1988). "Lactate-supported synaptic function in the rat hippocampal slice preparation." Science 240(4857): 1326-1328.

Schwartzkroin, P. A., Baraban, S. C. and Hochman, D. W. (1998). "Osmolarity, ionic flux, and changes in brain excitability." Epilepsy Res 32(1-2): 275-285.

Simard, M., Arcuino, G., Takano, T., Liu, Q. S. and Nedergaard, M. (2003). "Signaling at the gliovascular interface." J Neurosci 23(27): 9254-9262.

Simard, M. and Nedergaard, M. (2004). "The neurobiology of glia in the context of water and ion homeostasis." Neuroscience 129(4): 877-896.

Slezia, A., Kekesi, A. K., Szikra, T., Papp, A. M., Nagy, K., Szente, M., Magloczky, Z., Freund, T. F. and Juhasz, G. (2004). "Uridine release during aminopyridine-induced epilepsy." Neurobiol Dis 16(3): 490-499.

Smolders, I., Khan, G. M., Manil, J., Ebinger, G. and Michotte, Y. (1997). "NMDA receptor-mediated pilocarpine-induced seizures: characterization in freely moving rats by microdialysis." Br J Pharmacol 121(6): 1171-1179.

Sofroniew, M. V. and Vinters, H. V. (2010). "Astrocytes: biology and pathology." Acta Neuropathol 119(1): 7-35.

Solenov, E., Watanabe, H., Manley, G. T. and Verkman, A. S. (2004). "Sevenfold-reduced osmotic water permeability in primary astrocyte cultures from AQP-4-deficient mice, measured by a fluorescence quenching method." Am J Physiol Cell Physiol 286(2): C426-432.

Stringer, J. L. and Lothman, E. W. (1996). "During afterdischarges in the young rat in vivo extracellular potassium is not elevated above adult levels." Brain Res Dev Brain Res 91(1): 136-139.

Stringer, J. L. and Sowell, K. L. (1994). "Kainic acid, bicuculline, pentylenetetrazol and pilocarpine elicit maximal dentate activation in the anesthetized rat." Epilepsy Res 18(1): 11-21.

Strohschein, S., Huttmann, K., Gabriel, S., Binder, D. K., Heinemann, U. and Steinhauser, C. (2011). "Impact of aquaporin-4 channels on K+ buffering and gap junction coupling in the hippocampus." Glia 59(6): 973-980.

Su, G., Kintner, D. B. and Sun, D. (2002). "Contribution of Na(+)-K(+)-Cl(-) cotransporter to high-[K(+)](o)- induced swelling and EAA release in astrocytes." Am J Physiol Cell Physiol 282(5): C1136-1146.

Swann, J. W. and Brady, R. J. (1984). "Penicillin-induced epileptogenesis in immature rat CA3 hippocampal pyramidal cells." Brain Res 314(2): 243-254.

Sykova, E. (1983). "Extracellular K+ accumulation in the central nervous system." Prog Biophys Mol Biol 42(2-3): 135-189.

Sykova, E. (1997). "Extracellular space in the CNS: its regulation, volume and geometry in normal and pathological neuronal function." Neuroscientist 3: 28-41.

Sykova, E. (2004). "Diffusion properties of the brain in health and disease." Neurochem Int 45(4): 453-466.

Sykova, E. (2005). "Glia and volume transmission during physiological and pathological states." J Neural Transm 112(1): 137-147.

Syková, E. (1992). Ionic and Volume Changes in the Microenvironment of Nerve and Receptor Cells. Berlin, Heidelberg, New York, Springer-Verlag.

Syková, E. (1992). Ionic and volume changes in the miroenvironment of nerve and receptor cells. Progress in Sensery Physiology, Springer-Verlag, Heidelberg: 1-167.

Syková, E., Hník, P. and Vyklický, L. (1981). Ion-selective microelectrodes and their use in excitable tissues. New York, Plenum Press.

Sykova, E. and Chvatal, A. (1993). "Extracellular ionic and volume changes: the role in glia-neuron interaction." J Chem Neuroanat 6(4): 247-260.

Sykova, E. and Chvatal, A. (2000). "Glial cells and volume transmission in the CNS." Neurochem Int 36(4-5): 397-409.

Syková, E., Chvátal, A., Vargová, L., Voříšek, I. (1996). Extracellular space ionic composition, volume and geometry during neuronal activity and pathological stages, Springer-Verlag.

Sykova, E., Mazel, T., Hasenohrl, R. U., Harvey, A. R., Simonova, Z., Mulders, W. H. and Huston, J. P. (2002). "Learning deficits in aged rats related to decrease in extracellular volume and loss of diffusion anisotropy in hippocampus." Hippocampus 12(2): 269-279.

Sykova, E., Mazel, T. and Simonova, Z. (1998). "Diffusion constraints and neuron-glia interaction during aging." Exp Gerontol 33(7-8): 837-851.

Sykova, E. and Nicholson, C. (2008). "Diffusion in brain extracellular space." Physiological Reviews 88(4): 1277-1340.

Sykova, E., Svoboda, J., Polak, J. and Chvatal, A. (1994). "Extracellular volume fraction and diffusion characteristics during progressive ischemia and terminal anoxia in the spinal cord of the rat." J Cereb Blood Flow Metab 14(2): 301-311.

Sykova, E., Svoboda, J., Simonova, Z. and Jendelova, P. (1992). "Role of astrocytes in ionic and volume homeostasis in spinal cord during development and injury." Prog Brain Res 94: 47-56.

Sykova, E., Vargova, L., Prokopova, S. and Simonova, Z. (1999). "Glial swelling and astrogliosis produce diffusion barriers in the rat spinal cord." Glia 25(1): 56-70.

Sykova, E., Vorisek, I., Antonova, T., Mazel, T., Meyer-Luehmann, M., Jucker, M., Hajek, M., Ort, M. and Bures, J. (2005). "Changes in extracellular space size and geometry in APP23 transgenic mice: a model of Alzheimer's disease." Proc Natl Acad Sci U S A 102(2): 479-484.

Sykova, E., Vorisek, I., Mazel, T., Antonova, T. and Schachner, M. (2005). "Reduced extracellular space in the brain of tenascin-R- and HNK-1-sulphotransferase deficient mice." Eur J Neurosci 22(8): 1873-1880.

Tanaka, K., Watase, K., Manabe, T., Yamada, K., Watanabe, M., Takahashi, K., Iwama, H., Nishikawa, T., Ichihara, N., Kikuchi, T., Okuyama, S., Kawashima, N., Hori, S., Takimoto, M. and Wada, K. (1997). "Epilepsy and exacerbation of brain injury in mice lacking the glutamate transporter GLT-1." Science 276(5319): 1699-1702.

Taniguchi, M., Yamashita, T., Kumura, E., Tamatani, M., Kobayashi, A., Yokawa, T., Maruno, M., Kato, A., Ohnishi, T., Kohmura, E., Tohyama, M. and Yoshimine, T. (2000). "Induction of aquaporin-4 water channel mRNA after focal cerebral ischemia in rat." Brain Res Mol Brain Res 78(1-2): 131-137.

Taylor, C. P. and Dudek, F. E. (1982). "Synchronous neural afterdischarges in rat hippocampal slices without active chemical synapses." Science 218(4574): 810-812.

Theodosis, D. T., Pierre, K., Cadoret, M. A., Allard, M., Faissner, A. and Poulain, D. A. (1997). "Expression of high levels of the extracellular matrix glycoprotein, tenascin-C, in the normal adult hypothalamoneurohypophysial system." J Comp Neurol 379(3): 386-398.

Traynelis, S. F. and Dingledine, R. (1989). "Modification of potassium-induced interictal bursts and electrographic seizures by divalent cations." Neurosci Lett 98(2): 194-199.

Treiman, D. M., Walton, N. Y. and Kendrick, C. (1990). "A progressive sequence of electroencephalographic changes during generalized convulsive status epilepticus." Epilepsy Res 5(1): 49-60.

Turski, L., Ikonomidou, C., Turski, W. A., Bortolotto, Z. A. and Cavalheiro, E. A. (1989). "Review: cholinergic mechanisms and epileptogenesis. The seizures induced by pilocarpine: a novel experimental model of intractable epilepsy." Synapse 3(2): 154-171.

Ujec, E. (1988). "Differential DC amplifier for recording small and fast concentration changes with ion-selective microelectrodes." Physiol Bohemoslov 37(1): 87-90.

Ungerstedt, U. (1991). "Microdialysis--principles and applications for studies in animals and man." J Intern Med 230(4): 365-373.

Vajda, Z., Promeneur, D., Doczi, T., Sulyok, E., Frokiaer, J., Ottersen, O. P. and Nielsen, S. (2000). "Increased aquaporin-4 immunoreactivity in rat brain in response to systemic hyponatremia." Biochem Biophys Res Commun 270(2): 495-503.

van der Toorn, A., Sykova, E., Dijkhuizen, R. M., Vorisek, I., Vargova, L., Skobisova, E., van Lookeren Campagne, M., Reese, T. and Nicolay, K. (1996). "Dynamic changes in water ADC, energy metabolism, extracellular space volume, and tortuosity in neonatal rat brain during global ischemia." Magn Reson Med 36(1): 52-60.

van Eijsden, P., Notenboom, R. G., Wu, O., de Graan, P. N., van Nieuwenhuizen, O., Nicolay, K. and Braun, K. P. (2004). "In vivo 1H magnetic resonance spectroscopy, T2-weighted and diffusion-weighted MRI during lithium-pilocarpine-induced status epilepticus in the rat." Brain Res 1030(1): 11-18.

Vargova, L., Cicanic, M., Dmytrenko, L., Tureckova, J. and Anderova, M. (2013). Changes in astroglial volume, extracellular space geometry and K+ concentration in α-syntrophin deficient mice during cellular swelling. The 43th annual meeting of the Society for Neuroscience. San Diego, USA.

Vargova, L., Jendelova, P., Chvatal, A. and Sykova, E. (2001). "Glutamate, NMDA, and AMPA induced changes in extracellular space volume and tortuosity in the rat spinal cord." J Cereb Blood Flow Metab 21(9): 1077-1089.

Venero, J. L., Vizuete, M. L., Ilundain, A. A., Machado, A., Echevarria, M. and Cano, J. (1999). "Detailed localization of aquaporin-4 messenger RNA in the CNS: preferential expression in periventricular organs." Neuroscience 94(1): 239-250.

Verbavatz, J. M., Ma, T., Gobin, R. and Verkman, A. S. (1997). "Absence of orthogonal arrays in kidney, brain and muscle from transgenic knockout mice lacking water channel aquaporin-4." J Cell Sci 110 (Pt 22): 2855-2860.

Verkhratsky, A. (2006). "Glial calcium signaling in physiology and pathophysiology." Acta Pharmacol Sin 27(7): 773-780.

Verkhratsky, A. and Butt, A. (2007). Glial Neurobiology, Wiley.

Verkhratsky, A., Orkand, R. K. and Kettenmann, H. (1998). "Glial calcium: homeostasis and signaling function." Physiol Rev 78(1): 99-141.

Verkman, A. S. (2005). "More than just water channels: unexpected cellular roles of aquaporins." J Cell Sci 118(Pt 15): 3225-3232.

Verkman, A. S., Ratelade, J., Rossi, A., Zhang, H. and Tradtrantip, L. (2011). "Aquaporin-4: orthogonal array assembly, CNS functions, and role in neuromyelitis optica." Acta Pharmacol Sin 32(6): 702-710.

Vijayan, V. K., Lee, Y. L. and Eng, L. F. (1990). "Increase in glial fibrillary acidic protein following neural trauma." Mol Chem Neuropathol 13(1-2): 107-118.

Vitellaro-Zuccarello, L., Mazzetti, S., Bosisio, P., Monti, C. and De Biasi, S. (2005). "Distribution of Aquaporin 4 in rodent spinal cord: relationship with astrocyte markers and chondroitin sulfate proteoglycans." Glia 51(2): 148-159.

Vorisek, I. and Sykova, E. (1997). "Ischemia-induced changes in the extracellular space diffusion parameters, K+, and pH in the developing rat cortex and corpus callosum." J Cereb Blood Flow Metab 17(2): 191-203.

Vorisek, I. and Sykova, E. (2009). "Measuring diffusion parameters in the brain: comparing the real-time iontophoretic method and diffusion-weighted magnetic resonance." Acta Physiol (Oxf) 195(1): 101-110.

Walker, M. C., White, H. S. and Sander, J. W. (2002). "Disease modification in partial epilepsy." Brain 125(Pt 9): 1937-1950.

Wall, C. J., Kendall, E. J. and Obenaus, A. (2000). "Rapid alterations in diffusion-weighted images with anatomic correlates in a rodent model of status epilepticus." AJNR Am J Neuroradiol 21(10): 1841-1852.

Walls, A. B., Heimburger, C. M., Bouman, S. D., Schousboe, A. and Waagepetersen, H. S. (2009). "Robust glycogen shunt activity in astrocytes: Effects of glutamatergic and adrenergic agents." Neuroscience 158(1): 284-292.

Walz, W. and Hinks, E. C. (1986). "A transmembrane sodium cycle in astrocytes." Brain Res 368(2): 226-232.

Walz, W., Klimaszewski, A. and Paterson, I. A. (1993). "Glial swelling in ischemia: a hypothesis." Dev Neurosci 15(3-5): 216-225.

Wang, Y., Majors, A., Najm, I., Xue, M., Comair, Y., Modic, M. and Ng, T. C. (1996). "Postictal alteration of sodium content and apparent diffusion coefficient in epileptic rat brain induced by kainic acid." Epilepsia 37(10): 1000-1006.

Wasterlain, C. G., Fujikawa, D. G., Penix, L. and Sankar, R. (1993). "Pathophysiological mechanisms of brain damage from status epilepticus." Epilepsia 34 Suppl 1: S37-53.

Wen, H., Nagelhus, E. A., Amiry-Moghaddam, M., Agre, P., Ottersen, O. P. and Nielsen, S. (1999). "Ontogeny of water transport in rat brain: postnatal expression of the aquaporin-4 water channel." Eur J Neurosci 11(3): 935-945.

Whetsell, W. O., Jr. (1996). "Current concepts of excitotoxicity." J Neuropathol Exp Neurol 55(1): 1-13.

White, B. C., Sullivan, J. M., DeGracia, D. J., O'Neil, B. J., Neumar, R. W., Grossman, L. I., Rafols, J. A. and Krause, G. S. (2000). "Brain ischemia and reperfusion: molecular mechanisms of neuronal injury." J Neurol Sci 179(S 1-2): 1-33.

Wong, C. H. and Crack, P. J. (2008). "Modulation of neuro-inflammation and vascular response by oxidative stress following cerebral ischemia-reperfusion injury." Curr Med Chem 15(1): 1-14.

Wright, E. M., Wiedner, G. and Rumrich, G. (1977). "Fluid secretion by the frog choroid plexus." Exp Eye Res 25 Suppl: 149-155.

Wu, Y., Zhang, A. Q. and Yew, D. T. (2005). "Age related changes of various markers of astrocytes in senescence-accelerated mice hippocampus." Neurochem Int 46(7): 565-574.

Xie, Y., Zacharias, E., Hoff, P. and Tegtmeier, F. (1995). "Ion channel involvement in anoxic depolarization induced by cardiac arrest in rat brain." J Cereb Blood Flow Metab 15(4): 587-594.

Yamaguchi, Y. (2000). "Lecticans: organizers of the brain extracellular matrix." Cell Mol Life Sci 57(2): 276-289.

Yamamoto, N., Sobue, K., Miyachi, T., Inagaki, M., Miura, Y., Katsuya, H. and Asai, K. (2001). "Differential regulation of aquaporin expression in astrocytes by protein kinase C." Brain Res Mol Brain Res 95(1-2): 110-116.

Yang, B., Brown, D. and Verkman, A. S. (1996). "The mercurial insensitive water channel (AQP-4) forms orthogonal arrays in stably transfected Chinese hamster ovary cells." J Biol Chem 271(9): 4577-4580.

Yang, B. and Verkman, A. S. (1997). "Water and glycerol permeabilities of aquaporins 1-5 and MIP determined quantitatively by expression of epitope-tagged constructs in Xenopus oocytes." J Biol Chem 272(26): 16140-16146.

Yao, X., Hrabetova, S., Nicholson, C. and Manley, G. T. (2008). "Aquaporin-4-deficient mice have increased extracellular space without tortuosity change." J Neurosci 28(21): 5460-5464.

Yoneda, K., Yamamoto, N., Asai, K., Sobue, K., Fujita, Y., Fujita, M., Mase, M., Yamada, K., Nakanishi, M., Tada, T., Miura, Y. and Kato, T. (2001). "Regulation of aquaporin-4 expression in astrocytes." Brain Res Mol Brain Res 89(1-2): 94-102.

Zamecnik, J., Homola, A., Cicanic, M., Kuncova, K., Marusic, P., Krsek, P., Sykova, E. and Vargova, L. (2012). "The extracellular matrix and diffusion barriers in focal cortical dysplasias." Eur J Neurosci 36(1): 2017-2024.

Zamecnik, J., Vargova, L., Homola, A., Kodet, R. and Sykova, E. (2004). "Extracellular matrix glycoproteins and diffusion barriers in human astrocytic tumours." Neuropathol Appl Neurobiol 30(4): 338-350.

Zelenina, M. (2010). "Regulation of brain aquaporins." Neurochem Int 57(4): 468-488.

Zeynalov, E., Chen, C. H., Froehner, S. C., Adams, M. E., Ottersen, O. P., Amiry-Moghaddam, M. and Bhardwaj, A. (2008). "The perivascular pool of aquaporin-4 mediates the effect of osmotherapy in postischemic cerebral edema." Crit Care Med 36(9): 2634-2640.

Zhong, J., Petroff, O. A., Prichard, J. W. and Gore, J. C. (1993). "Changes in water diffusion and relaxation properties of rat cerebrum during status epilepticus." Magn Reson Med 30(2): 241-246.

Zhuo, L., Sun, B., Zhang, C. L., Fine, A., Chiu, S. Y. and Messing, A. (1997). "Live astrocytes visualized by green fluorescent protein in transgenic mice." Dev Biol 187(1): 36-42.

Zoli, M., Jansson, A., Syková, E., Agnati, L. F. and Fuxe, K. (1999). "Intercellular communication in the central nervous system. The emergence of the volume transmission concept and its relevance for neuropsychopharmacology." Trends in Pharmacological Sciences 20: 142-150.

Zoremba, N., Homola, A., Rossaint, R. and Sykova, E. (2007). "Brain metabolism and extracellular space diffusion parameters during and after transient global hypoxia in the rat cortex." Exp Neurol 203(1): 34-41.

Zoremba, N., Homola, A., Slais, K., Vorisek, I., Rossaint, R., Lehmenkuhler, A. and Sykova, E. (2008). "Extracellular diffusion parameters in the rat somatosensory cortex during recovery from transient global ischemia/hypoxia." J Cereb Blood Flow Metab 28(10): 1665-1673.

9. ATTACHMENT

List of author`s publications:

1. Šlais K., Voříšek I., Zoremba N., Homola A., **Dmytrenko L.,** Syková E. (2008) Brain metabolism and diffusion in the rat cerebral cortex during pilocarpine-induced status epilepticus. *Experimental Neurology*, Jan; 209(1):145-54, IF=4.156.

2. Bekku Y., Vargová L., Goto Y., Voříšek I., **Dmytrenko L.**, Narasaki M., Ohtsuka A., Fassler R., Ninomiya Y., Syková E., Oohashi T. (2010) Bral1: its role in diffusion barrier formation and conduction velocity in the CNS. *Journal of Neuroscience*, Feb 24; 30(8):3113-23, IF=7.178.

3. **Dmytrenko L.,** Cicanič M., Anděrová M., Voříšek I., Syková E., Vargová L. (2013) The impact of alpha-syntrophin deletion on the changes in tissue structure and extracellular diffusion associated with cell swelling under physiological and pathological conditions. *PLoS ONE* 8(7):e68044, IF=3.7.